NUMERICAL EVALUATION OF RETROFIT DESIGNS OF CABLE MEDIAN BARRIERS USING RECLAIMED TIRES

by

Amey G. Badar

A thesis submitted to the faculty of
The University of North Carolina at Charlotte
in partial fulfillment of the requirements
for the degree of Master of Science in
Mechanical Engineering

Charlotte

2017

Approved by:

_____
Dr. Howie Fang

_____
Dr. Alireza Tabarraei

_____
Dr. David Weggel

ABSTRACT

AMEY G. BADAR. Numerical evaluation of retrofit designs of cable median barriers using reclaimed tires. (Under the direction of DR. HOWIE FANG)

This thesis presents a research attempt at finding out a viable retrofit system design for cable median barriers using reclaimed tires. Finite element analysis was used to conduct simulations in order to evaluate the performance of retrofit barriers.

Four designs of the retrofit tire-cable median barriers were modeled and tested under impacts by a 1996 Dodge Neon and a 2006 Ford F250 according to MASH test level 3 impact conditions. The simulations were conducted on a flat median and the vehicles were impacted on the barrier at 62.1 mph and 25° impact angle at the post to find out a feasible design out of the four proposed designs. These simulations were conducted in a systematic manner and a viable design option was found amongst the four proposed retrofit options and named as EDC_J1. Further evaluation of EDC_J1 design was carried out by setting up simulations for back side and front side impacts on post and mid-span on flat and sloped medians.

The simulation results showed that the EDC_J1 barrier could successfully redirect the smaller sedan in most cases compared to the current cable median barrier without tires. The EDC_J1 tire-cable median barrier was also found to have less barrier deflection than the current design for impacts with smaller sedan.

ACKNOWLEDGEMENTS

Firstly, I would like to thank my graduate advisor Dr. Howie Fang for giving me an opportunity to work in his lab as a research assistant since last year. He has been a wonderful teacher and research guide to me and has constantly inspired and motivated me to do my best. I would also like to thank my committee members, Dr. David Weggel and Dr. Alireza Tabarraei, for their valuable reviews, comments and advice on my thesis.

I would like to thank the North Carolina Department of Transportation (NCDOT) for their financial support to me as a research assistant in NCDOT project 2017-13. I would especially like to thank my research colleague Matthew Gutowski for his help and advice throughout my time in this lab. My thanks also go out to Emre Palta for his valuable advice on modeling and writing for this thesis and to Oyeboade Fatoki for his post processing work on NCDOT project.

Last, but not least, I would like to thank my family in India for their support and encouragement to go for higher studies and my friends in India and US for all their help. Without their backing, this thesis would not have been possible.

TABLE OF CONTENTS

LIST OF TABLES

LIST OF FIGURES

CHAPTER 1 : INTRODUCTION

There are various types of roadside barriers installed on highways to prevent errant vehicles from entering dangerous areas such as steep slopes, rocks, or oncoming traffic. Highway median barriers are used on divided freeways to prevent vehicles from crossing over a median and striking an oncoming vehicle in a head on crash. Bridge barriers are an extension of the road side barriers to prevent vehicles from falling over a bridge. There are also work zone barriers that are used temporarily to redirect traffic and/or protect workers on site. Roadside barriers can also be categorized based on the overall rigidity of the barriers: flexible barriers such as cable barriers and weak post corrugated barriers, semi-rigid barriers such as W-beam and thrie-beam guardrails, and rigid barriers such as concrete barriers (e.g., Jersey and F-type barriers).

In this research, cable barriers are studied for their performance on highway medians and augmented with used tires. A typical cable barrier system consists of steel wire ropes mounted on weak posts. The cable median barriers (CMBs) come in two major types, high tension and low tension CMBs mainly distinguished by the tensions in the cables. The main role of a CMB is to safely retain and/or redirect an errant vehicle to avoid crashes with vehicles in the opposing travel lane. The CMB is commonly used in wide medians where there is enough room for the errant vehicle to be redirected. This type of barrier is not used for critical locations where there is no leeway. One advantage of the CMBs is that since they are flexible barriers, the damage caused to the striking vehicle and thereby the injuries to the occupants are relatively small. Also, compared to the other barrier systems, the CMB’s are relatively easy to repair and their service

time is short. The disadvantage of the CMBs is that these barriers might not be effective in certain crash scenarios involving large trucks and/or on high-slope medians

The goal of this research is to design and test a prototype of semi-flexible barrier that combines a cable barrier and reclaimed tires. This new barrier design can be used as a retrofit option to the current existing cable barriers and can be implemented with a small investment. The use of old/used tires is very limited as it very difficult and costly to recycle them. Some of the tires can't even be recycled and thus are just hogging the storage space. Use of such tires in this new barrier system will put these tires to good use and basically reduce the compliance of the barrier system as a whole. Furthermore, implementation of this system gives a good performance-to-cost ratio. The potential benefit on the performance of cable median barrier is as follows:

- The vehicles can be redirected in a shorter median
- There are less chances of vehicles under riding or overriding the barrier as is the case with present cable median barriers.
- The cost of post-impact repairs can be reduced.

1.1 Performance evaluation of cable barriers

This section gives a comprehensive summary of studies related to cable barriers as seen in Figure 1.1. The topics cover performance evaluation of in-service cable barriers, crash testing, and the application of finite element (FE) modeling and simulations for highway safety research.

Figure 1.1: Cable median barrier.

In 1967, Graham et al. submitted a report to the New York State Department of Public Works which included a study of current road side barrier systems. The study included a comprehensive theoretical analysis of the forces generated between vehicle and barrier during impact. Four mathematical models were developed to predict the trajectory of a vehicle in collision with a given barrier. Computers were used to solve these models and the solutions from three of these models included force deflection curves of the barrier in case of cable median barriers (tension rails), W-beam barrier (combination of tension and bending) and box beam barriers (pure bending). The fourth mathematical model was used to obtain the trajectory of the vehicle using appropriate

force-deflection curve as input. This research included forty-eight full scale collisions between standard passenger cars and various barrier configurations. These simulations included vehicle speeds up to 60 mph and impact angles up to 35 degrees to represent the worst possible accident conditions on the highways. Dynamic simulations on the guiderail posts embedded in different types of soil were carried out along with optimization of post size and embedment conditions. The highlight of this research was the development of the box beam barrier. In regards to the cable barrier systems, it was found that the best post was a standard 3I5.7 post with 0.75 in. steel cables. New York adopted a standard barrier height of 30 inches with a 3 inch spacing and the post spacing was decided to be 16 foot. Also, the 6x6 inch soil plate and spring tension compensators were incorporated in the barrier design. A test on the bridge rail variant of the cable barrier was performed. In this test, the vehicle was not redirected and suffered sufficient damage concluding that design modifications in the cable barrier or installation of other barriers was necessary at the bridge rails.

In 1990, Phillips et al. submitted a report titled “Cable guiderail breakaway terminal ends” to the U.S. Department of Transportation. This research focused on the performance of terminal ends of the cable barrier systems in the event of crash. The original design of the terminal ends were supposed to redirect and decelerate the vehicles impacting the sloped ends of the cable median barriers as the cables were being lowered into the terminal ends. It was assumed that upon impact, the slotted member will release the cables and prevent snagging of the vehicle and eventual rollover which is unacceptable behavior. In order to address this problem, the anchor design was revised in which the retention slots were fixed at an angle and thus the rods and cables were able to pull free on impact at the terminals. This change also ensured that the

integrity of the barrier remained intact for all other impact scenarios. Twelve full scale tests were conducted in accordance to the NCHRP report 230 to evaluate this design change. Tests were conducted on three distinct designs including modified original design, 45-degree turndown with solid anchor rod and 45-degree cable turndown. It was concluded from the tests that long cable turndown used in the previous standard cable guiderail terminal could snag and overturn the vehicle in departure impacts. The current terminal end design did not allow for lateral loads to be transmitted by the cables to the angles for quick release. The new terminal concept which included a 45-degree cable turndown and a slip-base end post. Various crash simulations by vehicles weighing 1800-lb, 2500-lb and 4850-lb confirmed that the new terminal end design demonstrated acceptable characteristics.

In 1993, Laker et al. submitted a paper to the Transportation Research Record titled “Development and Proving Tests of a Four-Rope Safety Fence”. This research was conducted to design a new cable barrier to overcome the deficiencies of an earlier two cable barrier system and that could be installed on any surface. This research was carried out in collaboration with Bridon PLC. The initial design had two ropes at two different heights and upon impact, the lower cable was over ridden and the upper cable was under ridden. For the new cable barrier, several new designs were proposed which included the use to two additional cables. Ten different impact tests were carried out at the Motor Industry Research Association (MIRA) in the UK. The new designs included a second pair of ropes added in the slot provided at the center of the z-shaped cross-section post. In the final design chosen, the post was manufactured from a 6-mm gauge steel having yield strength of 335 N/mm^2. The two upper ropes in the slot were at a height of 585 mm and lower pair of ropes were supported by small brackets on either

side of the posts at a height of 490 mm from the ground. The posts were held in concrete sockets with good clearance for easy removal and replacement in case of damage. The static tension in the rope was kept at a constant value of 22.25 kN. Various design changes were made by altering the heights of the cables and changing the static tension. Another important variation was the crisscrossing of the lower pair of cables utilize post retention more effectively. The post spacing was fixed at 2.4 m and another system was tested with the post spacing of just 1 m to be used on roads with a narrow median. The results of tests proved that the new cable barriers met the impact performance standards of the UK Department for Highways. Two vehicles with different weight class were used to test the barrier system. The barrier was able to redirect both the vehicles safely and with minimum damage to the vehicle and its occupants. At the time of this report, this barrier design was being tested according to the NCHRP 350 guidelines for use in the United States.

In 1993, Yang et al. submitted a report to the Transportation Research Record titled “Performance of Cable Guiderail in New York”. The report describes the efforts taken by the New York State Department of Transportation to investigate causes of tension loss in cable guiderail and formulate corrective measures for the same. This study was conducted in two phases. In the first phase, the performance of new cable barriers and the results of laboratory testing were documented. In the second phase, field performance of selected modified installations were documented from 1984 to 1987. During the first phase studies, anchor movement and permanent cable stretch were identified as major causes of tension loss in the barrier and several changes were proposed in regards to soil compaction and initial and long-term cable tension. In addition to these studies, prestressed cables were used at some of the locations to study

its effectiveness in reducing tension loss due to cable stretch. Laboratory tests were conducted using normal and prestressed cables to determine if any significant differences are present in cable strain due to long term loading. Four tensioning procedures have been described and discussed in this report and detailed analysis of the effectiveness of each method has been presented. Some of the findings included that barriers installed using either normal or revised tensioning procedures experienced greatest tension loss after the first tensioning and over the first winter. It was also established that tension losses would continue to occur in spite of re-tensioning procedures and periodic re-tensioning efforts need to be made. The pre-stretched cables loose tension at the same rate as normal cable.

In 1997, Hunter et al. published a paper in which they conducted a statistical study to perform in service evaluation of three cable barrier system on the segment of I-40 in North Carolina interstate highway. The crash data was collected from the years 1990 to 1997. Several regression-type models were developed which were used to estimate the effects of the installation of cable median barrier on crash rates for several crash types. The variables used in the model development were crash year, median type, median width, right shoulder width, number of lanes etc. The study showed that crashes increased on the section where cable median barriers were installed however, the number of fatal crashes and head on collisions had gone down. The overall severity index values were greatly reduced after the cable median barrier installation.

In 1998, Sposito et al. conducted a study on the effectiveness of the three cable barrier in preventing crossover accidents on interstate and to evaluate the maintenance and repair costs in order to make future recommendations for installations for these barrier systems. They found out that cable barrier system is cost effective compared to

the concrete barrier system and that it works best in medians with a minimum of 7m width. It was also found out that the fatality rate dropped from 0.6 per year for 1987 through 1996, to zero per year for the study period. However, the injury accident rate increased from 0.7 per year from 1987 through 1996, to 3.8 per year for the study period. It was concluded that the annual costs of the cable barrier system will always be less than the annual costs of the concrete median barrier system for this specific study location.

In 2008, Cooner et al. submitted a report to the Texas Department of Transportation titled “Performance evaluation of cable medina barrier systems in Texas”. This report summarizes efforts of the performance evaluation of various cable barrier systems in Texas. The parameters used for evaluation included installation costs, recurring maintenance costs and experiences, crash history before and after implementation and the field performance. The cable barrier systems in this study included proprietary designs by Trinity, Gibraltor and Brifen. The findings from the cost evaluation point of view suggested that the unit costs for the cable barrier systems dropped significantly over time because of stiff competition between manufacturers and increased demand. The cost of cable barrier implementation was the lowest in the state of Texas and the comprehensive cable barrier installation costs are the lowest compared to any type of concrete barrier. The report also includes findings for the maintenance and repair evaluation which suggested that majority of locations did not have break in the cable median barrier for patrol crossovers. Soil and weather conditions caused problems with post sockets and terminal anchor foundations. There were at least 75 reported cases where the damaged cable barrier was hit a second time. It was also found that government personnel performed more repair works compared to private

contractors. Research showed that there were on an average 7 impacts to a cable median barrier per mile per year, consistent with the findings of Ohio State. Data from the research showed that more frequent collisions occurred in rain and snow, and when the barrier was placed near the travel lane instead when placed within the median. A life-cycle cost analysis of the cable barrier showed that these barriers had a lower overall cost over 15-year lifespan. The report also indicated that overall fatalities caused due to cross over crashes have reduced significantly since the installation of the cable median barriers.

In 2013 Stolle et al conducted a study to investigate the conditions associated with cable median barrier containment failures and crash severity. The 85th percentile trajectory angle associated with severe cable median barrier crashes was calculated to be 39 degrees. It was also found that low tension cable barriers had lowest severe crash rate of 1.7% despite penetration and rollover rates of 9.1% and 7.8% respectively compared to the high tension cable barrier system. It was suggested for future full scale crash test with a large car or SUV should be conducted at a CG trajectory angle of 39 degrees.

In 2014 Stolle et al conducted a study to identify contributing circumstances to cable median barrier penetrations. Tools such as crash report scene diagrams and measurements, median geometries, photographs, vehicle geometries and inertial properties, and finally computer simulations were used to identify the said factors. They found that the most common type of underride penetration was caused by vehicles oriented nearly perpendicular to the barrier at impact, even at moderate impact angles. The high tension cable median barriers experienced override due to cable entrapment by the post flange or web. The low tension cable barriers experienced several

penetrations related to low strength of bottom and middle cable to post attachment, but relatively few overrides that were mainly caused by launching over the barriers. Some suggestions to prevent underrides were provided which stated that bottom cables should be located between 13 and 15 in. (330 and 381 mm), and strong cable-to-post attachments should be used. To prevent overrides, the top cables of systems located on approach slopes of 6:1 V-ditches or steeper should be weakly attached to the post with a height of 35 in. (889 mm) or higher.

In 2015, Burns et al. conducted a similar performance evaluation of a section on US-26 in Oregon. The cable median barrier is installed on a non-freeway road and the median is narrow (many locations have width less than 4 ft.). The design of this cable barrier system differs from the typical freeway cable median barriers in terms of post spacing. Typical median barriers have about 15 to 20ft distance between two posts, however, the US-26 CMB has only 6ft of spacing between two consecutive posts. This cable barrier meets the NCHRP 350 TL-4 standards. The study showed that crash rate increased by 72% following the installation of the barrier, however the number of fatal crashes and head on collisions were reduced by a significant amount.

1.2 Numerical simulations for performance evaluation

In 2005, Hiser et al. published a paper titled “Modeling slip base mechanisms” in the International Journal of Crashworthiness. The main objective of this research was to develop improved methods of modeling slip base structures using finite element analysis. Two bolt preloading techniques were developed and evaluated. The first method utilized a discrete spring element to preload the bolt and had a rigid bolt and nut. The second method utilized the pre-stressed bolt shaft solid elements. Both the models were impacted by rigid cylinders in three cases including, weak axis impact 137

mm above the slip plane, weak axis impact 437 mm above the slip plane, and strong axis impact at 437 mm above the slip plane. The second and third impact tests were conducted at bumper height. It was found that both models produced desired preload however, the discrete spring based model required 20% more energy than the solid model. In the second case, the first model locked up but the second model separated as desired. Based on these results, it was concluded that the solid bolt model displayed bolt overload and failure accurately in both strong and weak axis impacts and its use in further full scale simulations was suggested.

In 2007, Marzougui et al. conducted a study using finite element analysis along with vehicle dynamics analysis to observe the effect of sloped terrain on the safety performance of cable median barriers. The numerical simulations were validated by actual full scale crash testing. It was concluded from the study that on flat terrain, both the modeled and the Washington State cable barrier designs perform similarly in meeting the NCHRP report 350 crashworthiness criteria. On 6:1 sloped terrain, the simulations showed that the cable barrier will redirect the pickup truck even if the barrier is 1.22 m (4ft) offset from the center of a v-shaped median. The simulation also showed and full-scale crash tests confirmed that the cable barrier may not redirect mid-size sedans and small vehicles if the barrier is placed more than 0.3 m (1ft) from center of a v-shaped median. It was determined that suspension on the mid-sized vehicles tended to be fully compressed due to dynamic forces imposed by the terrain, speed and angle when the vehicle starts up the slope on the opposite side of the median. These conditions are likely to place the nose of the vehicle below the lowest cable and hence allow underride of the barrier. The sloped-front end designs of many vehicles also contribute to this problem. Variations in the specific suspension on a vehicle, its

loading, steering input, and stiffness of the median surface would also influence the propensity to underride the barrier. Based on the results from this study, several retrofit designs were developed. These retrofit designs were divided into two groups based on the need for further testing and analysis.

In 2010, Mohan et al, published a paper detailing finite element modeling and validation of 3-strand cable system. In this paper, computationally efficient and accurate models of the soil, posts, cable, hook bolts etc. was modeled and were used in full scale simulations as well. The results were compared with physical crash tests for validation and subsequent improvements in the models were made to make it suitable for future use in full scale barrier evaluation simulations.

In 2010, Fang et al. submitted a report to the North Carolina Department of Transportation titled “Finite Element Evaluation of Two Retrofit Options to Enhance the Performance of the Cable median Barriers”. This report summarizes the finite element modeling and simulation efforts on evaluating the performance of cable median barriers including the current and several proposed retrofit designs. The first option experimented with changing of the cable heights for the current design and it was found out that cable heights affect cable-vehicle interactions to a great extent. The first option consisted of five designs which did not necessarily perform better than current cable median design in front and back side simulations. Based on the results of the first retrofit option, a new retrofit option called “sixth design retrofit” was made and it was found that this design works for both front side and back side impacts rather well. A second retrofit option consisted of adding a fourth cable to the current design. This second option had two designs based on the height of the fourth cable. It was found that the second option had the same performance for the front side impacts as the current design,

however, it had an improved performance for the back side impacts. The important conclusions drawn from these experiments is that by using the two retrofit design options, the performance of the cable barrier system would be improved in the back side impacts without sacrificing its performance for the front side impact.

In 2011, C. S. Stolle et al developed a nonlinear finite element model of the 19mm cable. Prior to this, wire rope FE models were created based on the discretion of the researcher as component testing of wire rope was not available to validate material properties. To validate the model, quasi static tension tests, cantilever bending test and high speed jerk tests and perpendicular impact tests were conducted. The Belytshcko-Schwer resultant beam elements and the moment-curvature material model were chosen for the FE model because of good agreement between physical testing and simulations. A mesh sensitivity analysis was carried out to find out the optimum mesh size. It was found that optimum computational efficiency and accuracy was obtained for element length between 10-15mm. The new model was found to be significantly more accurate than previous model. Full scale simulations were performed using the new wire rope FE model and results were compared to physical tests, which agreed well.

In 2012, Bielenberg, Stolle and Reid submitted a report to the Midwest states regional pooled fund program. In this report, computer simulations were performed to analyze and evaluate a new cable to post attachment for high tension cable barriers. This model of the attachment, replicates the currently used keyway bolt. Using a solid element model of a rod with ASTM A449 material properties, a beam element model of the keyway bolt was generated and validated against the component tests. A numerical simulation of a bogie test was performed for the same. It was shown that

usage of solid element for keyway bolt was impractical for full scale simulations and that the beam model was computationally efficient.

In 2012, Fang et al. submitted a report to the North Carolina Department of Transportation titled “Recommendations for Placement of Cable Median Barriers on 6:1 and 4:1 Sloped Medians with Horizontal Curvatures”. This report summarizes the research efforts of using finite element modeling and simulations to evaluate the performance of generic low tension cable median barriers (CMBs) on four-lane and six-lane freeways with a 46-foot median, horizontal curvature, and 6:1 and 4:1 median slopes. Some of the important findings from this project were, the horizontal curvature affected the CMB performance because of the difference in departure and impact angles of the vehicles. The current NCDOT design was effective in retaining small car within the median for most of the cases, however the system unperformed for the truck in back side impacts. A retrofit CMB design was also incorporated in this study showing that performance of this design was only marginally better than the current CMB design. One of the major conclusions from this study was in regards to the CMB placement on 4:1 slope 6 lane highway. It was found that in this particular configuration, the CMB performed worst for front and back side impacts by the truck.

In 2013, Wang et al. conducted a study about using beam elements for representing slender members like hook bolts and cables used in cable median barriers. Solid and shell elements models were also developed for comparison with the beam models. To verify the quality of the beam-element model, numerical simulations of hook bolt pullout tests were performed under quasi-static and dynamic loading conditions. It was observed that solid models were very accurate, however they also 15-20 times more expensive than beam elements. The shell models were inaccurate in

the presence of edge contacts and required an expensive contact routine (automatic general interior contact) to get results comparable to that of the beam elements. It was also found that beam elements with 12 to 18 elements were reasonably accurate and inexpensive compared to solid models and shell models. Overall, the beam models provided stable, accurate and cheaper option for slender members such as cables and hook bolts in crash simulations. A full scale crash simulation using beams for cables and hook bolts was performed and showed a 19.2% increase in efficiency in comparison to use of shell model.

1.3 Use of tires in crash attenuation devices

In 1972, Brooks Walker got a patent (US3661359) titled “Energy absorber”. This device uses automotive tires along with a rim as a crash attenuation device. An individual tire is fixed to the rigid barrier in such a way that the axis of revolution of the tire is perpendicular to the direction of impact. Holes are made on the top surface of the tire and water is filled inside the tire and then the holes are plugged back in by inexpensive plugs. The tire and rim together seal the water inside the tire. A plurality of such tires are attached with each other to form a continuous barrier. On impact, the rim deforms and the water is pushed out of the orifices thus absorbing the brunt of the crash and dissipating energy.

In 1974, Merton Way and John Pas got a patent (US3848853) titled “Highway safety tire device”. This device utilizes discarded automobile tires arranged on top of each other with their sidewalls facing each other to make a cylindrical shaped barrier. The tires are fastened to each other by means of long bolts or individual bolts. A minimum of three tires must be used to form this vertical barrier. The inner side of this cylindrical barrier is to be filled with a filler material like soil. This device is to be used

at select locations on the highway to act as safety device, warning or barricade to protect an automobile or its occupants from injury.

In 1974, Clarence Vincent filed for a patent (US4090694A) titled “Go-cart guard rail”. This system comprises used automobile tires lined up along the inner and outer curvature of the race track. The tires are lined up with their treads facing each other form a continuous, ribbon-like flexible barrier. Each tire is individually attached to a stationary anchor by bolts. On the opposite side of the anchor, the tire tread is attached to the impact rail by bolts. The advantage of this system is that after the vehicle impacts this barrier, the tires are not displaced from their original position and remain in the same position for next possible impact without any manual intervention. This arrangement saves time and man-hours which would have otherwise been wasted in repositioning the impacted tires.

In 1976, Leland Yoho filed a patent (US4066244) titled “Vehicular energy absorber”. This barrier system utilizes waste tires to form a barrier around a specific traffic hazard. The unique feature of this barrier system is its design simplicity and effectiveness. The barrier consists of minimum two rows of tires arranged tread to tread perpendicular to the anticipated direction of impact. Between each of these rows, a pair of tires are placed to form another row of equi-spaced tires arranged with their sidewalls facing each other. All the tires are tied to each other by fasteners and the row nearest to the hazard is tied to vertical posts or stanchions. The height of the barrier is kept constant throughout. Excessive vertical movement of the barrier upon impact is prevented by the stanchions. This barrier dissipates impact energy efficiently and is very cost effective.

In 1993, Danial Moon got a patent (US5238228) titled “impact absorbing barrier and the method of constructing same”. This patent describes the use of tires as impact attenuation devices. The inventor has various sizes of the tires cut up in half along the radial direction. Then these tires are stacked inside each other and glued on top of each other, sidewalls facing each other. The tires are then tied up with bands and covered with a shield. This forms a single unit of the barrier. Provision has been made such that multiple units can be interlinked to form a chain and a continuous barrier can be formed.

In 1996, Normand Bernaquez and Ivan Sabourin received a patent (US5480255) titled “Impact- absorbing barriers for highways”. This barrier system comprises of recycled tires arranged in specific order to form a low cost crash attenuation device. This system mainly consists of inner and outer wall made of tires. The inner wall is made up of half-tires (here half-tire refers to a tire cut in half along the tread such that it has a half toroidal shape) and the outer wall is made up of full tires. First the half-tire layer is laid on the ground and a dense filler material like sand is poured into the tire. Then a new layer of half-tires is arranged on top of the pre-filled layer facing upwards and sand is filled. This cycle is continued to build an inner wall consisting of sand filled half-tires up to the required height. Then an outer layer wall is constructed by arranging tires on top of each other where the tire treads face each other. Tie-bands are to be used to secure the tires and half-tires to each other. The inventors foresee the use of this barrier system on highways, river embankments and in mountainous regions to halt avalanches and rock-falls.

In 1997, Henry Yunick got a patent (US5645368) titled “Race Track with novel crash barrier and method”. In this method a novel crash barrier consisting of the use of

tires to attenuate the crash forces has been described. The invention talks about a crash barrier in which, the tires are stacked on top of each other in a total of 4 layers such that their sidewalls are touching each other. Retainers have been used to hold the tires in place and the tires themselves have been arranged in a zigzag manner like a brickwork for better interlocking. On impact, this barrier deflects inwards and slows down the race car incrementally in such a way that the crash forces and total energy are dissipated in a systematic way and the vehicle remains clear of the other vehicles coming from behind.

In 2001, Rick Kramer filed for a patent (US20030081997 A1) titled “Vehicle crash wall”. In this patent, a new crash barrier to be used for race tracks (primarily NASCAR) and public highways has been described. This device utilizes a new arrangement of the steel impact plate along with metal sleeve. A filler material consisting of tires is used for shock absorption and dissipation. The tires are grouped into an arbitrary number and bolted to each other to restrict their degree of freedom. A cover has been provided to the barrier to make it aesthetic and restrict the debris. The said semi flexible barrier is primarily to be used instead of conventional rigid barriers and thus will cause less damage to the vehicle, driver and the barrier itself.

In 2003, Reinhard Diem got a patent (US6505993B1) titled “Method and device for braking vehicles”. In this method, a novel device crash barrier has been described. This barrier is to be used on race tracks in areas with high probabilities of accidents. The barrier consists of tires attached with each other by means of elastic bands. According to the inventor, the length and height of the barrier should be proportional to the weight of the vehicle being raced. The tires at the end of the barrier section are

tied to a fixed post. The retaining wall has enough room for the oncoming vehicle and guarantees soft and linear deceleration of the vehicle.

In 2005, Alex Talbott filed a patent (US20050236609) titled “Tire fence”. In this patent, a novel tire barrier has been described which can be used as median barrier on highways. The tires are always arranged in stacks 3 or 4 level high on top of each other, sidewalls facing each other. They are connected to each other by binding rods which serve dual purpose of restricting degree of freedom of the tires and eliminating water accumulation in the tire. The entire barrier section can be arranged in various shapes. The maintainability and cost effectiveness are considered while designing this barrier.

The current research related to cable median barriers suggest that these barriers are effective in preventing cross-median crashes in most cases. However, for certain cases involving high median gradients and smaller vehicles, penetration has been observed. The smaller vehicles tend to underride or penetrate the cables easily owing to a smaller ride height. Thus, continuous research is being carried out to prevent the penetration of cable median barriers. Research efforts have focused on creating new designs by changing cable heights and cable to post attachments. Median barrier placements for sloped medians have also been studied to find out the optimum location for installation. This work is an attempt at creating a retrofit design utilizing reclaimed tires combined with the cable median barriers. As a proven cost effective tool, finite element simulations were chosen as preferred method to find out a good retrofit design. The following chapters provide detailed report in the use of finite element method to evaluate the tire-cable median barrier designs. Chapter 2 provides a theoretical explanation of the contact methods used in this research. Chapter 3 provides a detailed

description of finite element models and simulation setups used in this research. Chapter 4 gives a comprehensive report on the simulation results obtained and Chapter 5 provides a detailed comparison between the tire-cable median barriers and current existing cable median barriers in order to evaluate formers performance. Finally Chapter 6 gives the conclusion for this work along with recommendations for future work.

CHAPTER 2 : CONTACT THEORY

In this research, finite element (FE) analysis has been used to solve for nonlinear dynamic problems of vehicular crashes. This makes the problem a non-continuum mechanics problem and needs special FE algorithms to solve it. The effectiveness of an FE solutions depends on the handling of the contact algorithms. Contact is defined by two separate objects interfering with each other (e.g. vehicle impacting a post) or a single object touching itself (e.g. crushing of highly deformable materials). The FE contact algorithm should be able to detect both of these cases and ensure that the same physical space is not being occupied by two different entities at a given time. There are different contact handling algorithms used in LS DYNA to solve this problem. Each method has its own advantages and disadvantages in terms of accuracy, computational cost, and complexity. Among the three methods described below, penalty method has been used to handle the contact problem in this research.

An interface in LS-DYNA is defined as the point at which two distinct objects interact. The objects are meshed with either triangular or quadrilateral elements or a combination of both. At the interaction, one side is designated as the slave side and the other is the master side. The nodes lying on the slave side are called slave nodes and those on the master side are called master nodes. An interface can also be defined in three dimensions by listing in arbitrary order, all triangular and quadrilateral segments, which comprise each side of the point of contact (interface). Treatment of sliding and impact along these interfaces is an important capability of LS-DYNA.

2.1 Methods for handling sliding and impact along interfaces

LS-DYNA uses three distinct methods for handling sliding and impact along interfaces. These methods are listed below.

- Kinematic constraint method
- Distributed parameter method
- Penalty method

2.1.1 Kinematic constraint method

This method uses the impact and release conditions of Hughes et al., [1976]. The problem with this method is that when the master surface mesh is finer than slave mesh, the master nodes can penetrate through the slave surface and create kinks in the slide line. A slide line in this case refers to the contact zone (Ibrahimbegovic 2006). During high velocity impact analysis, the kinetic energy between the impacting objects might give rise to high interface pressures. In such cases, using one point integration or more quadrature points for integration of the elements cannot prevent formations of the kinks. Hence, this method was not used in the thesis.

2.1.2 Distributed parameter method

In the distributed parameter formulation, one half of the slave element mass of each element in contact is distributed to the covered master surface area. Also, the internal stresses in each element determines a pressure distribution for the master surface area that receives the mass. After the distribution of mass and pressure is completed, the acceleration of the master surface is updated. Then, constraints are imposed on the slave node accelerations and velocities to insure their movement along the master surface. In this method, the slave nodes are not allowed to penetrate the master surface so the need to calculate the penetration distance and the corresponding

contact force is eliminated. This method has not been used in this research as no further improvements were made to this algorithm for a very long time and thus it may not be able to handle the complex geometry and the need for specialized contact handling requirement of this research.

2.1.3 Penalty method

The commonly used contact formulations in LS-DYNA are the penalty method and the Lagrange multiplier method. The Lagrange multiplier method has high accuracy but it involves handling unknowns in the form of Lagrange multipliers (Kikuchi and Oden 1988). This is the reason for the high computational cost for this method. The penalty method, is simpler and less computationally expensive in comparison to the Lagrange multiplier method. In addition to this, the penalty method has the flexibility to be used in both implicit and explicit analyses. In this chapter, three formulations of the penalty methods and their associated contact algorithms in LS-DYNA are discussed.

The penalty method was developed to solve contact problems in numerical methods. The main advantage of this method is that it can be implemented in a comparatively easy manner to other contact algorithms and the convergence rate (speed at which a solution is reached) for the method is also good. The solution accuracy of the penalty method is sufficient for many engineering applications. An important parameter in the penalty approach is the calculation of the contact stiffness. Currently, there are three formulations for the calculation of contact stiffness.

2.1.3.1 Standard penalty formulation

In this method, contact treatment is internally represented by linear springs between the slave nodes and the nearest master segments. Imaginary springs are placed between two offending surfaces and the forces in the spring are calculated based on the amount of penetration. The stiffness of this imaginary spring is called the contact stiffness. When there is a penetration between two surfaces, the contact force is calculated such that it redirects the penetrating nodes away from the surface it penetrates. In the standard penalty formulation, the contact stiffness is calculated using material constants and geometry of the discretized surface. If the two materials in contact have the same material properties (i.e. bulk modulus), this method gives very efficient results for the treatment of such contact problems. Another advantage of this method is that the contact stiffness is not affected by the time step size because in this case, the penetration of individual nodes or segments on the slave surface through the master surface is checked at each time step.

The contact force F^c is calculated by

$$F^c = kD \tag{2.1}$$

Where k is the contact stiffness and D is the depth of penetration. Distinct geometrical elements lead to various contact stiffness formulations. For shell elements, the contact stiffness is defined by

$$k = \frac{SKA}{\left(\text{Maximum shell diagonal length}\right)} \tag{2.2}$$

Where S is the stiffness scale factor, K is the bulk modulus of the material, and A is the area of the shell element. For solid elements, the contact stiffness is defined by

$$k = \frac{SKA^2}{V} \tag{2.3}$$

Where V is the volume of the solid element.

When the contact forces between the slave and master segments are calculated and distributed to individual nodes, the force vector is inserted into the equation of motion given by

$$M\ddot{d}(t) + F^{\text{int}}\left(d(t)\right) + F^{c}\left(d(t)\right) = F^{ext}(t) \tag{2.4}$$

Where M is the mass matrix, $d(t)$ is the displacement vector, $\ddot{d}(t)$ is the acceleration vector, F^{int} is the internal force vector, F^{c} is the contact force vector and F^{ext} is the external force vector.

2.1.3.2 Soft constraint formulation

Many times, there is contact between two materials whose stiffness varies greatly (e.g., soft foam and structural steel components). The soft materials have an undesirable effect on the contact stiffness value, they lower it and cause excessive penetration. To tackle this problem, the soft constraint penalty formulation is used. This formulation is best suited to handle the local interactions between bodies of dissimilar materials in contact. The soft constraint formulation uses a different formulation for the contact stiffness. This is done by calculating an additional stiffness based on the stability criterion (Courant's criterion). This additional stiffness is then added to the master and slave contact stiffness. The soft constraint contact stiffness is defined by

$$k = 0.5 S_{sc} m^{*} \left(\frac{1}{\Delta t_c} \right) \tag{2.5}$$

Where S_{sc} is the scale factor for the soft-constraint penalty formulation, m^{*} is a function of the masses of the slave nodes and master nodes and Δt_c is the current time step. The

soft constraint contact stiffness is compared to the values calculated from the standard penalty formulation and the maximum amongst the two is selected for calculating the contact force.

2.1.3.3 Segment based formulation

This formulation will check the penetration of the slave segment with the master segment instead of checking the slave nodes penetration with the master segment. This method is usually used for contact geometries where penalty based contact formulations will fail to prevent penetration (complicated geometries). The segment based formulation has the advantage in solving complex contact problems such as those involving edge-to-edge and surface-to-surface interactions. An advantageous feature of this formulation is that contact stiffness is calculated using the actual time step. The time step is updated if the solution time step grows 5% larger than initial time step. This allows the time increment to remain constant in most cases, even if the solution time step grows slightly. The penalty stiffness in the segment based formulation is given by

$$k_{cs} = 0.5 S_{sg} \left(S_{fs} \text{ or } S_{fm} \right) \left(\frac{m_1 m_2}{m_1 + m_2} \right) \left(\frac{1}{\Delta t_c} \right) \tag{2.6}$$

Where S_{sg}, S_{fs} and S_{fm} are the scale factors for the sliding interface penalty, the default slave penalty, and the default master stiffness penalty, respectively. Δt_c is the current time step, m_1 and m_2 are the masses of the slave and master segment, respectively. For shell elements, the segment mass is equal to the element mass. For solid elements, the segment mass is equal to the half of the solid element mass. In the segment based method, the initial penetration depths are not only eliminated but are also stored as a

baseline to calculate additional penetration depth which produces contact forces given by

$$F^c = k(\mathrm{d} - \mathrm{d}_i) \tag{2.7}$$

Where F^c is the contact force, d is the current penetration depth, and d_i is the initial penetration depth.

2.2 Contact modeling in LS-DYNA

LS-DYNA has a number of contact algorithms that can be selected based on material properties of the parts in contact, geometry etc. The contact algorithm types are classified as follows:

- One-way treatment
- Two-way treatment
- Single surface
- Tied contact
- Contact entity

In LS-DYNA, a contact can be defined by using parts, segments, or nodes to check for penetrations on the master surface using the slave nodes/segments. The penetration is checked at each time step regardless of which contact formulation is used. If a penetration is detected, the contact force necessary to separate the slave node/segment from the master segment is calculated and applied. In order to provide a stable and robust contact model, certain parameters are provided by LS-DYNA which control various aspects of the contact treatments. These parameters include static and dynamic friction coefficients between master and slave segments, optional thickness for slave and master surface which overrides true thickness etc. Apart from the above mentioned contact treatments, there are some automatic contact options, which provide better suited contact treatment for many large deformation engineering problems.

2.2.1 One-way contact treatment

The “one-way” term in one way contact is used to indicate that only the user-specified slave nodes are checked for penetration on the master segments. These contacts may be appropriate when the master side is a rigid body (e.g. the road in crash simulations). Also, one more instance in which this contact type can be used is when the slave part has fine mesh and the master has a relatively coarser mesh. One-way contact types allows for compression loads to be transferred between slave and master segments. If relative sliding occurs between the two offending surfaces, tangential loads can also be transmitted if contact friction is active. A coulomb friction formulation is used with an exponential interpolation function to allow for transition from static to dynamic friction. This requires that the decay coefficient be defined and the static friction coefficient be larger than the dynamic friction coefficient. The coefficient of friction is calculated by the following equation (2.8).

$$\mu = \mu_d + (\mu_s - \mu_d)\,\mathrm{e}^{-c|v|} \tag{2.8}$$

Where, μ is the coefficient of friction, μ_d and μ_s are the dynamic and static coefficient of friction respectively, c is the decay constant and v is the relative velocity between slave node and master segment.

Other applications of the one-way contact type are in beam-to-surface or shell-edge-to-surface interactions, wherein, the beam nodes or shell edge nodes are defined in the slave node set.

One of the most common one way contact treatment is nodes-to-surface contact where each slave node is checked for penetration against the master surface. As mentioned above, nodes-to-surface contact is suitable when the master surface is a rigid

body or the slave surface is a deformable body, which has a relatively fine mesh compared to the master surface. In this research, the automatic nodes to surface contact has been used to define contact between the master (road) and the slave (barrier tires, cables, and posts). Figure 2.1 shows nodes to surface contact.

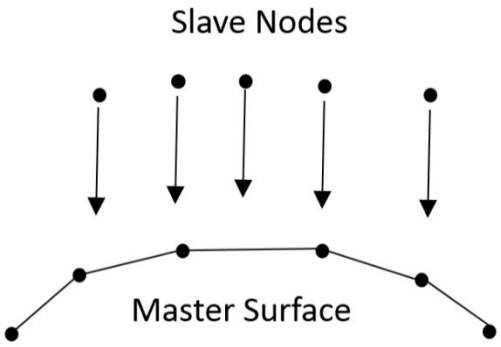

Figure 2.1: Nodes to surface contact.

Another contact categorized as a one-way contact is the one-way surface-to-surface contact as represented by Figure 2.2. In the nodes-to-surface contact, the slave nodes are represented by discrete points and only they are checked for penetration against a master surface. This method is similar to the nodes-to-surface contact, however, the main difference is that unlike nodes-to-surface contact, only the slave nodes whose normal vectors are oriented towards the master surface are checked for penetration. In these one-way contact types, the slave and master surfaces should be carefully and strategically selected so as to make the most out of this computationally efficient contact type. A complete list of one-way contacts is as follows:

- CONTACT_AUTOMATIC_NODES_TO_SURFACE
- CONTACT_ONE_WAY_SURFACE_TO_SURFACE
- CONTACT_AUTOMATIC_ONE_WAY_SURFACE_TO_SURFACE
- CONTACT_FORMING_NODES_TO_SURFACE
- CONTACT_FORMING_ONE_WAY_SURFACE_TO_SURFACE

- CONTACT_CONSTRAINT_NODES_TO_SURFACE
- CONTACT_ERODING_NODES_TO_SURFACE
- CONTACT_RIGID_NODES_RIGID_BODY
- CONTACT_RIGID_BODY_ONE_WAY_TO_RIGID_BODY

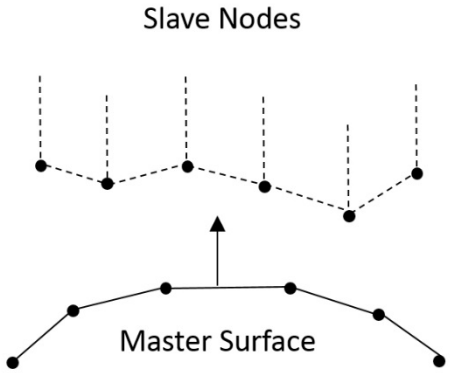

Figure 2.2: One way surface to surface contact.

2.2.2 Two-way contact treatment

In two-way contact treatment, the slave nodes are checked for penetration against the master surface similar to the one way treatment. Then a second subroutine is added to check the master nodes against the slave segments. The advantage of this treatment is that it removes the process of careful selection of master and slave segments since contact is checked in both directions. The downfall of this method is that it requires almost double the computational time compared to one-way contact treatments. However, this increase in time becomes a necessity when dealing with complex geometries, large deformations, and unpredictable deforming parts. A popular contact that belongs to the two-way contact treatment is the surface-to-surface contact shown in Figure 2.3.

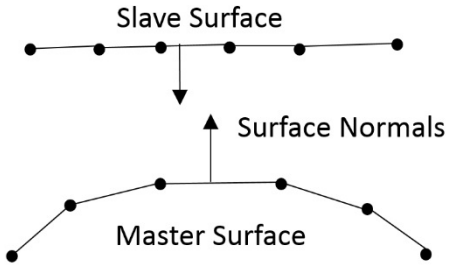

Figure 2.3: Surface to surface contact.

LS-DYNA has an automatic surface-to-surface contact as well. This has been used to define contact between the master (road) and slave (car tires and some external sheet metal parts). The difference between the two is that the automatic option gives the software freedom to assign the parts as slave and master automatically and their tasks can be changed from time step to time step. A complete list of two-way contacts is as follows

- CONTACT_SURFACE_TO_SURFACE
- CONTACT_AUTOMATIC_SURFACE_TO_SURFACE
- CONTACT_FORMING_SURFACE_TO_SURFACE
- CONTACT_FORMING_TWO_WAY_NODES_TO_SURFACE
- CONTACT_CONSTRAINT_SURFACE_TO_SURFACE
- CONTACT_ERODING_SURFACE_TO_SURFACE
- CONTACT_RIGID_BODY_TWO_WAY_TO_RIGID_BODY

2.2.3 Single surface contact

These contact types are the most widely used in LS-DYNA, especially for crashworthiness applications. The unique feature of this contact type is that all parts are defined in a single set and penetrations are checked among all the parts, including self-penetrations. This renders the definition of a master set unnecessary. This contact is efficient and dependable if defined properly. Among the popular contacts in the single

surface contact types, automatic single surface shown in Figure 2.4 and automatic general contact are widely used. The automatic-single-surface contact implements a segment-based penalty formulation in which, segments, instead of nodes, are used to check for penetrations through other segments. The main feature of the general contact type is that, shell edge-to-edge and beam-to-beam contacts are treated automatically. All free edges of shell and beam elements are checked for contact with other free edges and beams. A variation of automatic general contact, automatic general interior shown in Figure 2.5, can also detect interior edge penetrations. However, it tends to be very expensive.

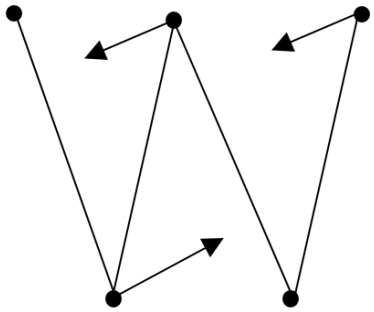

Figure 2.4: Automatic single surface contact (self-contact checking).

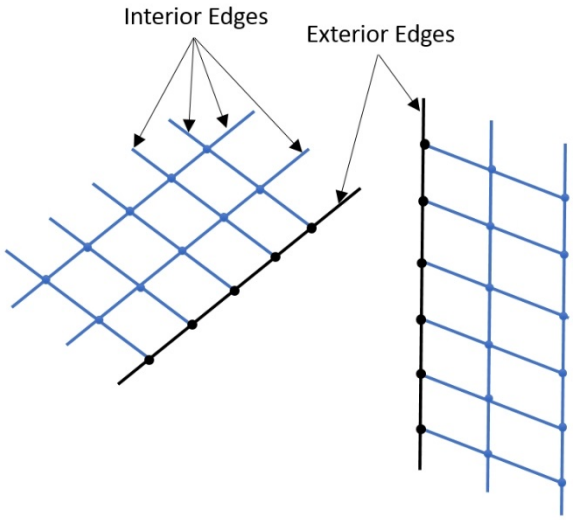

Figure 2.5: Automatic general interior (external and internal edge check).

2.2.4 Tied contact

In tied contact types, the slave nodes are constrained to move with the master surface. At the beginning of the simulation, the nearest master segment is located for each slave node based on an orthogonal projection of that slave node to the master segment. There is a preset criteria to determine if the slave node is close enough to the master segment and when this criteria is met, the slave node is moved to the master surface. This allows for initial geometry to be modified without invoking any stresses. It is helpful to define tied contacts by a set of nodes or segments rather than as a set of part Ids because this gives user more control over what gets tied to what and can prevent unintentional constraints. As the simulation progresses, kinematic constraint equations are used to hold the isoparametric position of the slave nodes with respect to its master surface. Tied contacts are generally used only with solid elements since the rotational degrees of freedom of the slave nodes are not constrained. If this contact is used for shell elements, it may produce unrealistically soft behavior. Tied contacts can be one-

way tied (i.e. only slave nodes are tied to the master surface) or two-way tied (slave nodes are tied to the master surface and vice versa). Tied contacts have translational degree of freedom and can have rotational degree of freedom for the slave nodes as well. A failure criteria can also be preset with this contact and an offset can also be defined. Figure 2.6 and Figure 2.7 show tied contact schematic for one way tied and two way tied algorithms respectively.

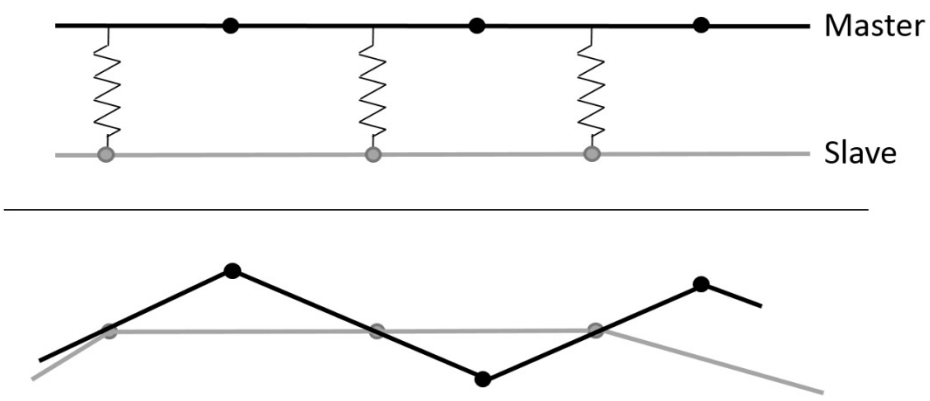

Figure 2.6: One-way tied interface schematic (Suri Bala – d3view.com).

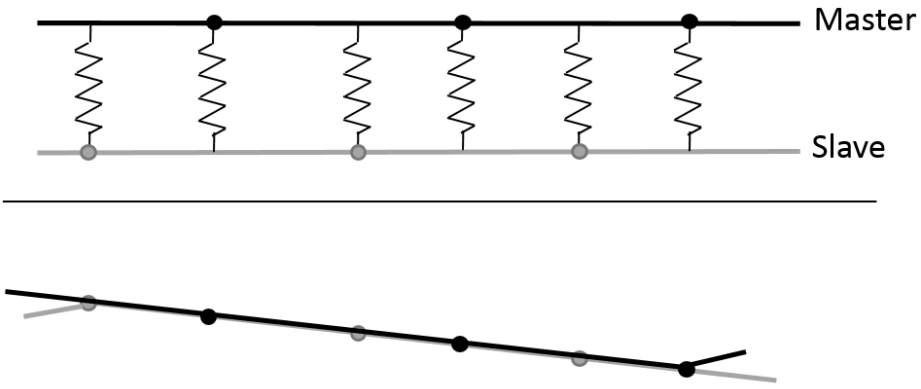

Figure 2.7: Two-way tied interface schematic (Suri Bala – d3view.com).

2.2.5 Contact entity

This contact type is used for treating deformable nodes against rigid geometric surfaces. The analytical equations defining the geometry of the surface are used in the contact calculations. So instead of a regular segmented (meshed) surface, only a regular geometric shaped entity is used. A penalty based approach is used in calculating the forces that resist penetration. This contact is used to couple LS-DYNA with rigid body dummies having surfaces approximated by nice geometric shapes such as ellipsoids (e.g. Head). An automatic mesh is generated using a mesher to aid in visualizing the results however, this mesh is not used in the contact calculations. Some examples of the analytical rigid surfaces are as follows:

- Flat
- Sphere
- Cylinder
- Hyper-ellipsoid
- Torus
- Load curve defining the line
- CAL3D/MADYMO plane
- CAL3D/MADYMO ellipsoid
- VDA surface (read from a file)
- IGES surface (read from a file)

Figure 2.8 shows some of the analytical models that are used as contact entities.

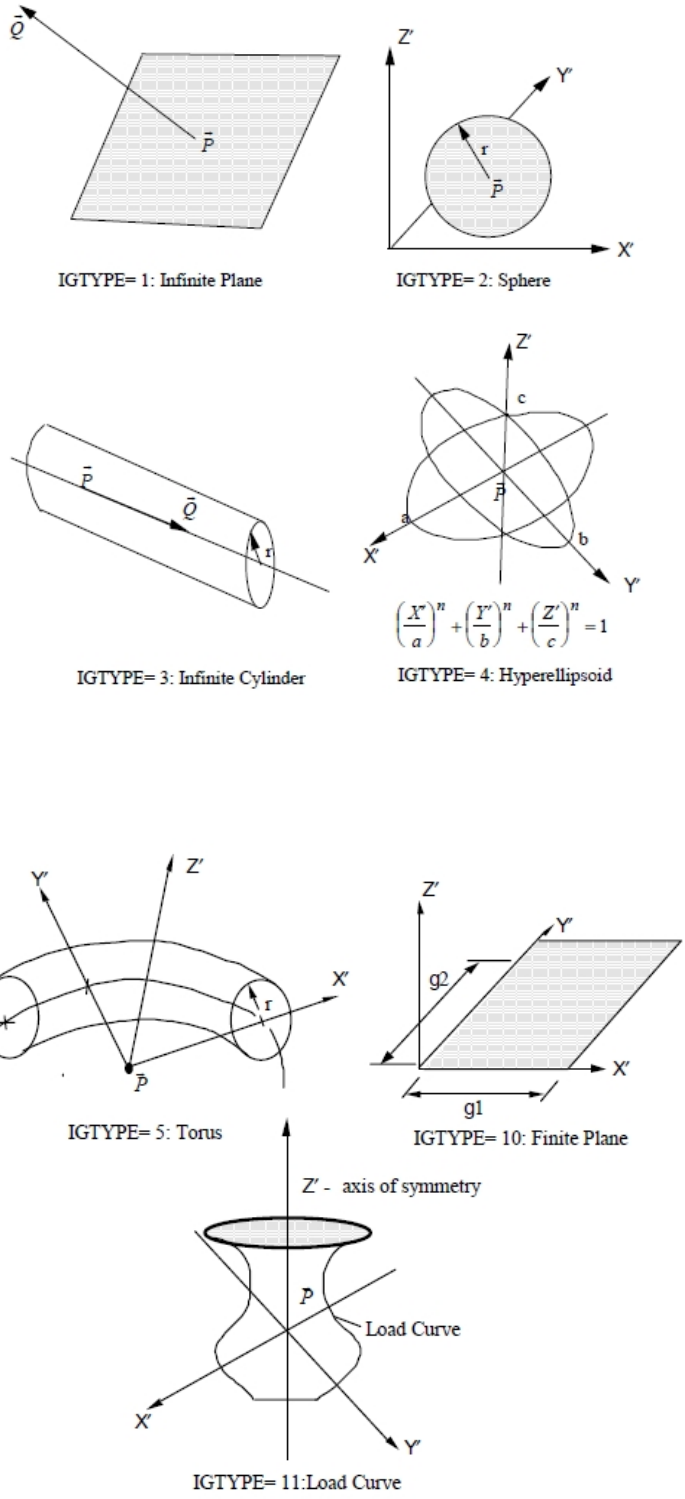

Figure 2.8: Contact entities (LS-DYNA keyword user's manual).

CHAPTER 3 : FINITE ELEMENT MODELING OF VEHICLES AND CABLE BARRIERS

The objective of this research was to design and evaluate the performance of retrofit options of cable median barrier utilizing reclaimed tires. The barrier was to be evaluated according to the MASH TL-3 conditions. There were four proposed barrier design variants. The barriers were evaluated on flat median and the best design was also evaluated on sloped median.

The simulation work outlined in Table 3.1, Table 3.2 and Table 3.3 includes two vehicle models, a 1996 Dodge Neon and a 2006 Ford F250 truck along with the tire-cable median barrier models. Initially all the simulations were performed on Dodge Neon and later same cases were run for the Ford truck. The FE models of the sedan and the truck were obtained from the National Crash Analysis Center (NCAC) and modified to correct modeling issues. The barrier model was developed in house and tires were appended to it for the purpose of this study. Crash simulations were performed under MASH TL-3 conditions. MASH TL-3 conditions include a passenger car between 2,365 and 2,475 lbs. (1,075 and 1,125 kg) or a pickup truck between 4,890 and 5,110 lbs. (2,220 and 2,320 kg). The test conditions were a vehicle speed of 62.1 mph (100 km/h) and an impact angle of 25 degrees.

3.1 FE models of testing vehicles

3.1.1 1996 Dodge Neon

The FE model of 1996 Dodge Neon contains a total of 339 parts that were discretized into 283,683 nodes and 270,953 elements (2,852 solid, 92 beam, 267,775

shell, and 234 other elements). Ten different constitutive models were used including the piecewise linear plasticity model defined for most steel components, the elastic model for the tires and a few other components, the viscous damping model for the shock absorbers, the low-density foam model for the radiator core, the spot-weld model for sheet metal connections, the Blatz-Ko rubber model for nearly incompressible rubber cushions, the rigid model for most mounting hardware, and the null material model defined for contact purposes. Hourglass control was used on various components that could potentially experience large deformations. The FE model of Dodge Neon was originally developed at NCAC and validated with the National Highway Traffic Safety Administration (NHTSA)'s Frontal New Car Assessment Program (NCAP) tests. The Dodge Neon model is shown in Figure 3.1 and its specifications are as follows:

- Curb weight: 2414 lbs. (1095 kg)
- Overall length: 171.8 in (4.36 m)
- Overall width: 67.5 in (1.71 m)
- Overall height: 52.8 in (1.34 m)
- Ground clearance: 5.7 in (145 mm)

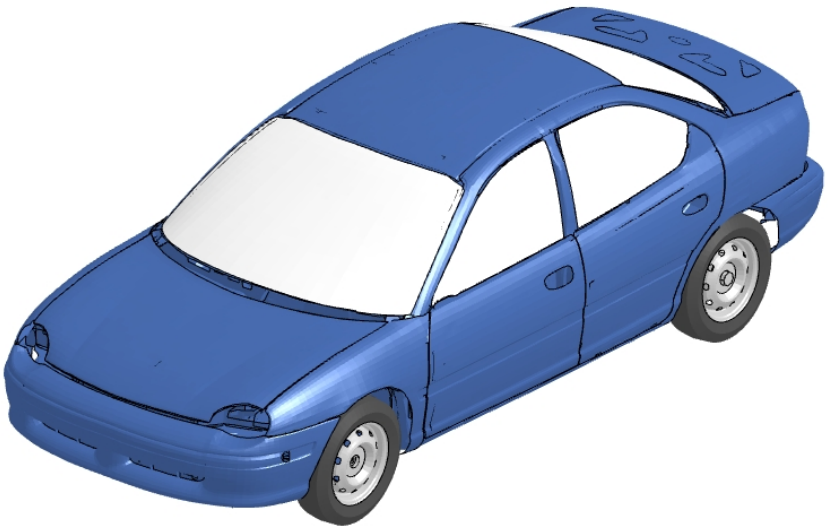

Figure 3.1: FE model of Dodge Neon.

3.1.2 2006 Ford F250

The FE model of the 2006 Ford F250 contains a total of 746 parts that were discretized into 737,986 nodes and 736,096 elements (25,905 solid, 2,305 beam, 707,656 shell, and 230 other elements). Eleven different constitutive models were used including the piecewise linear plasticity model defined for most steel components, the linear and nonlinear elastic spring model for the suspension springs, the viscous damping model for the shock absorbers, the low-density foam model for the radiator core, the spot-weld model for sheet metal connections, the visco-elastic model for rubber cushions, and the null material model defined for contact purposes. Hourglass control was used on various components that could potentially experience large deformations. The FE model of Ford F250 was originally developed at NCAC and validated with the National Highway Traffic Safety Administration (NHTSA)'s Frontal New Car Assessment Program (NCAP) tests. The Dodge Neon is within the acceptable

range of mass for MASH TL-3, while the Ford F250 is slightly higher. The Ford F250 model is shown in Figure 3.2 and its specifications are as follows:

- Curb weight: 5690 lbs. (2581 kg)
- Overall length: 226.4 in (5.75 m)
- Overall width: 79.9 in (2.03 m)
- Overall height: 76.5 in (1.94 m)
- Ground clearance: 8.3 in (211 mm)

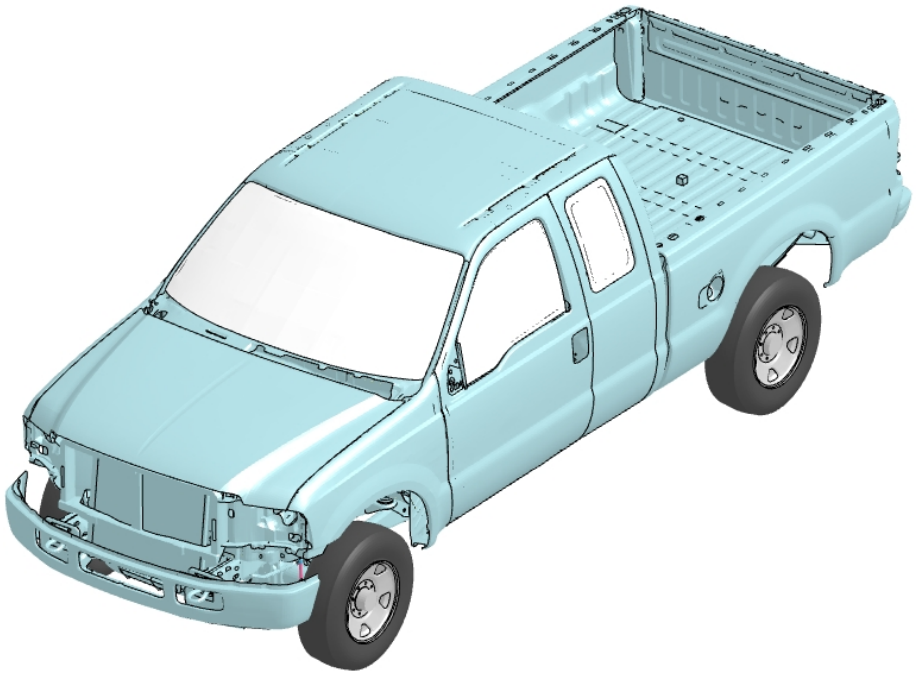

Figure 3.2: FE model of Ford F250.

3.2 FE model of the barrier tire

The tire modeled for the tire-cable median barrier is a Chevrolet Silverado tire. The tire nomenclature is P245/70R17. This means that the tire has a sidewall width of 245 mm and an aspect ratio of 70. This tire is made to fit a 17 inch wheel. The original tire model was composed of two separate part numbers for the tread and the sidewall. This tire was remeshed as a single part and the mesh size was in the range of 12-15 mm.

The tire has been modeled as a simplified tire using only 2D shell elements and elastic material. It contains 4380 shell elements. The density of tire is 2.272e-009 tonne/m^3, modulus of elasticity is 3000 tonne/m^2 and the poisson's ratio is 0.45. These properties were taken from the Chevrolet Silverado FE model developed at the Center for Collision Safety and Analysis (CCSA). The thickness of the shells has been kept uniform at 7.5 mm and the mass of the tire is 35 lb. A detailed model of the tire was not computationally feasible because of the size of simulations and limited resources. The Silverado tire is shown in Figure 3.3

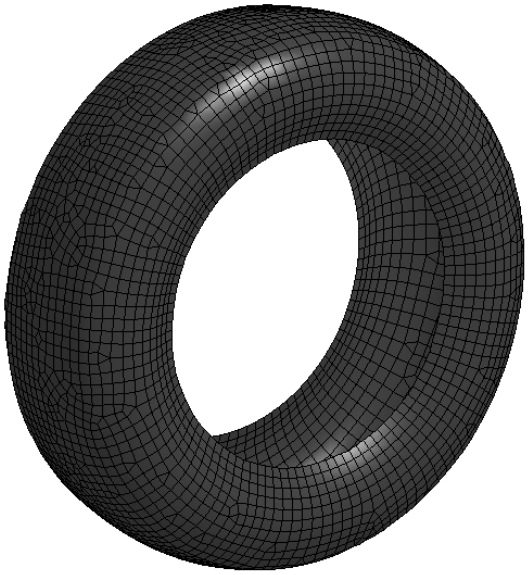

Figure 3.3: FE model of barrier tire.

3.3 FE models of the retrofit median barriers

The tire-cable median barrier FE models were made using the current design cable median barrier FE model from NCDOT RP2017-13 as the base model. It contains 1054260 nodes, 6689 beams, 817147 shells and 197612 solids. This model is an approximately 400 foot section of the barrier which consists of 27 posts spaced at a

distance of 16 feet between each other. Terminals have been modeled to anchor the cables and provide tension via turnbuckles. The material models used include elastic for the tires and cables, Piecewise linear plasticity for hook bolts, post web and flange, CSCM for concrete block, soil and foam failure for the soil and MAT_NULL for null shell around the soil.

The tires are attached to the barrier having two cables on one side and is called the front side while the side with just one cable is called as the back side for a flat median. Figure 3.5 shows the front and back side of the barrier for a flat median. The tire outer diameter is 768 mm and is attached to the cable by rigid nodal bodies. Figure 3.4 shows attachment of the barrier tire to the cables by rigid nodal bodies. Between two posts, there are a total of six tires placed equidistant from each other. A realistic model of the concrete block embedded in the soil has been modeled so that the concrete block pullout, if any, can be observed.

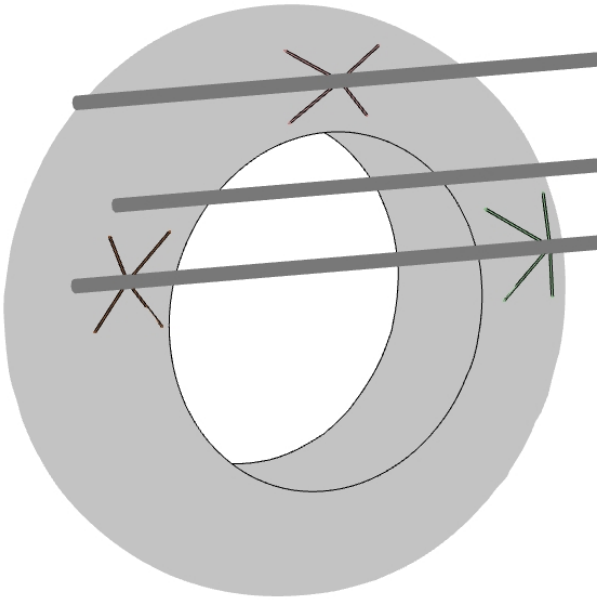

Figure 3.4: Representation of barrier tire and cable attachment.

In case of 6:1 sloped medians, the arrangement of barrier tire and cable attachment has been retained however the front side and back side nomenclature change. The front side impacts for a sloped median include all scenarios when the vehicle crashes into the barrier before reaching the ditch and the back side impacts include all scenarios when the vehicle crashes into the barrier after traversing through the ditch. Figure 3.6 shows the front and back side of the barrier for a sloped median.

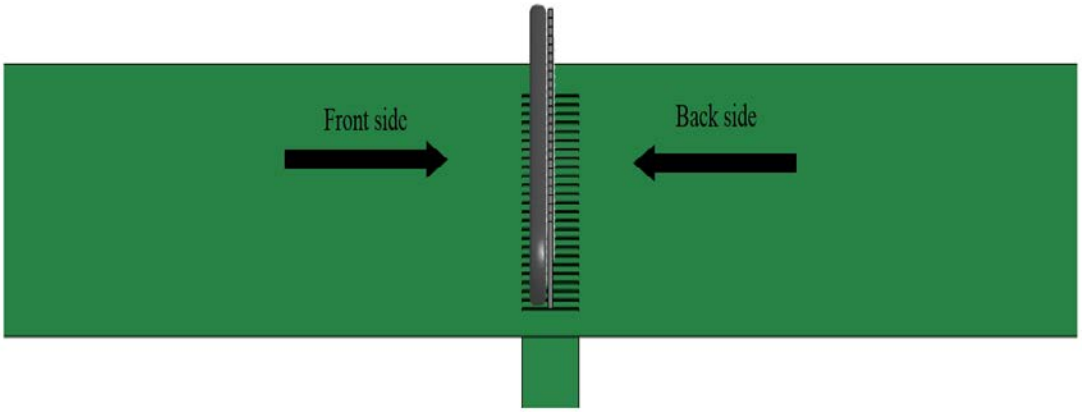

Figure 3.5: FE model of flat median - front and back side.

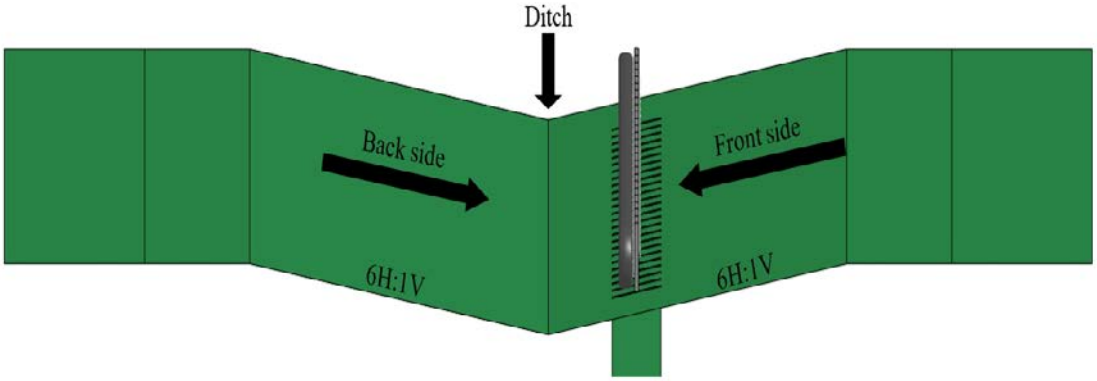

Figure 3.6: FE model of sloped median - front and back side.

In simulations conducted with the current cable median barrier design on sloped median, the posts were located at a distance of 4 feet from the ditch. Thus, the placement

of tire-cable median barrier on the sloped median led to two placement scenarios. The first scenario was called placement 1 and involved positioning of the tire-cable median barrier after the ditch such that the distance between the front face of the tire sidewall and the ditch was 4 feet. Figure 3.7 shows placement 1 for the sloped median. The second scenario was called placement 2 and involved positioning of the tire-cable median barrier before the ditch such that the distance between the post and the ditch was 4 feet. Figure 3.8 shows placement 2 for the sloped median.

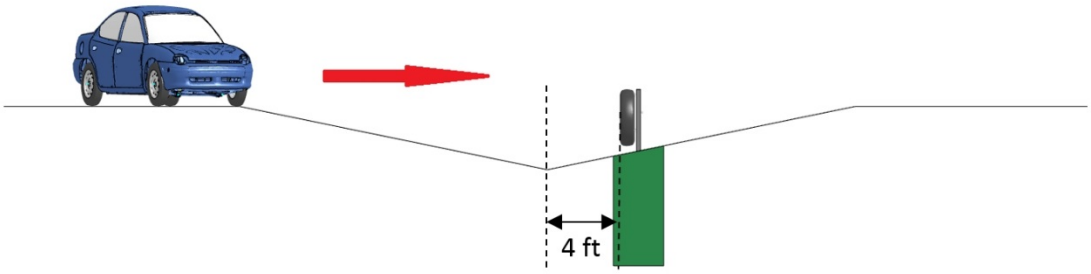

Figure 3.7: Sloped median (placement 1).

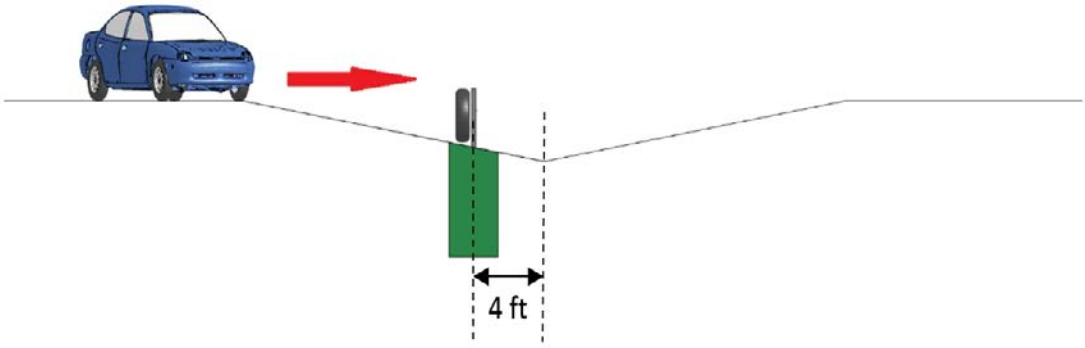

Figure 3.8: Sloped median (placement 2).

Four variants of the tire-cable median barrier were evaluated in this work. The variation in design mainly focused on changes to hook bolt shapes and cable heights.

The designs were conceived by implementing a least retrofitting approach which ensured that they would deviate minimally from the current design of cable median barriers used by the North Carolina Department of Transportation (NCDOT). Figure 3.9 shows the side view of NCDOT current design and the tire-cable median barrier variations are described thereafter.

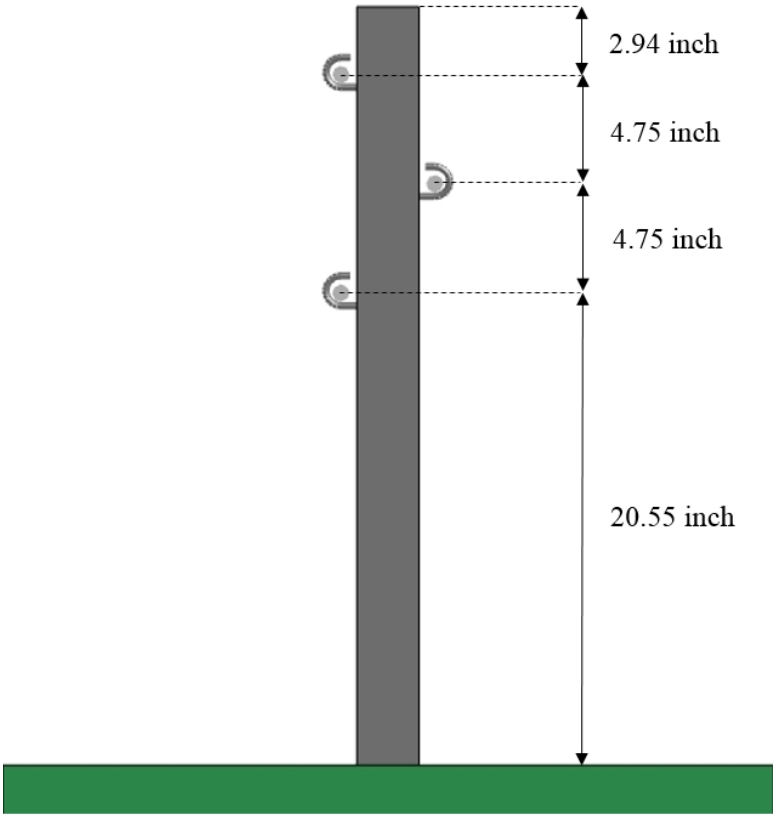

Figure 3.9: Side view of NCDOT current design

3.3.1 TCMB_J1

In this model, the NCDOT current design of cable median barrier was retrofitted with the tires without any alteration. The top and bottom cables are equidistant from the middle cables and no failure criteria has been defined for the hook bolt to post attachment. The contact definitions used in this model include automatic general for

cables, hook bolts and post with soil null shells. Automatic surface to surface contact has been used between terminal concrete block and soil, and also between vehicle tires and road. Automatic nodes to surface was used for contact between the road (master) and cables, barrier tires (slave). Automatic general interior contact was used between vehicle parts and barrier tires with cables and posts. All internal contacts for the vehicle are defined as single surface contact. Figure 3.10 gives the side view of the TCMB_J1 tire-cable median barrier and shows the cable heights.

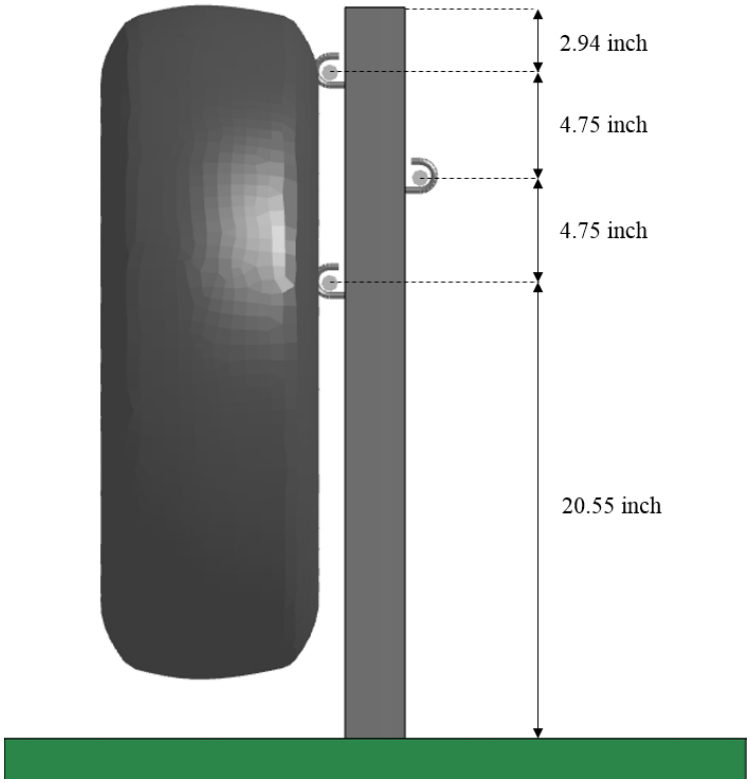

Figure 3.10: Side view of TCMB_J1.

3.3.2 TCMB_U1

In this model, the J-shaped hook bolts of the current design were replaced by U-shaped hook bolts. No failure criteria was defined at the point where the hook bolt is

attached to the post. Thus, this design was made artificially rigid. This barrier design followed the same tire attachment method used for TCMB_J1 design (i.e. rigid nodal bodies). The contact definitions used are same as those used for TCMB_J1 design. Figure 3.11 gives the side view of the TCMB_U1 along with the cable heights.

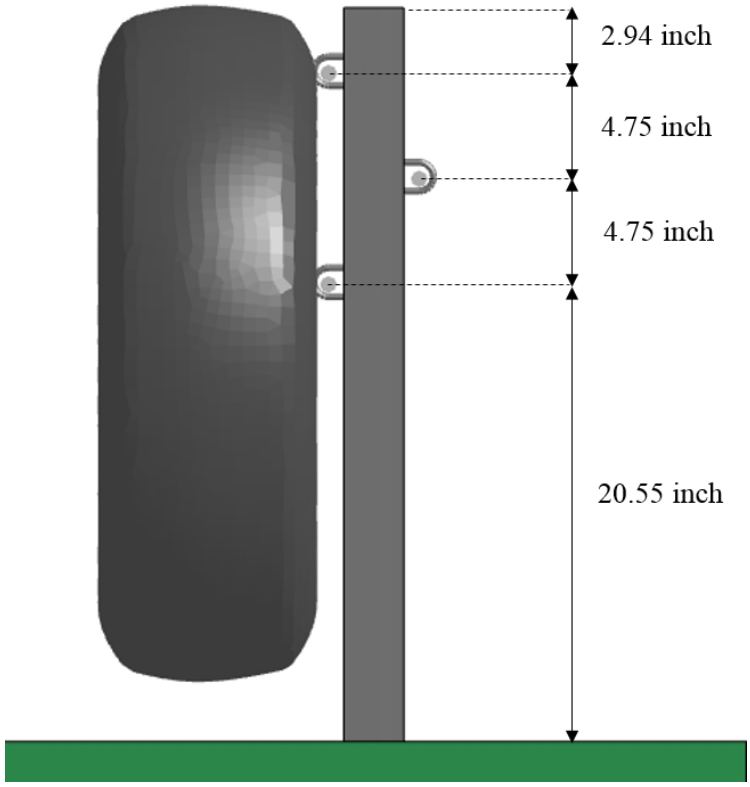

Figure 3.11: Side view of TCMB_U1.

3.3.3 EDC_J1

In this model, the heights of the cables were changed such that the top and bottom cable were equidistant from the middle cable. To achieve this, the top cable was retained in its original position and the middle cable was moved down to the height of the bottom cable and the new distance was measured. Then the bottom cable was moved down by the same distance to restrict the movement of the lower half of the barrier tire

and support it in a better way. Similar to previous designs, the tire was attached to the side having two cables by rigid nodal bodies. The contact definitions used are same as those used for TCMB_J1 design. Figure 3.12 gives the cross-sectional view of EDC_J1 along with the cable heights.

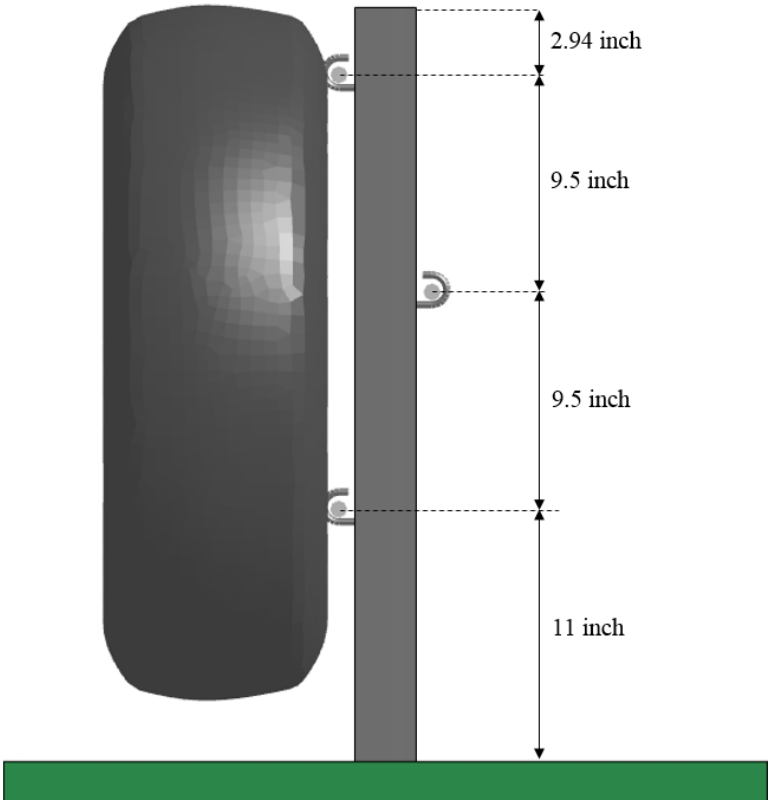

Figure 3.12: Side view of EDC_J1.

3.3.4 EDC_U1

In this model, the J-shaped hook bolts of the EDC_J1 were replaced by U-shaped hook bolts. No failure criteria was defined at the points where the hook bolt was attached to the post. Thus, this design was made artificially rigid.This barrier design followed the same tire attachment method used for previous designs of tire-cable median barriers (i.e. rigid nodal bodies). The contact definitions used are same as those

used for TCMB_J1 design. Figure 3.13 gives the cross-sectional view of the EDC_U1 along with the cable heights.

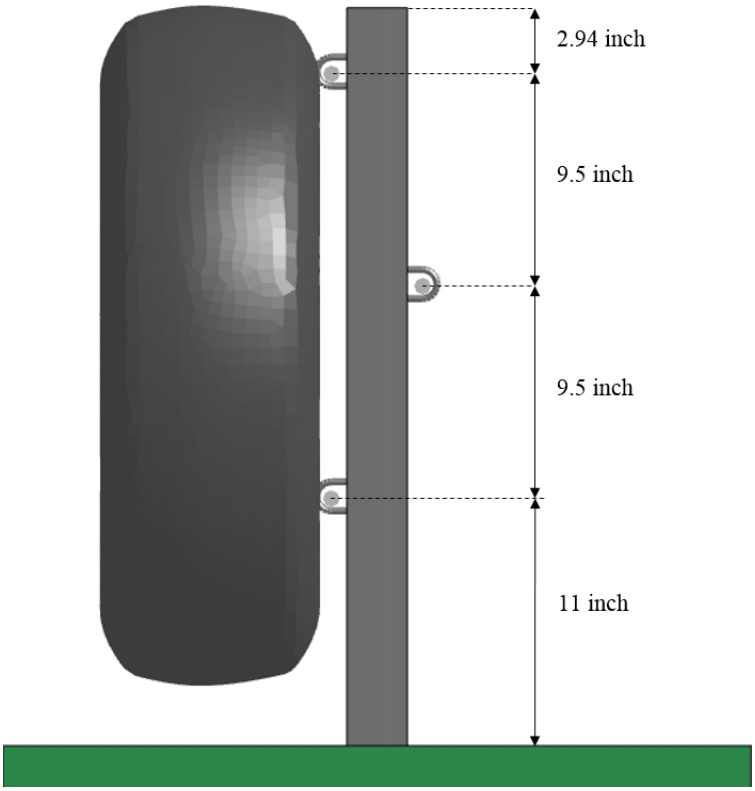

Figure 3.13: Side view of EDC_U1.

3.4 Simulation setup

The experimental methodology was designed with a goal to find out a good design for handling front and back side impact by a small sedan. All the designs were also to be tested by impact with the truck. The experiments were also designed in order of minimum changes/least retrofitting to the current design cable median barrier. Based on this criterion, a total of 4 simulations were carried out according to the simulation matrix in Table 3.1

Table 3.1: Simulation matrix - Case 1.

Vehicle	Barrier	Median	Impact side	Impact point
NEON	TCMB_J1	Flat	Front	Post
	TCMB_U1			
	EDC_J1			
	EDC_U1			

The impact simulations were carried out only on the barrier front side and the impact point was chosen as one of the posts located approximately in the middle of the barrier section. Once it was confirmed that the design was viable, other cases involving back side and front side impact on the post and mid-span were performed.

After the completion of Case 1, it was observed that EDC_J1 tire-cable median barrier design was a viable option and further investigation was necessary in order to better evaluate barrier performance. The simulation matrix in Table 3.2 shows the simulation setup for evaluating the viable EDC_J1 tire-cable median barrier design. The barrier was evaluated on flat median and on the two placement options for sloped median.

Table 3.2: Simulation matrix - Case 2.

Vehicle	Median	Impact side	Impact point
NEON	Flat	Front	Mid-span
		Back	Post
		Back	Mid-span
	Sloped (Placement 1)	Front	Post
		Front	Mid-span
		Back	Post
		Back	Mid-span
	Sloped (Placement 2)	Front	Post
		Front	Mid-span
		Back	Post
		Back	Mid-span

After completion of simulations with the Neon model, a simulation matrix was designed for the Ford F250 truck. It was decided to run all scenarios as those run for Dodge Neon to observe the performance of the tire-cable median barrier designs on impact with a truck. EDC_J1 design was to be evaluated on sloped median as well. Table 3.3 shows the Case 3 simulation matrix.

Table 3.3: Simulation matrix - Case 3.

Vehicle	Barrier	Median	Impact side	Impact point
FORD F250	TCMB_J1	Flat	Front	Post
	TCMB_U1	Flat	Front	Post
	EDC_U1	Flat	Front	Post
	EDC_J1	Flat	Front	Post
			Front	Mid-span
			Back	Post
			Back	Mid-span
		Sloped (Placement 1)	Front	Post
			Front	Mid-span
			Back	Post
			Back	Mid-span
		Sloped (Placement 2)	Front	Post
			Front	Mid-span
			Back	Post
			Back	Mid-span

CHAPTER 4 : PERFORMANCE EVALUATION OF TIRE-CABLE MEDIAN BARRIERS

In this chapter, FE simulation results for the cases listed in Table 3.1, Table 3.2 and Table 3.3 are presented and studied to determine the performance of the tire-cable median barrier system. The simulations were conducted using the vehicle models of Dodge Neon and Ford F250 impacting the barrier at 62.1 mph (100 km/h) and a 25° angle of impact. It should be observed that these deterministic simulation results can be used to predict the performance of the tire-cable median barrier only up to a certain level of accuracy. These results should not be used to draw definitive conclusions about their performance and further examination for the same is recommended

In order to estimate the vehicular responses after impacting the tire-cable median barrier, relevant data was collected and analyzed. The data collected included the vehicles displacement, velocity and acceleration along the x, y and z axes along with the resultant velocity calculated at the center of gravity (CG). The yaw, pitch and roll angles were also calculated. Figure 4.1 shows the yaw, pitch and roll directions used to calculate the respective angles. The yaw is rotation around the vertical axis, the pitch is rotation around the horizontal axis and the roll is rotation around the axis mutually perpendicular to the other two, directed from the back side to the front side of the vehicle.

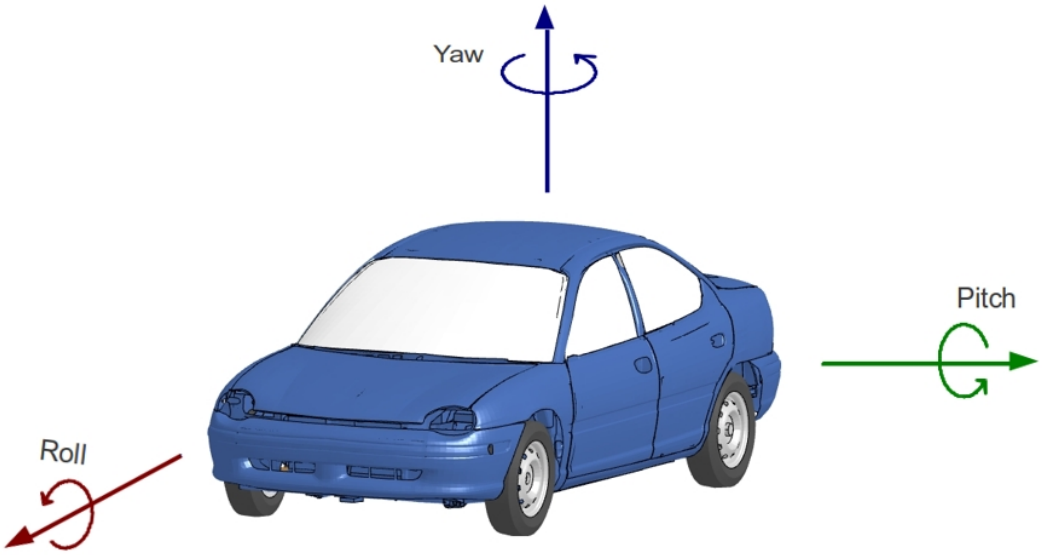

Figure 4.1: Definition of yaw, pitch and roll angles.

The Manual for Assessing Safety Hardware (MASH) is a detailed document written by the American Association of State Highway and Transportation Officials (AASHTO) which provides guidance for crash testing and performance evaluation of roadside safety features. The MASH exit box criterion was used to evaluate the post impact trajectory of the vehicle for MASH evaluation criteria N. Figure 4.2 illustrates the definition of the exit box, which begins at the last point of contact of the vehicle with the initial face of the barrier. The size of the exit box is determined by the size and type of vehicle impacting the barrier. Table 4.1 gives the dimensions of the exit box for the Dodge Neon and the Ford truck. Distance A is calculated by the formula $7.2 + V_W + 0.16V_L$ (meters), where V_W and V_L are the width and length of the vehicle respectively. Distance B is constant at 10 meters for sedans or pickup trucks. For a simulation to be considered safe, all four tire tracks should travel the distance B all the while being inside the distance A. Another scenario that MASH evaluation criterion N recognizes as safe is, if the vehicle remains upright and in constant contact with the

barrier while the vehicle velocity reduces and it comes to a halt. In this scenario, an exit box is not required. Other cases for which an exit box is not required is when the vehicle rolls over after impact or penetrates the barrier and lands up on the other side of the barrier. High vehicular exit angles and spinout are not desirable as they indicate towards the ability of the vehicle to possibly reenter into the travel lane and cause secondary collisions. Although the exit box is an important tool to evaluate post impact vehicular trajectories, snagging or pocketing of the vehicle may cause spinouts even for cases deemed safe by the exit box criterion. In addition to the exit box criterion, MASH evaluation criterion F was also used which specifies that the vehicle should remain upright during and after collision and the maximum roll and pitch angle are not to exceed 75°.

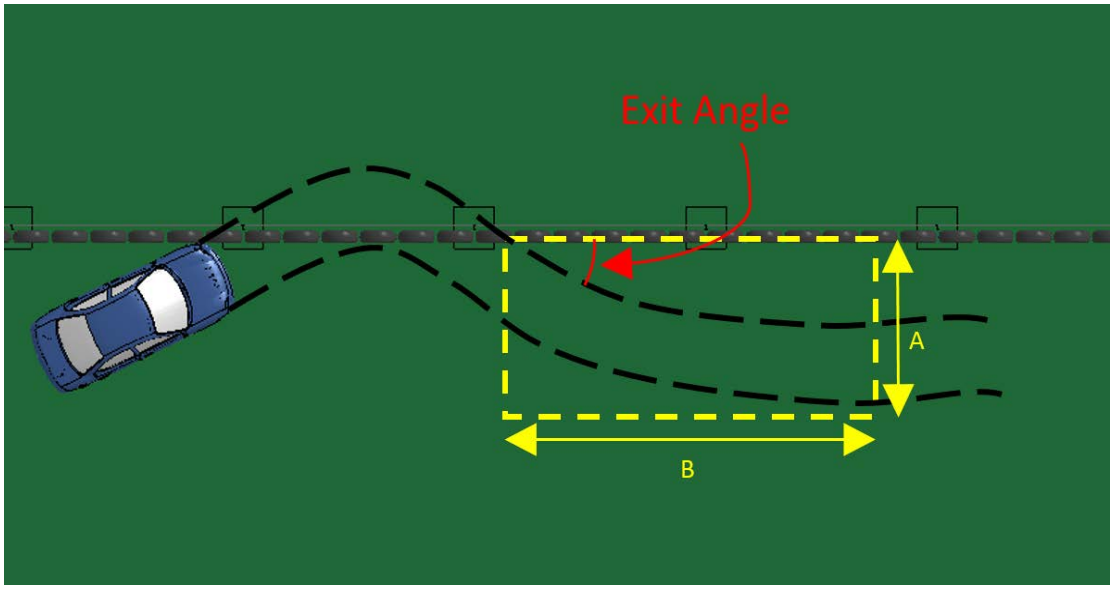

Figure 4.2: Exit box criterion.

Table 4.1: Exit box dimensions.

Vehicle	A	B
Dodge Neon	4.6 m	10 m
Ford F250	5.15 m	10 m

4.1 Case 1 simulations results

The selection of a good tire-cable median barrier design was done by analyzing the crash simulation results according to Table 3.1. MASH TL-3 impact conditions were used for the simulations and the vehicle used was Dodge Neon. Table 4.2 lists the barrier designs and gives a brief summary of the performance of respective barrier designs in terms of vehicular responses.

Table 4.2: Results for Case 1.

Barrier	Results
TCMB_J1	Vehicle underrides the barrier and continues to move forward with considerable velocity into the opposing travel lane
TCMB_U1	Vehicle snags on the post and is flipped up in the air landing at a steep angle on the ground
EDC_J1	Vehicle is redirected and passes the exit box criterion
EDC_U1	The barrier tires act as a ramp to launch the vehicle in air. The vehicle lands on the barrier itself before rolling more than 90 degrees to contact the ground.

4.1.1. The TCMB_J1 Design

This barrier design was the first design iteration because it involved no change to the current three cable design in terms of hook shape or cable height. Figure 4.3 shows the vehicle trajectory of Dodge Neon impacting the TCMB_J1 tire-cable median barrier. The TCMB_J1 barrier is shown in its deformed state with the Neon tire tracks marked in white. From the vehicle trajectory, it is evident that the barrier completely failed to redirect the vehicle and hence an exit box has not been shown.

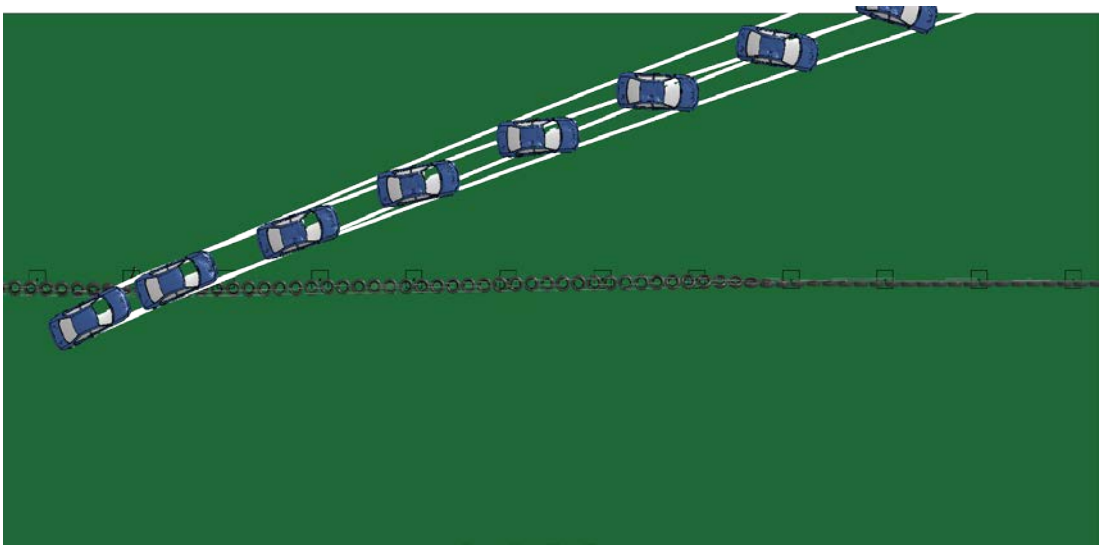

Figure 4.3: Vehicle trajectory for Neon impacting TCMB_J1.

Figure 4.4 shows the yaw, pitch and roll angles of the vehicle. Both the pitch and roll angle values remain within a range of 5° for most part of the simulation and the sudden increase in their values toward the end is because the vehicle ran out of ground. Thus in this case, the barrier passes MASH evaluation criteria F. The

continuous increase in the yaw angle shows that after impact, the vehicle spins continuously till it reaches the end of the road.

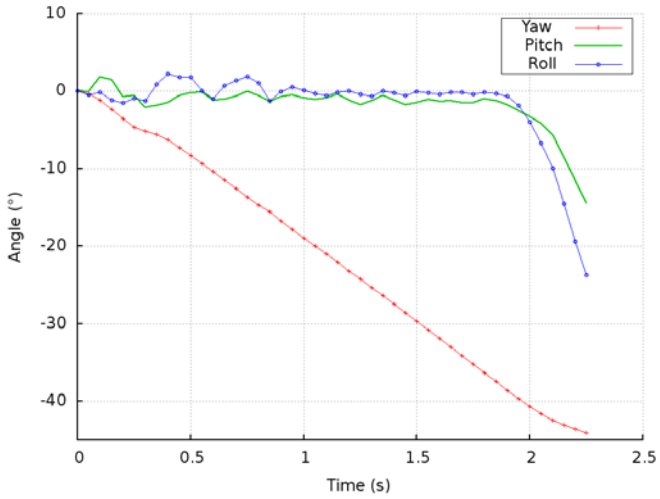

Figure 4.4: Yaw, pitch and roll angles for Neon impacting TCMB_J1.

Figure 4.5 shows vehicle barrier interaction in which it is clear that TCMB_J1 barrier overrode the vehicle completely. For TCMB_J1 design, the lower end of the barrier tires have unrestricted degree of freedom in the transverse direction. Thus, during the initial stage of the impact, Neon lifts the lower end of the barrier tires in contact and it sets of a chain reaction among the adjacent tires which helps in under-riding of the barrier.

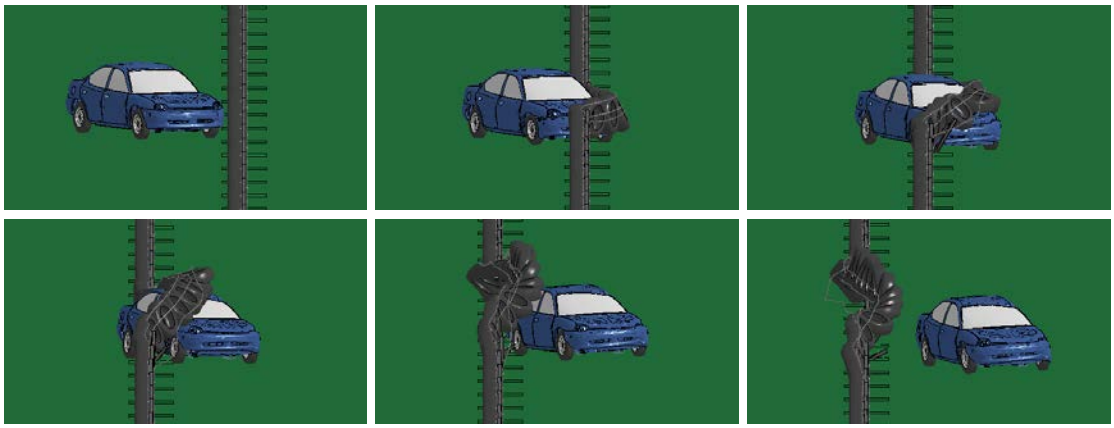

Figure 4.5: Neon interaction with TCMB_J1.

The vehicle displacement in Y direction (transverse displacement) and the velocity in Y direction (transverse velocity), calculated at the CG (center of gravity) of the vehicle are shown in Figure 4.6. It can be observed that the displacement graph appears to be linear indicating non-redirection of the vehicle. The transverse velocity also appears to have reduced but does not go below 20 km/h indicating a high possibility of secondary collision with the oncoming vehicles in the opposing lane. Since this design failed to redirect the vehicle completely, a new design alternative was needed.

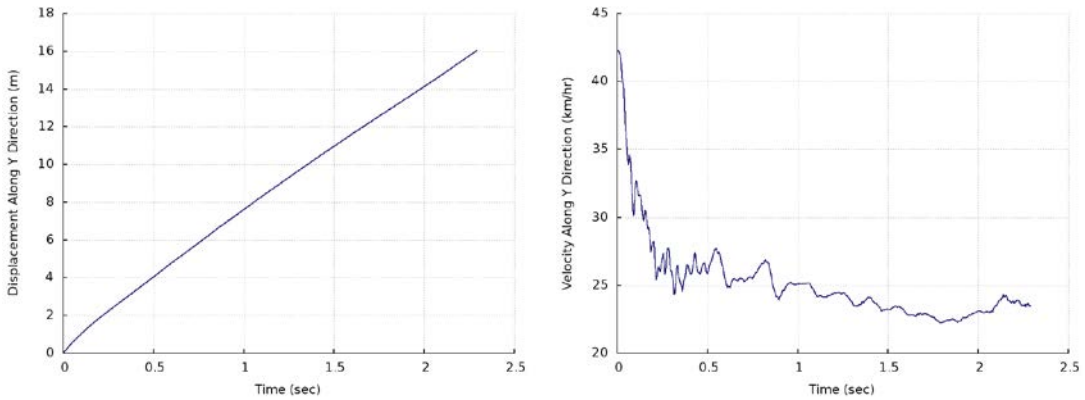

Transverse displacement Transverse velocity

Figure 4.6: Transverse displacement and velocity of Neon impacting TCMB_J1.

4.1.2. The TCMB_U1 Design

Barrier design TCMB_J1 failed because the lower part of barrier tires was easily displaced by the vehicle. In this design, to reduce the ease of barrier tire displacement, the hook bolts were changed to a U shape (i.e. the hook bolts were attached to the post at two distinct points instead on one). It was expected that rigidity of the barrier would increase by restricting movement of barrier tires and cables compared to TCMB_J1 barrier.

Figure 4.7 shows the vehicle trajectory of Dodge Neon impacting the TCMB_U1 tire-cable median barrier. The TCMB_U1 barrier is shown in its deformed state with the Neon tire tracks marked in white and the exit box marked in yellow. It can be observed that the vehicle is not redirected within the exit box and hence fails the MASH exit box criterion.

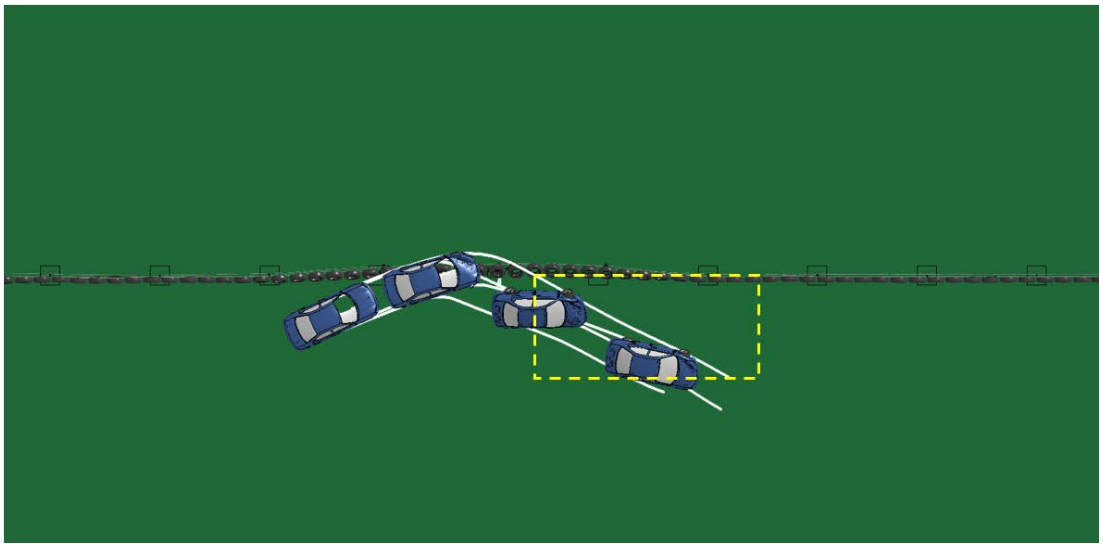

Figure 4.7: Vehicle trajectory and exit box for Neon impacting TCMB_U1.

Figure 4.8 shows the yaw, pitch and roll angles of the vehicle. The pitch and roll angle values remain within the 75° limit prescribed in the MASH criterion.

However, the high values of pitch and roll angles here are indicative of the fact that the vehicle was not smoothly redirected.

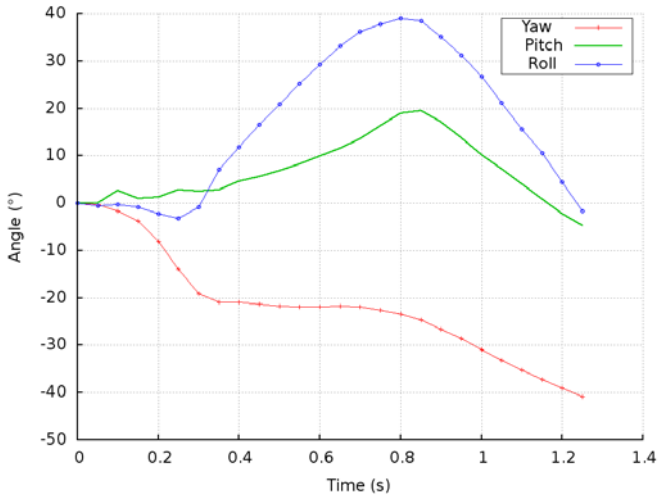

Figure 4.8: Yaw, pitch and roll angles for Neon impacting TCMB_U1.

Figure 4.9 shows the vehicle barrier interaction in which it is clearly seen that the post impact behavior of the vehicle is not ideal. For TCMB_U1 design an extra rigidity has been observed in the barrier due to the usage of U shaped hook bolts instead of J shaped hook bolts. The extra rigidity combined with movement of the lower part of the barrier tires makes this barrier inherently unstable. Due to this, the vehicle is unable to displace the barrier tires and cables in the transverse direction for a longer period of time resulting into excessive reaction force on the vehicle itself. The front side of the vehicle in contact with the barrier displaces the lower part of the barrier tires but is unable to separate the cables from the U shaped hook bolts. This causes the vehicle front left tire to engage with a post and the vehicle is violently launched in the direction opposite to the impact direction. This is not a smooth redirection and can possibly be very dangerous to the passengers sitting inside the vehicle.

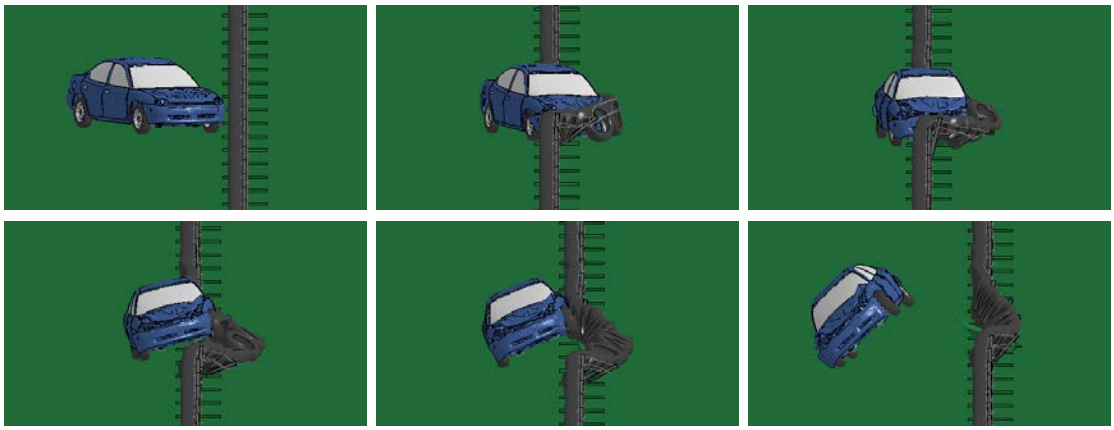

Figure 4.9: Neon interaction with TCMB_U1.

The vehicle displacement in Y direction (transverse displacement) and the velocity in Y direction (transverse velocity), calculated at the CG (center of gravity) of the vehicle are shown in Figure 4.10. It can be observed from the transverse velocity plot that the change in velocity is sudden in the initial phase of the impact. The transverse velocity reduces sharply from around 42 km/h to 0 km/h in just 0.2 seconds generating high G forces which may cause injuries to the occupants.

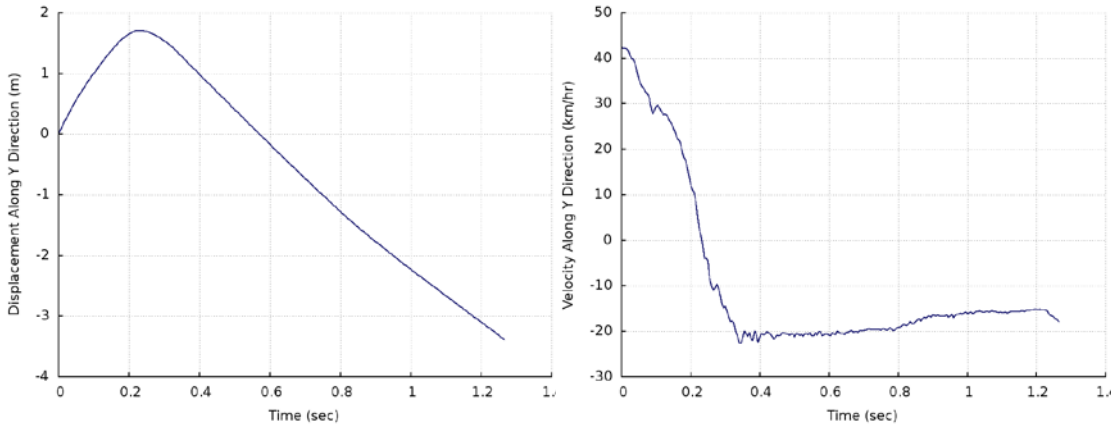

Transverse displacement Transverse velocity

Figure 4.10: Transverse displacement and velocity of Neon impacting TCMB_U1.

4.1.3. The EDC_J1 Design

The approach of changing hook shape did not give good results on impact scenarios with the Neon. Hence, it was decided to revert back to the original hook shape and change the cable height instead. In the case of TCMB_J1 it was observed that the lower half of barrier tire was unrestricted and was a major reason for the failure of the barrier. Thus, it was decided to change the cable heights such that the top cable is attached to the upper half of the tire sidewall and the bottom cable is attached to the lower half. This created a barrier design in which the top and bottom cables were equidistant from the middle cable and supported the tire sidewall in a better way compared to TCMB_J1 barrier.

Figure 4.11 shows the vehicle trajectory of Dodge Neon impacting the EDC_J1 tire-cable median barrier. The EDC_J1 barrier is shown in its deformed state with the Neon tire tracks marked in white and the exit box shown in yellow. It can be observed that all four tire tracks of the vehicle fit in the exit box and thus this barrier design passes MASH exit box criterion N.

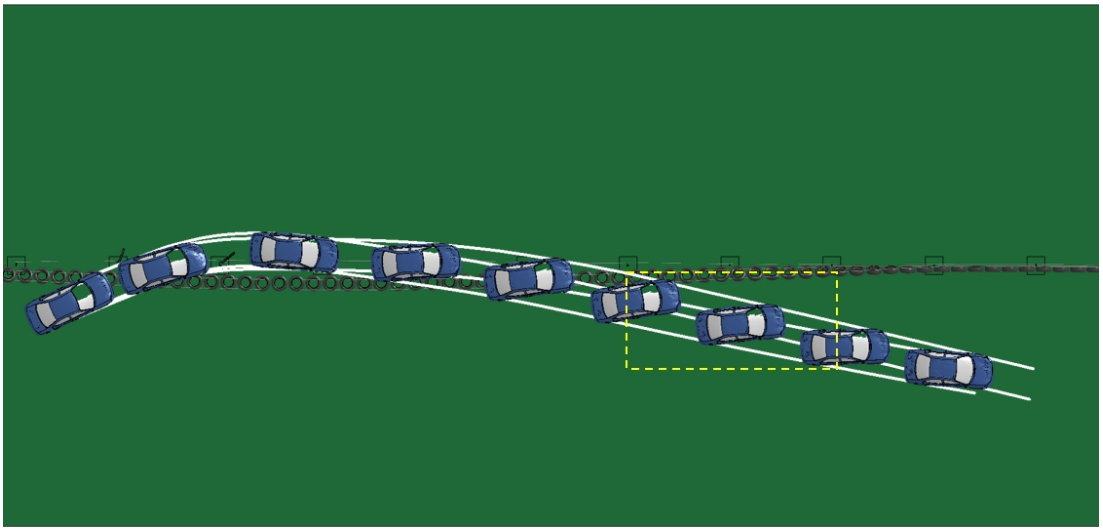

Figure 4.11: Vehicle trajectory and exit box for Neon impacting EDC_J1.

Figure 4.12 shows the yaw, pitch and roll angles of the vehicle. Both the pitch and roll angle values remain well within a range of 5° and thus the simulation passes MASH evaluation criterion F. The changes in yaw angle suggest that vehicle does not follow a smooth redirecting pattern and possibility of reentering the travel lane is present.

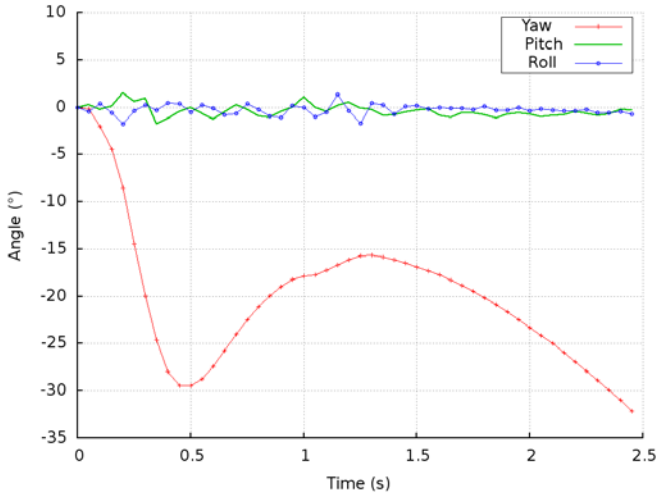

Figure 4.12: Yaw, pitch and roll angles for Neon impacting EDC_J1.

Figure 4.13 shows the vehicle barrier interaction and it is clear that EDC_J1 is capable of redirecting the vehicle. The maximum lateral deflection of the barrier occurs at 0.47 seconds into the simulation. For EDC_J1 tire-cable median barrier, the balanced design of two cables, one on each side of the tire sidewall prevents unrestricted movement of the lower part of the tire. This helps in preventing a chain reaction of twisting tires as was the case with TCMB_J1 design. The J shaped hook bolts yield and provide necessary freedom for the tires and cables to detach from the post and draw the vehicle inside. This prevents exertion of an excessive reaction force by the barrier on the vehicle as was the case with TCMB_U1 design. As in case of all cable barriers, the

energy from the initial impact gets transmitted to the adjacent cables and causes transverse (Y direction) oscillations of the cables. In current cable median barriers, the hook bolts are strong enough to contain these oscillations. However, the tire-cable median barrier has additional weight of the tires attached to the cables and hence detaches easily from the hook bolts when compared to current design cable median barriers.

Figure 4.13: Neon interaction with EDC_J1.

The vehicle displacement in Y direction (transverse displacement) and the velocity in Y direction (transverse velocity), calculated at the CG (center of gravity) of the vehicle are shown in Figure 4.14. The transverse displacement plot shows that the vehicle was able to displace the barrier laterally and the redirection was smooth. It can be observed from the transverse velocity plot that the change in velocity is gradual and it stabilizes around 1.5 seconds to a speed of 15 km/h.

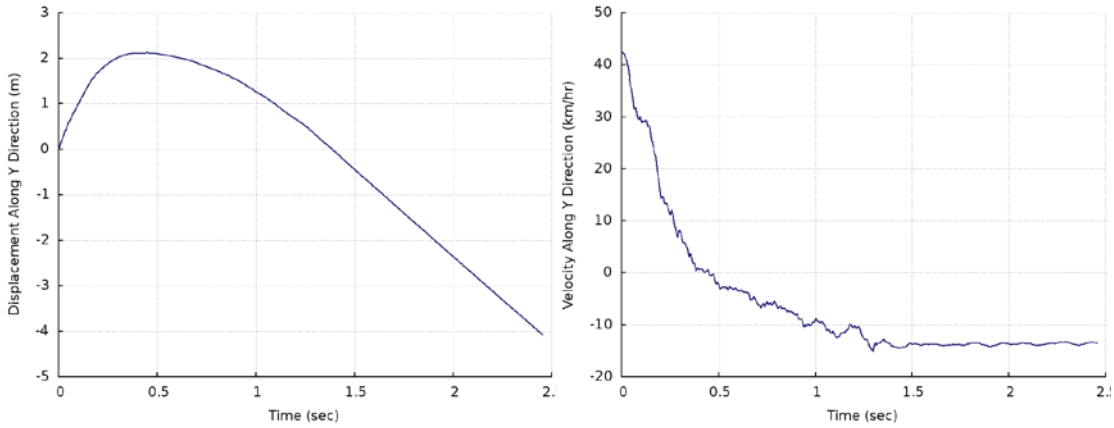

Transverse displacement Transverse velocity

Figure 4.14: Transverse displacement and velocity of Neon impacting EDC_J1.

4.1.4. The EDC_U1 Design

The EDC_J1 tire-cable median barrier showed promise after the failure of TCMB_J1 and TCMB_U1 barrier designs. As an additional effort, the EDC_J1 barrier was modified to create EDC_U1 barrier. The only change made was to the shape of hook bolts. EDC_U1 uses the same U shaped hook bolts found in TCMB_U1. Based on the results of TCMB_U1 design, it was expected that this barrier too would be very rigid and the simulation results proved the same.

Figure 4.15 shows the vehicle trajectory of Dodge Neon impacting the EDC_U1 tire-cable median barrier. The EDC_U1 barrier is shown in its deformed state with Neon tire tracks marked in white. The vehicle rolled over and fell on the ground on its side and hence an exit box is not shown.

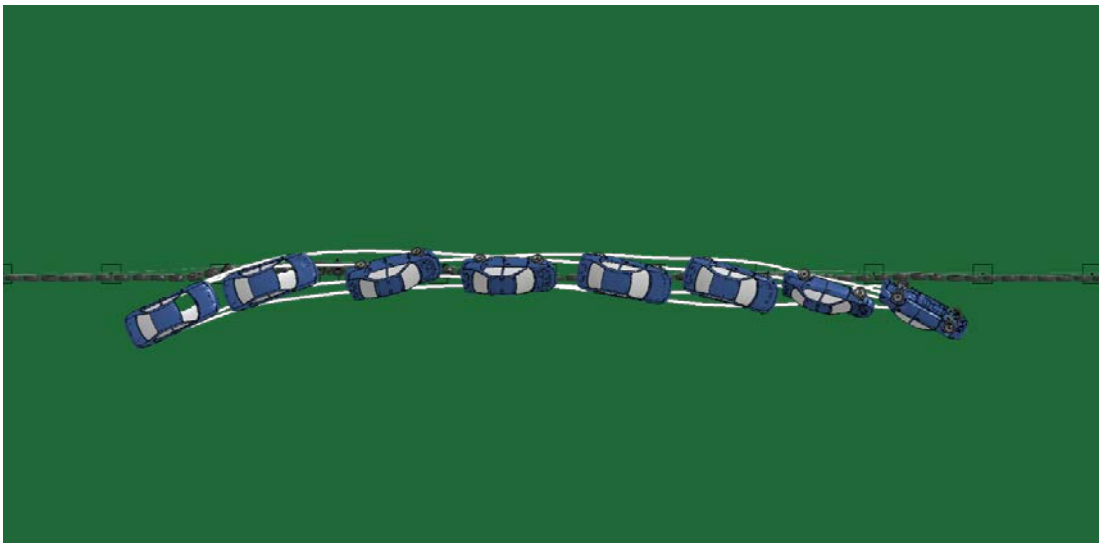

Figure 4.15: Vehicle trajectory for Neon impacting EDC_U1.

Figure 4.16 shows the yaw, pitch and roll angles of the vehicle. It can be clearly seen that the value of roll angle exceeds 75° limit and thus the barrier fails to comply with MASH evaluation criterion F.

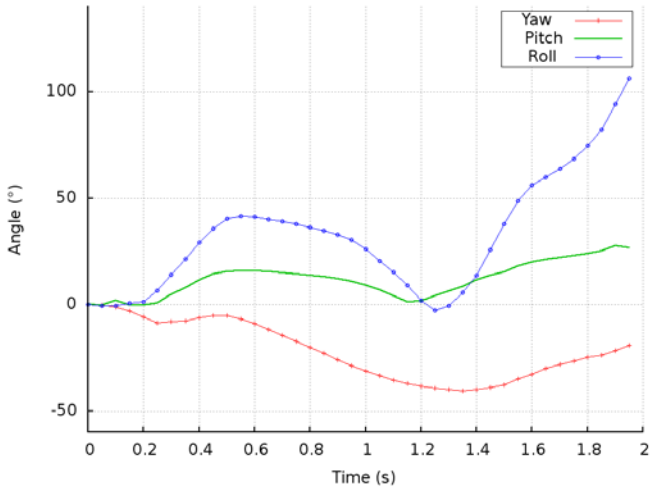

Figure 4.16: Yaw, pitch and roll angles for Neon impacting EDC_U1.

Figure 4.17 shows the vehicle barrier interaction and it can be seen that EDC_U1 was not able to redirect the vehicle safely. For EDC_U1 design an extra

rigidity was observed in the barrier due to the usage of U shaped hook bolts similar to the TCMB_U1 design. Due to this, the vehicle is unable to displace the barrier tires and cables in the transverse direction for a longer period of time resulting into excessive reaction force on the vehicle. Also as vehicle advances into the barrier, the extra rigidity forces cables and posts to bend which in turn bends the barrier tires creating a ramp. The vehicle is launched violently in the air due to the formation of this ramp and lands on top of the barrier before rolling over to its side.

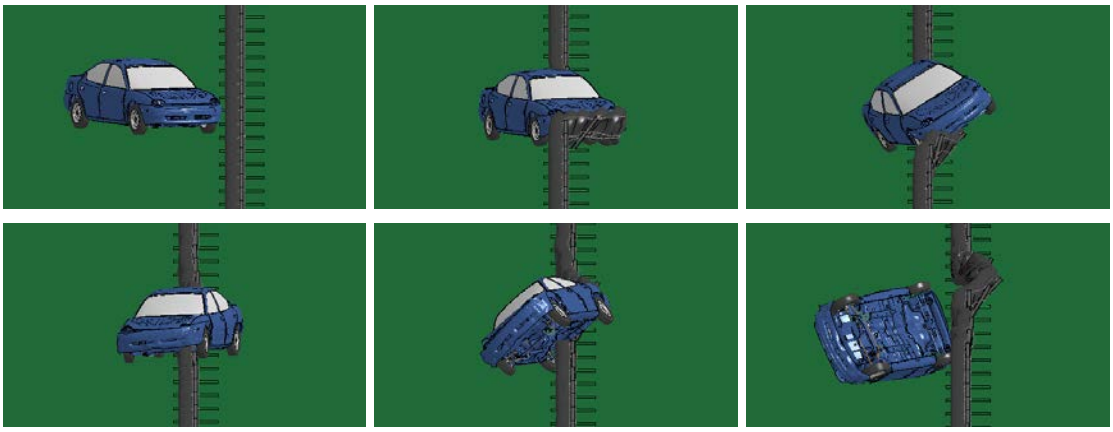

Figure 4.17: Neon interaction with EDC_U1.

The vehicle displacement in Y direction (transverse displacement) and the velocity in Y direction (transverse velocity), calculated at the CG (center of gravity) of the vehicle are shown in Figure 4.18. The transverse velocity plot bears a close resemblance to the one for TCMB_U1 barrier. There is a sudden drop in velocity from 42 km/h to 0 km/h within 0.2 seconds creating high G forces and would be dangerous for occupants.

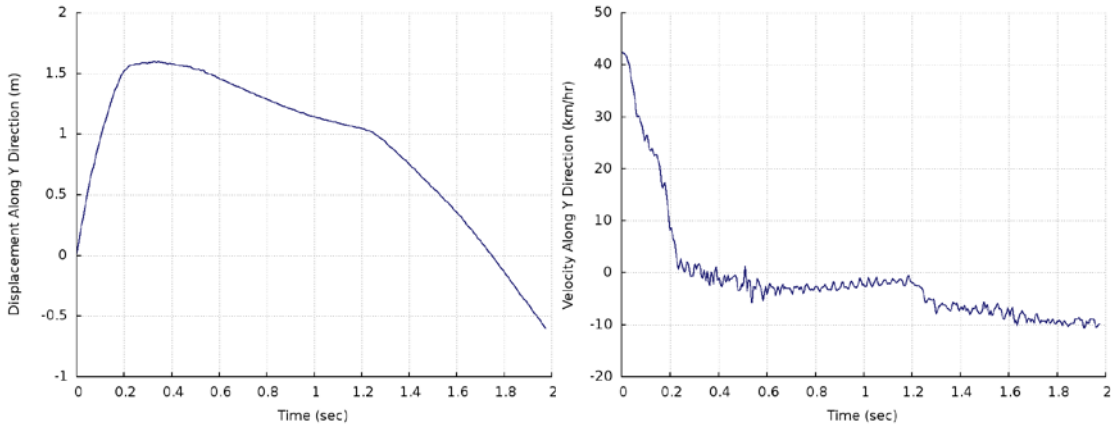

Transverse displacement Transverse velocity

Figure 4.18: Transverse displacement and velocity of Neon impacting EDC_U1.

4.2 Case 2 simulations results

Simulation results from Case 1 proved that EDC_J1 tire-cable median barrier design was a viable option. Hence additional simulations were conducted to evaluate the design on flat and sloped medians and critical locations were chosen for front and back side impacts. Table 4.3 gives the summary of results obtained from Case 2 simulations with respect to vehicle redirection.

Table 4.3: Results for Case 2.

Median	Impact side	Impact point	Results
Flat	Front	Mid-span	Redirected (outside exit box)
	Back	Post	Redirected (outside exit box)
	Back	Mid-span	Redirected (outside exit box)
Sloped (placement 1)	Back	Post	Vehicle underrode the barrier
	Back	Mid-span	Redirected (exit box criterion satisfied)
	Front	Post	Redirected (exit box criterion satisfied)
	Front	Mid-span	Redirected (exit box criterion satisfied)
Sloped (placement 2)	Front	Post	Vehicle overrode the barrier
	Front	Mid-span	Redirected (exit box criterion satisfied)
	Back	Post	Redirected (exit box not applicable)
	Back	Mid-span	Redirected (exit box not applicable)

4.2.1 Flat median

4.2.1.1 Front side mid-span impact

Figure 4.19 shows the vehicle trajectory of Dodge Neon impacting the EDC_J1 tire-cable median barrier. The EDC_J1 barrier is shown in its deformed state with the Neon tire tracks marked in white and the exit box shown in yellow. It can be observed that the vehicle is not redirected within the exit box and hence the barrier fails the MASH exit box criterion.

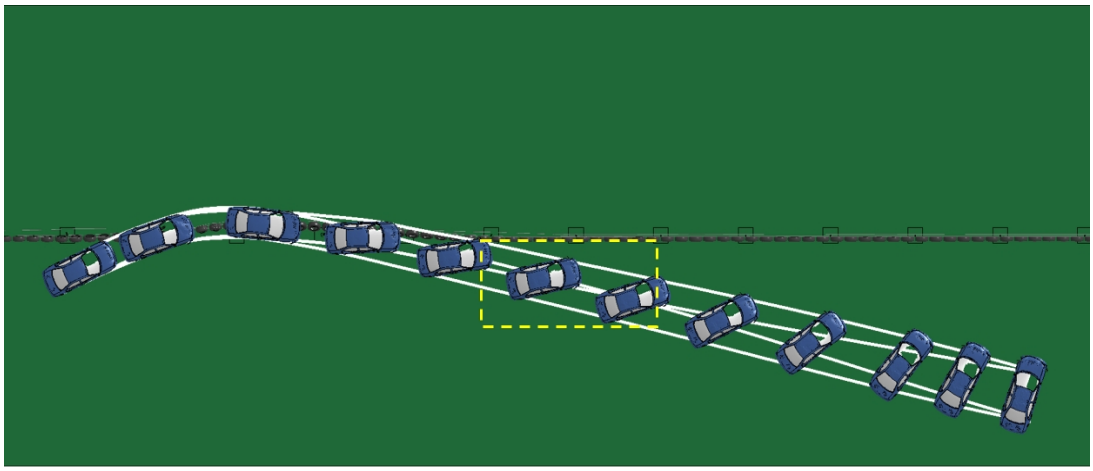

Figure 4.19: Vehicle trajectory and exit box for front side mid-span impact of Neon with EDC_J1 on flat median.

Figure 4.20 shows the yaw, pitch and roll angles of the vehicle. Both the pitch and roll angle values remain well within a range of 5° and thus the barrier passes MASH evaluation criterion F. The changes in yaw angle suggest that vehicle continues to spin out as it is being redirected. This increases the chance for secondary collisions significantly.

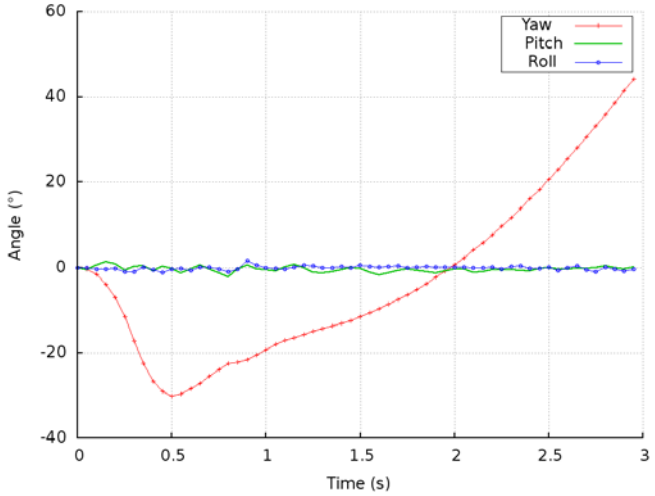

Figure 4.20: Yaw, pitch and roll angles for front side mid-span impact of Neon with EDC_J1 on flat median.

Figure 4.21 shows the state of maximum deflection of the barrier. The maximum deflection of the barrier is 1.88 meters and occurs at 0.48 seconds into the simulation. The vehicle displacement in Y direction (transverse displacement) and the velocity in Y direction (transverse velocity), calculated at the CG (center of gravity) of the vehicle are shown in Figure 4.22. It can be observed from the transverse velocity plot that the change in velocity is gradual and it stabilizes around 1.5 seconds to a speed of 12 km/h.

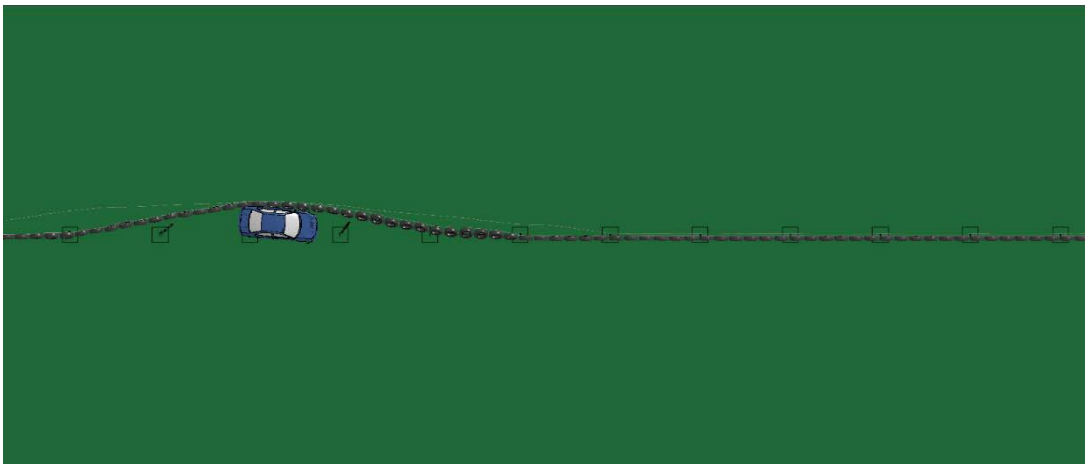

Top view

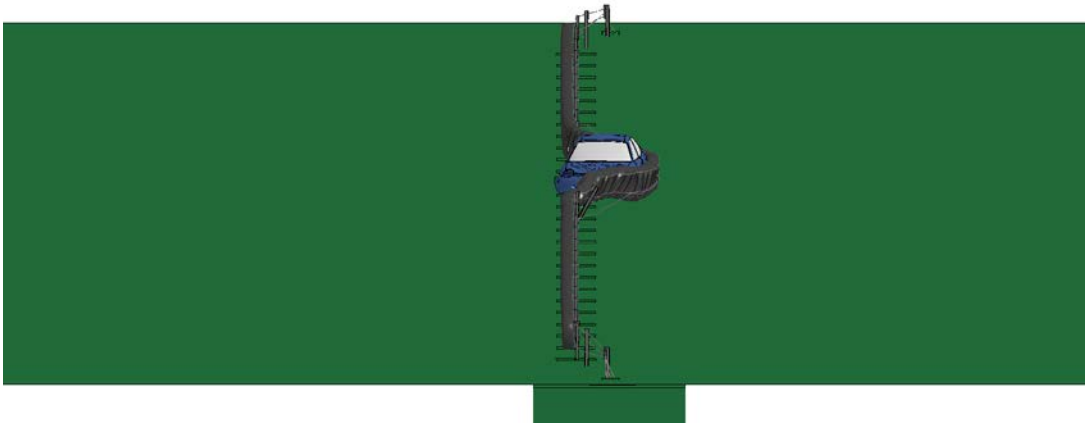

Front view

Figure 4.21: Maximum deflection of EDC_J1 for front side mid-span impact on flat median.

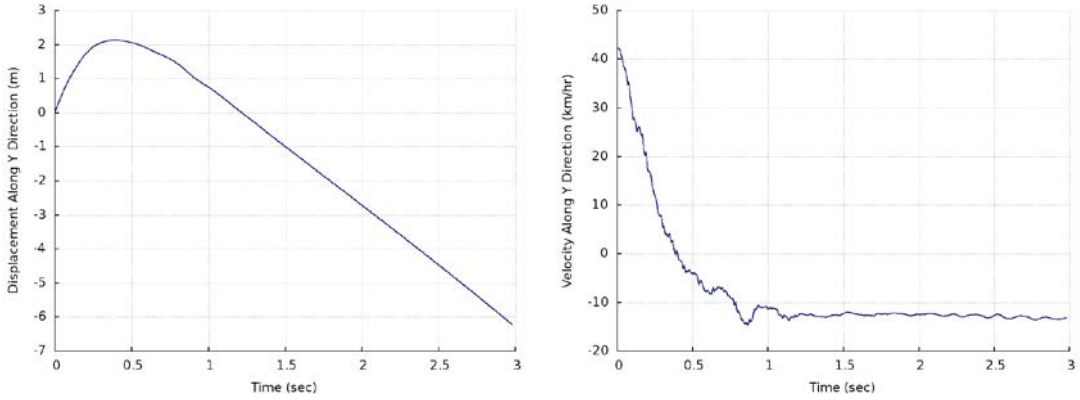

Transverse displacement Transverse velocity

Figure 4.22: Transverse displacement and velocity of Neon impacting the front side mid-span of EDC_J1 on flat median.

4.2.1.2 Back side post impact

Figure 4.23 shows the vehicle trajectory of Dodge Neon impacting the EDC_J1 tire-cable median barrier. The EDC_J1 barrier is shown in its deformed state with the Neon tire tracks marked in white and the exit box shown in yellow. It can be observed that the vehicle was not redirected within the exit box and hence fails the MASH exit box criterion.

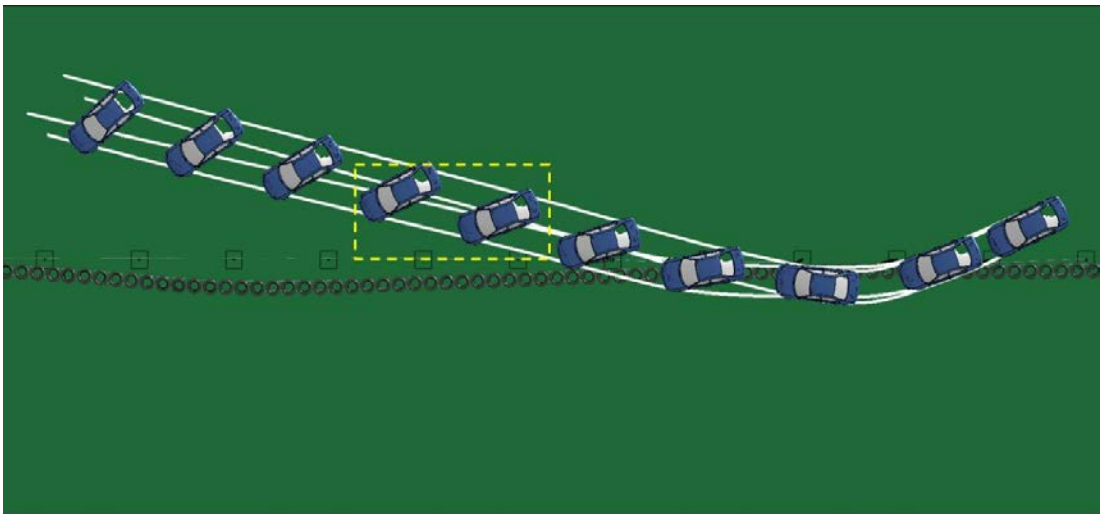

Figure 4.23: Vehicle trajectory and exit box for back side post impact of Neon with EDC_J1 on flat median.

Figure 4.24 shows the yaw, pitch and roll angles of the vehicle. Both the pitch and roll angle values remain well within a range of 5° and thus the barrier passed MASH evaluation criterion F. The changes in yaw angle suggest that vehicle continues to spin out as it is being redirected increasing the risk of a secondary impact due to loss of control.

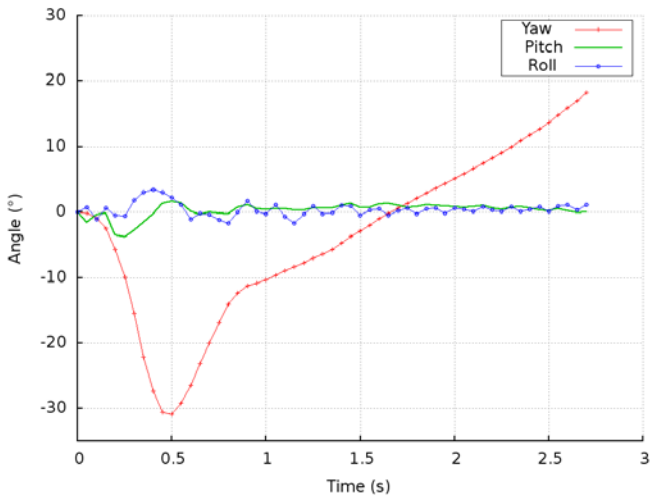

Figure 4.24: Yaw, pitch and roll angles for back side post impact of Neon with EDC_J1 on flat median.

Figure 4.25 shows the state of maximum deflection of the barrier. The maximum deflection of the barrier was 2.23 meter and occurred at 0.46 seconds into the simulation. The vehicle displacement in Y direction (transverse displacement) and the velocity in Y direction (transverse velocity), calculated at the CG (center of gravity) of the vehicle are shown in Figure 4.26. It can be observed from the transverse velocity plot that the change in velocity was gradual and stabilized around 1.5 seconds to a speed of 13 km/h.

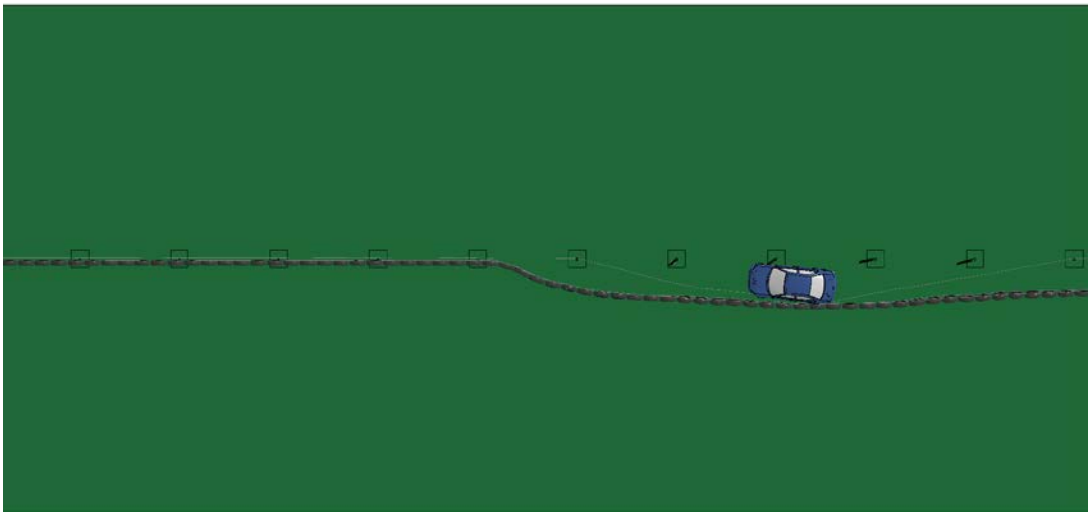

Top view

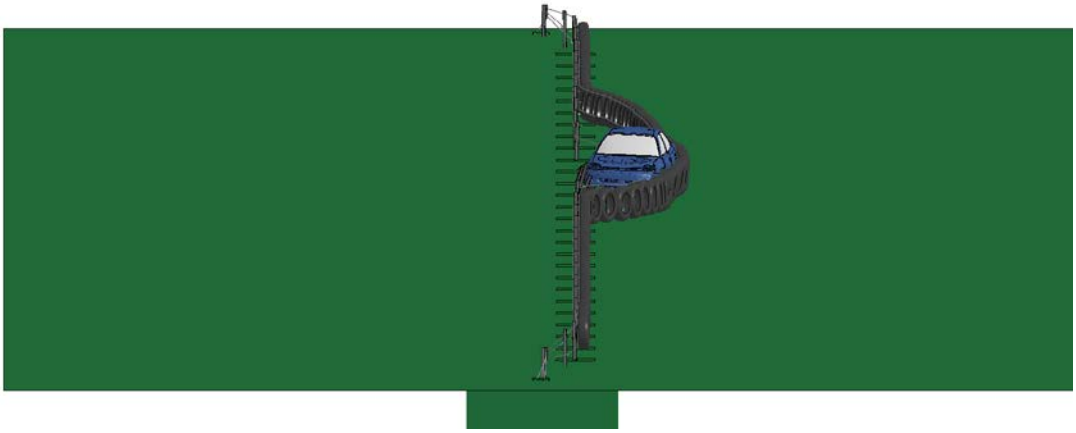

Front view

Figure 4.25: Maximum deflection of EDC_J1 for back side post impact on flat median.

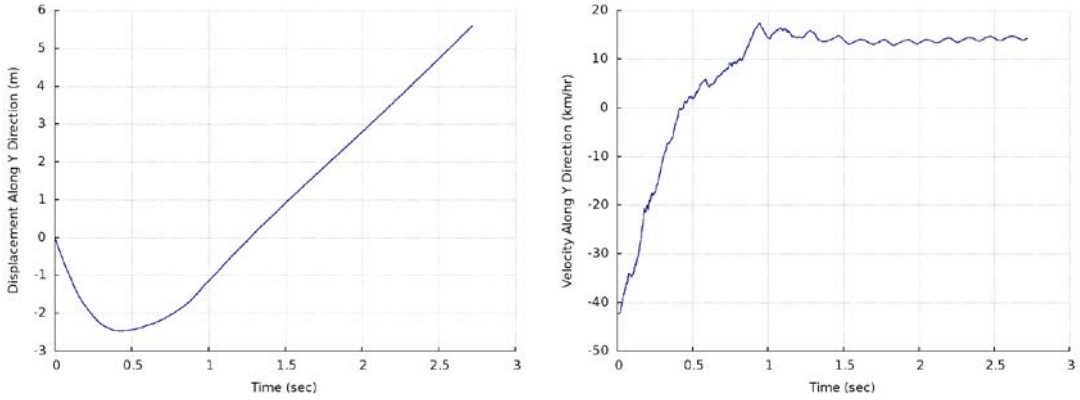

Transverse displacement Transverse velocity

Figure 4.26: Transverse displacement and velocity of Neon impacting the back side post of EDC_J1 on flat median.

4.2.1.3 Back side mid-span impact

Figure 4.27 shows the vehicle trajectory of Dodge Neon impacting the EDC_J1 tire-cable median barrier. The EDC_J1 barrier is shown in its deformed state with the Neon tire tracks marked in white and the exit box shown in yellow. It can be observed that the vehicle was not redirected within the exit box and hence failed the MASH exit box criterion.

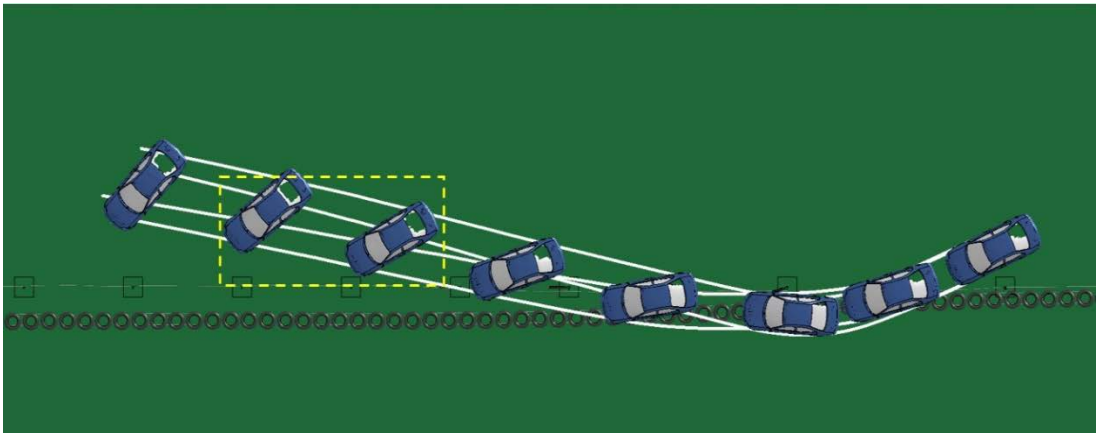

Figure 4.27: Vehicle trajectory and exit box for back side mid-span impact of Neon with EDC_J1 on flat median.

Figure 4.28 shows the yaw, pitch and roll angles of the vehicle. Both the pitch and roll angle values remain well within a range of 5° and thus the barrier passed MASH evaluation criterion F. The changes in yaw angle suggest that vehicle continues to spin out as it is being redirected increasing the risk of a secondary impact due to loss of control.

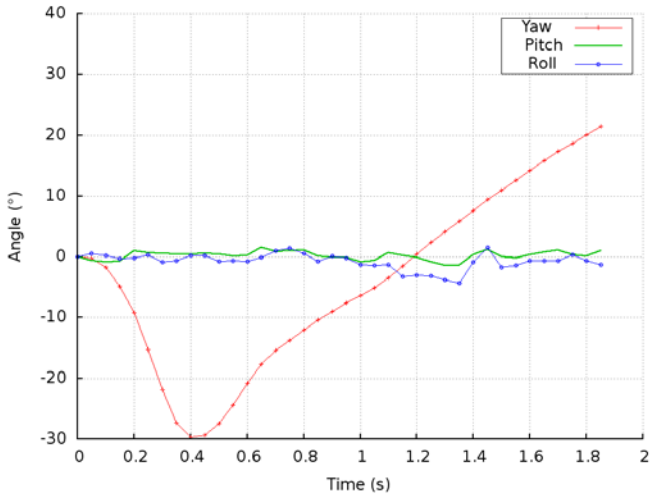

Figure 4.28: Yaw, pitch and roll angles for back side mid-span impact of Neon with EDC_J1 on flat median.

Figure 4.29 shows the state of maximum deflection of the barrier. The maximum deflection of the barrier was 2.11 meter and occurred at 0.42 seconds into the simulation. The vehicle displacement in Y direction (transverse displacement) and the velocity in Y direction (transverse velocity), calculated at the CG (center of gravity) of the vehicle are shown in Figure 4.30. It can be observed from the transverse velocity plot that the change in velocity was gradual and stabilized around 1.5 seconds to a speed of 14 km/h.

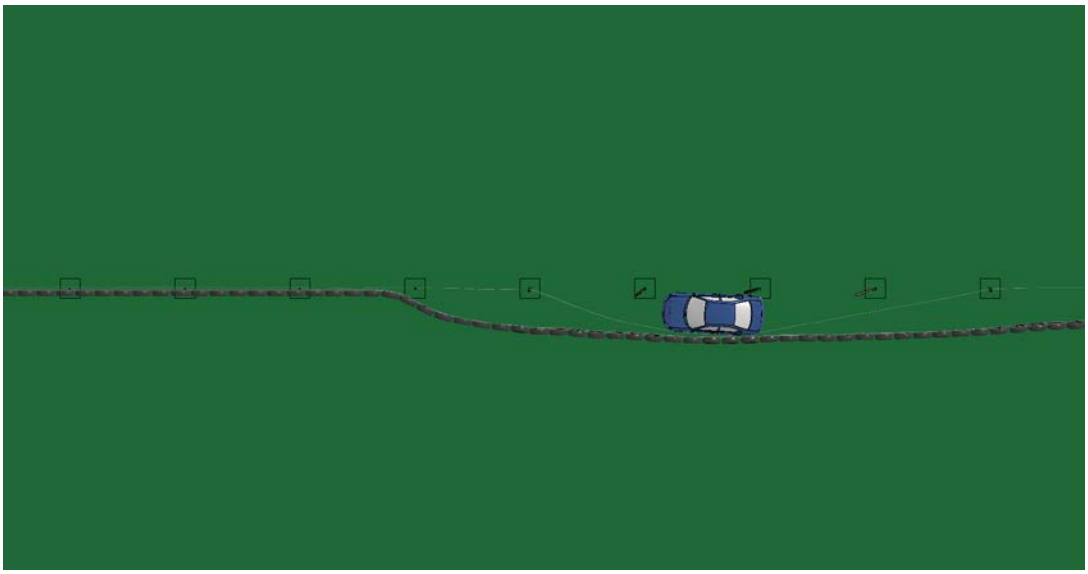

Top view

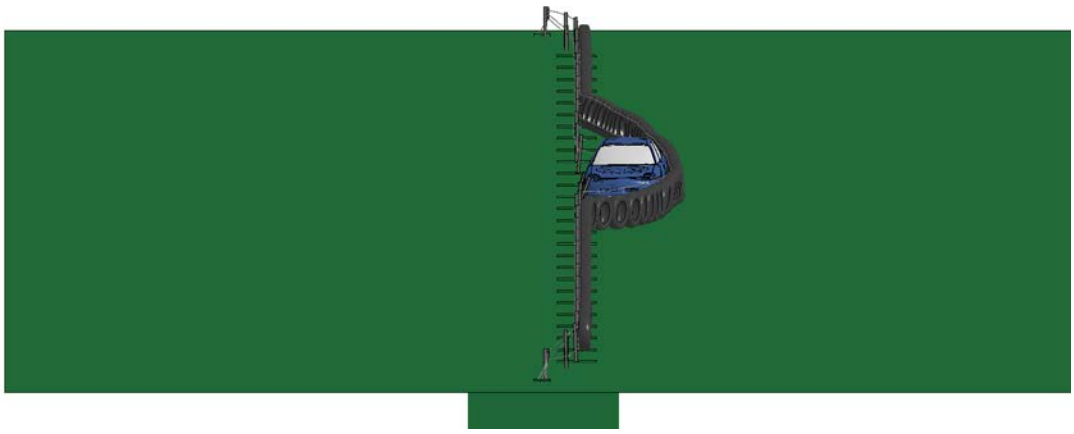

Front view

Figure 4.29: Maximum deflection of EDC_J1 for back side mid-span impact on flat median.

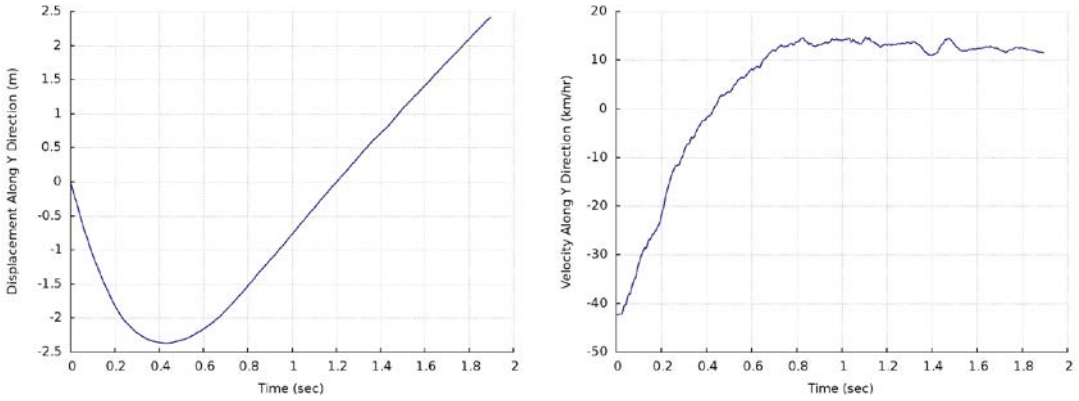

Transverse displacement Transverse velocity

Figure 4.30: Transverse displacement and velocity of Neon impacting the back side mid-span of EDC_J1 on flat median.

4.2.2 Sloped median (placement 1)

4.2.2.1 Back side post impact

Figure 4.31 shows the vehicle trajectory of Dodge Neon impacting the EDC_J1 tire-cable median barrier. The EDC_J1 barrier is shown in its deformed state with the Neon tire tracks marked in white. It can be observed that the vehicle penetrated the barrier and ended up on the other side. The vehicle continued to redirect in the ditch till the end of the simulation but since it had penetrated the barrier, no exit box was shown.

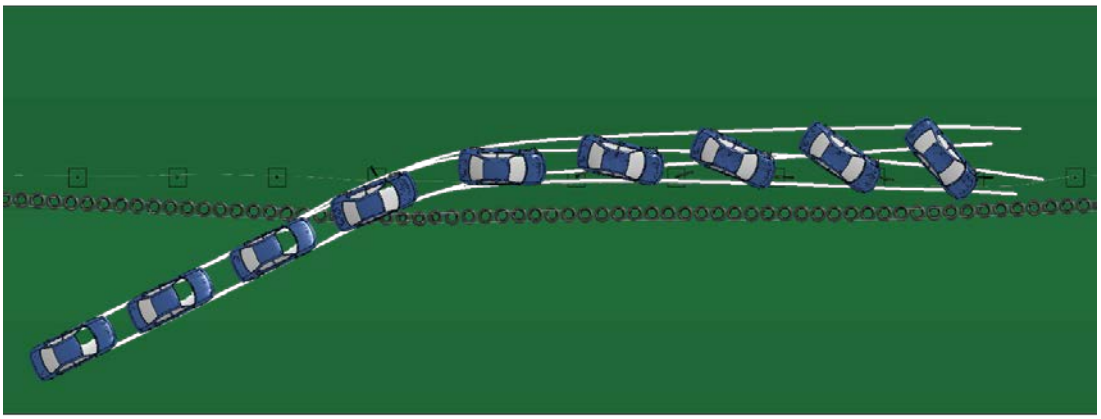

Figure 4.31: Vehicle trajectory for back side post impact of Neon with EDC_J1 on sloped (placement 1) median.

Figure 4.32 shows the yaw, pitch and roll angles of the vehicle. Both the pitch and roll angle values remain well within a range of 20° and thus the barrier passed MASH evaluation criterion F. The changes in yaw angle combined with the velocity profile suggest that vehicle will continue to spin in the ditch and come to rest there.

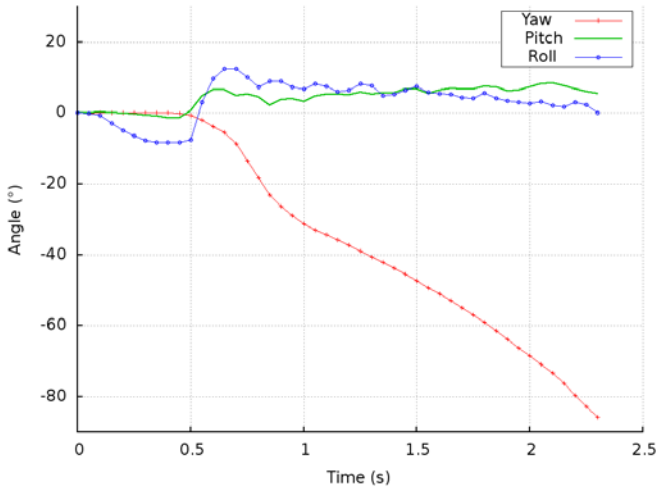

Figure 4.32: Yaw, pitch and roll angles for back side post impact of Neon with EDC_J1 on sloped (placement 1) median.

Figure 4.33 shows the state of maximum deflection of 1.02 meters for the barrier before the vehicle underrode it. The maximum deflection occurs at 0.7 seconds into the

simulation. In this case, the impact of the vehicle with the post on the sloped median creates a unique scenario in which the barrier tires push the post down upon impact and the vehicle height is already low due to a compressed suspension. This causes the vehicle front side to lift the tires upwards while continuing to travel forward. Continuous contact with the barrier tires causes some reduction in the velocity of the vehicle and some redirection is also observed as the vehicle underrides the barrier. Figure 4.34 shows vehicle barrier interaction.

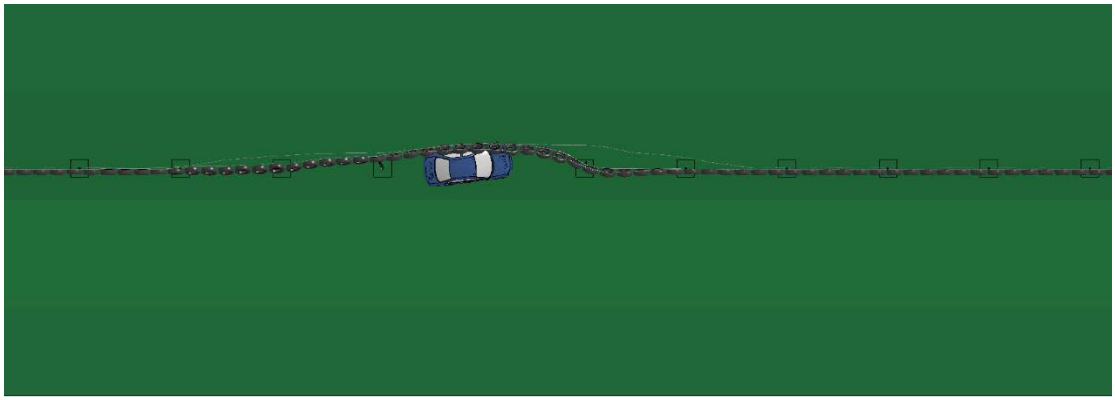

Figure 4.33: Maximum deflection of EDC_J1 for back side post impact on sloped (placement 1) median.

Figure 4.34: Neon interaction with EDC_J1 on sloped (placement 1) median for back side post impact.

The vehicle displacement in Y direction (transverse displacement) and the velocity in Y direction (transverse velocity), calculated at the CG (center of gravity) of

the vehicle are shown in Figure 4.35. It can be seen in the displacement plot that vehicle could not be redirected. It can be observed from the velocity plot that the transverse velocity of the vehicle stabilizes to a great extent and combined with the trajectory and yaw angle profile, it can be predicted that the vehicle will not enter the travel lane.

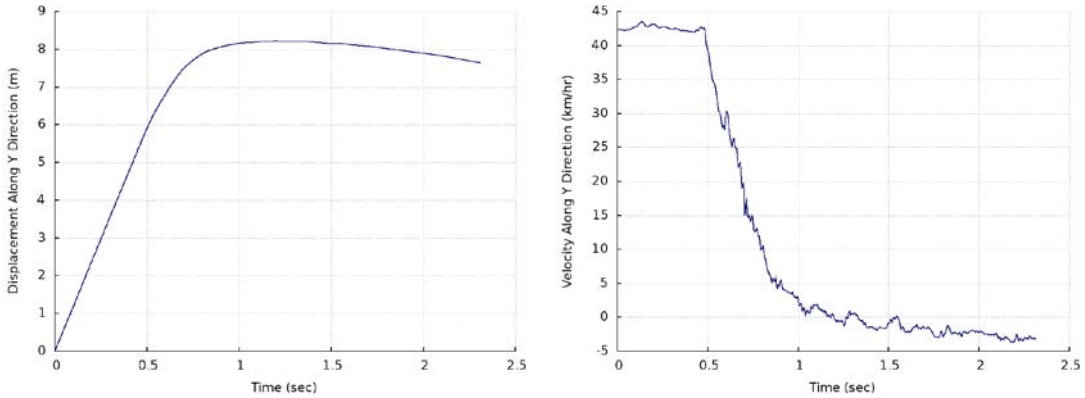

Transverse displacement Transverse velocity

Figure 4.35: Transverse displacement and velocity of Neon impacting the back side post of EDC_J1 on sloped (placement 1) median.

4.2.2.2 Back side mid-span impact

Figure 4.36 shows the vehicle trajectory of Dodge Neon impacting the EDC_J1 tire-cable median barrier. The EDC_J1 barrier is shown in its deformed state with the Neon tire tracks marked in white and the exit box shown in yellow. It can be observed that all four tire tracks of the vehicle fit in the exit box and thus this barrier design passes MASH exit box criterion N.

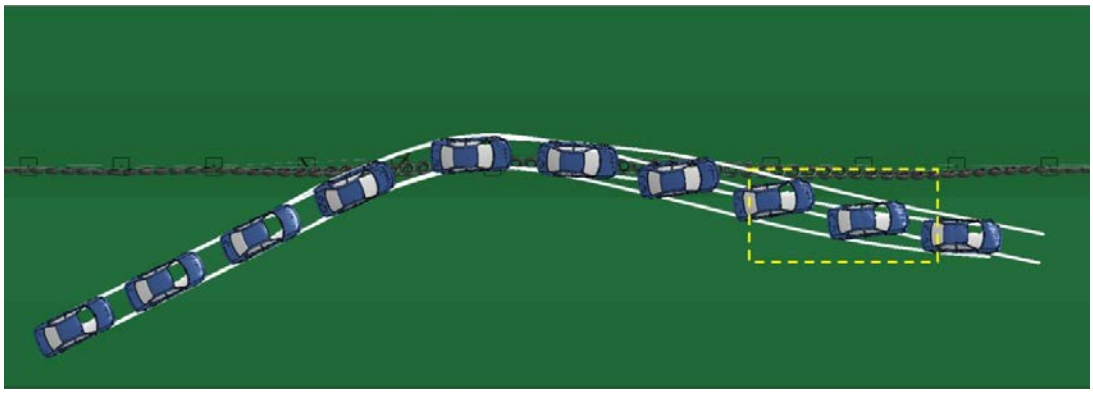

Figure 4.36: Vehicle trajectory and exit box for back side mid-span impact of Neon with EDC_J1 on sloped (placement 1) median.

Figure 4.37 shows the yaw, pitch and roll angles of the vehicle. Both the pitch and roll angle values remain well within a range of 15° and thus the barrier passes MASH evaluation criterion F. The changes in yaw angle suggest that vehicle does not spin out while being redirected and thus provides better control to the driver post impact.

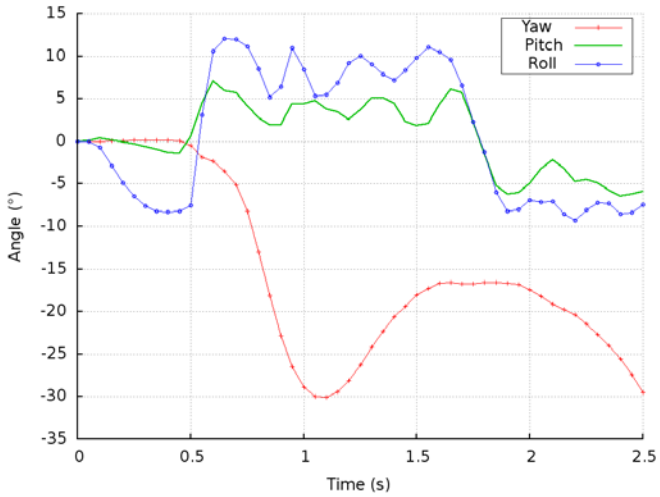

Figure 4.37: Yaw, pitch and roll angles for back side mid-span impact of Neon with EDC_J1 on sloped (placement 1) median.

Figure 4.38 shows the state of maximum deflection of the barrier. The maximum deflection was 1.89 meter and occurred at 1.02 seconds into the simulation.

The vehicle displacement in Y direction (transverse displacement) and the velocity in Y direction (transverse velocity), calculated at the CG (center of gravity) of the vehicle are shown in Figure 4.39. It can be observed from the transverse velocity plot that the change in velocity is gradual and it stays below 15 km/h after 1.5 seconds.

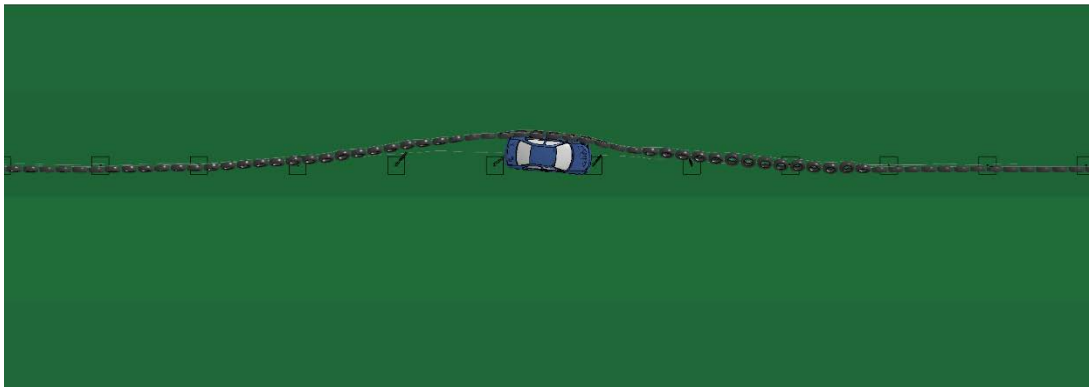

Top view

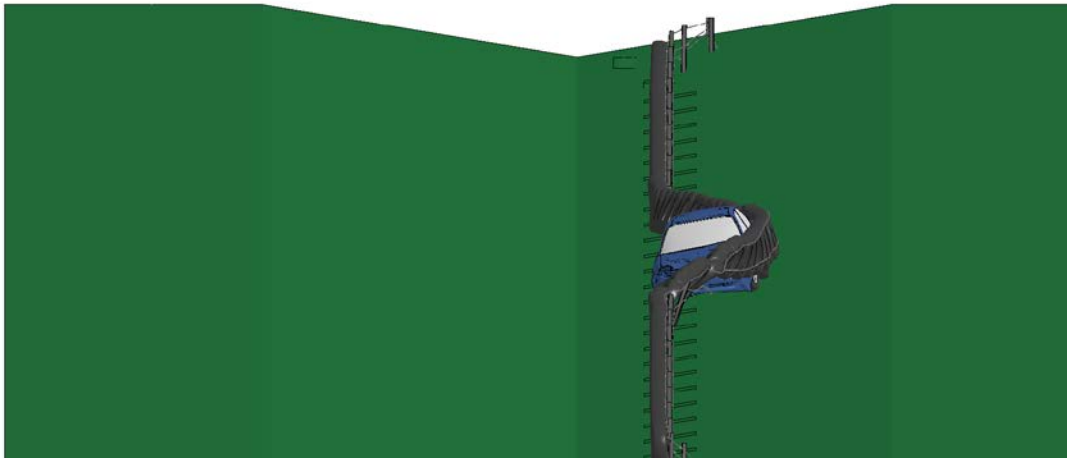

Front view

Figure 4.38: Maximum deflection of EDC_J1 for back side mid-span impact on sloped (placement 1) median.

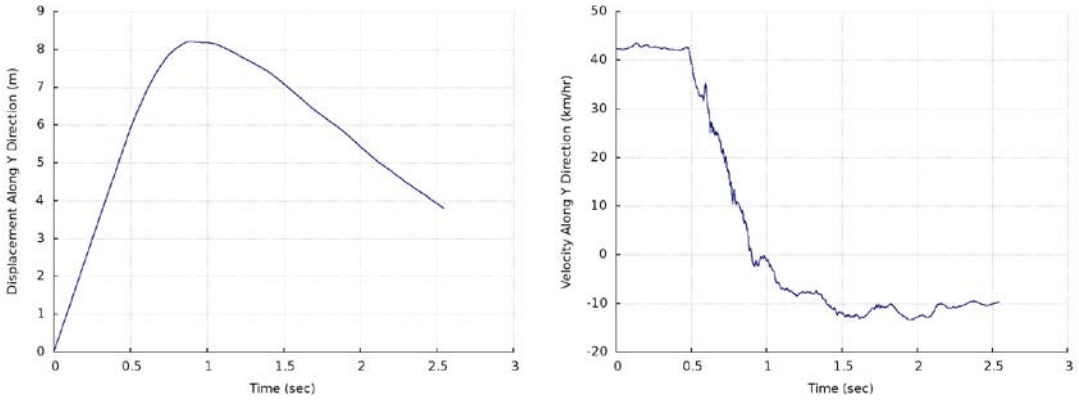

Transverse displacement Transverse velocity

Figure 4.39: Transverse displacement and velocity of Neon impacting the back side mid-span of EDC_J1 on sloped (placement 1) median.

4.2.2.3 Front side post impact

Figure 4.40 shows the vehicle trajectory of Dodge Neon impacting the EDC_J1 tire-cable median barrier. The EDC_J1 barrier is shown in its deformed state with the Neon tire tracks marked in white and the exit box shown in yellow. It can be observed that all four tire tracks of the vehicle fit in the exit box and thus this barrier design passes MASH exit box criterion N.

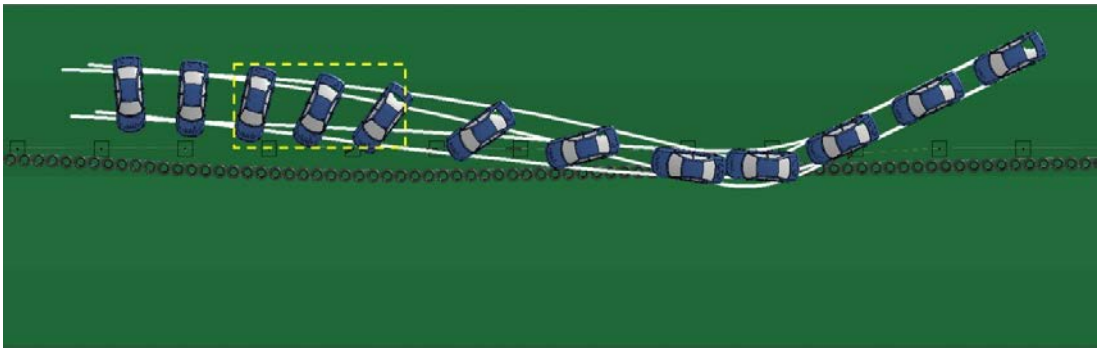

Figure 4.40: Vehicle trajectory and exit box for front side post impact of Neon with EDC_J1 on sloped (placement 1) median.

Figure 4.41 shows the yaw, pitch and roll angles of the vehicle. Both the pitch and roll angle values remain within a range of 15° and thus the barrier passes MASH

evaluation criterion F. The changes in yaw angle suggest that vehicle continues to spin out as it is being redirected resulting in loss of control for the driver.

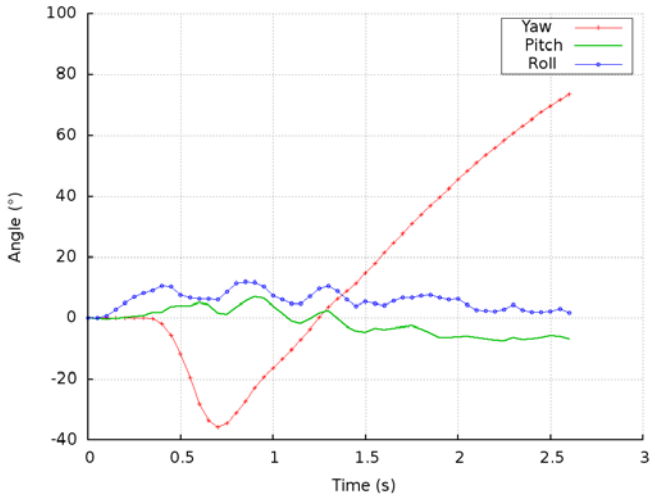

Figure 4.41: Yaw, pitch and roll angles for front side post of Neon with EDC_J1 on sloped (placement 1) median.

Figure 4.42 shows the state of maximum deflection of the barrier. The maximum deflection of the barrier was 2.19 meter and occurred at 0.69 seconds into the simulation. The vehicle displacement in Y direction (transverse displacement) and the velocity in Y direction (transverse velocity), calculated at the CG (center of gravity) of the vehicle are shown in Figure 4.43. It can be observed from the transverse velocity plot that the change in velocity is gradual and starts approaching zero at 2.5 seconds into the simulation.

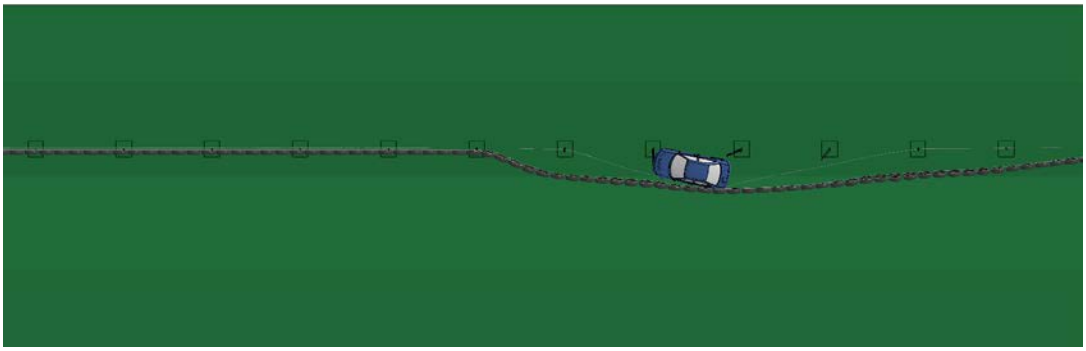

Top view

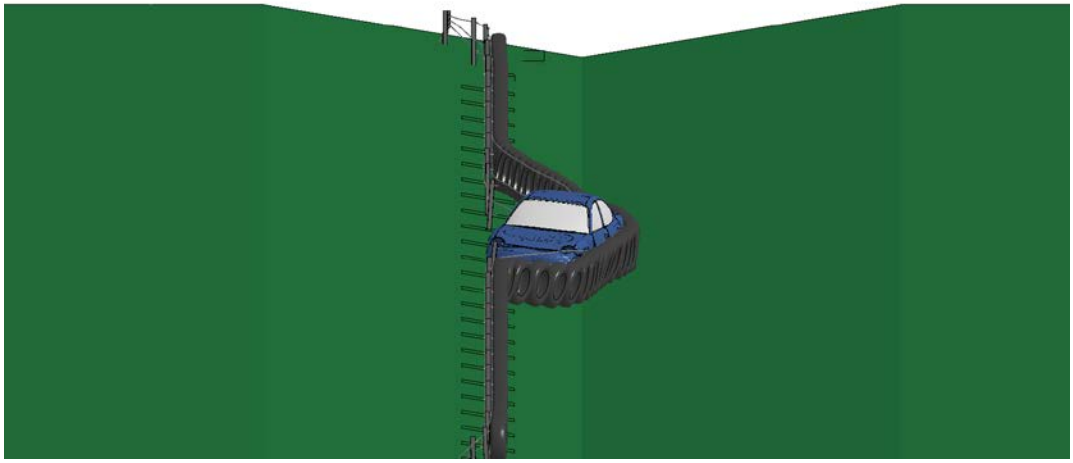

Front view

Figure 4.42: Maximum deflection of EDC_J1 for front side post impact on sloped (placement 1) median.

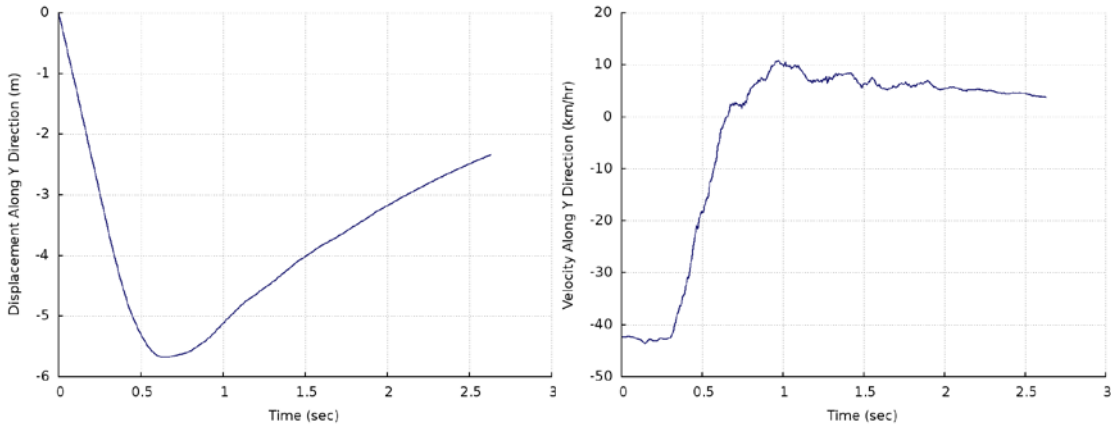

Transverse displacement

Transverse velocity

Figure 4.43: Transverse displacement and velocity of Neon impacting the front side post of EDC_J1 on sloped (placement 1) median.

4.2.2.4 Front side mid-span impact

Figure 4.44 shows the vehicle trajectory of Dodge Neon impacting the EDC_J1 tire-cable median barrier. The EDC_J1 barrier is shown in its deformed state with the Neon tire tracks marked in white and the exit box shown in yellow. It can be observed that all four tire tracks of the vehicle fit in the exit box and thus this barrier design passes MASH exit box criterion N.

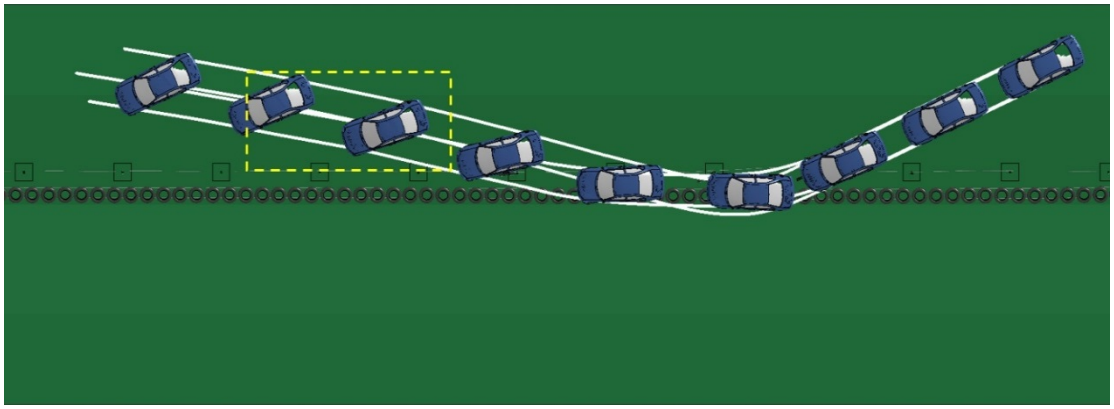

Figure 4.44: Vehicle trajectory and exit box for front side mid-span impact of Neon with EDC_J1 on sloped (placement 1) median.

Figure 4.45 shows the yaw, pitch and roll angles of the vehicle. Both the pitch and roll angle values remain well within a range of 15° and thus the simulation passes MASH evaluation criterion F. The changes in yaw angle suggest that vehicle continues to spin out as it is being redirected resulting in loss of control for the driver.

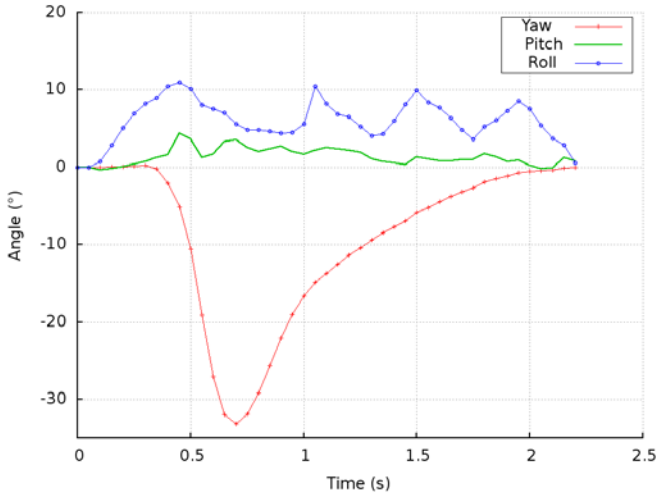

Figure 4.45: Yaw, pitch and roll angles for front side mid-span of Neon with EDC_J1 on sloped (placement 1) median.

Figure 4.46 shows the state of maximum deflection of the barrier. The maximum deflection of the barrier was 2.11 meter and occurred at 0.68 seconds into the simulation. The vehicle displacement in Y direction (transverse displacement) and the velocity in Y direction (transverse velocity), calculated at the CG (center of gravity) of the vehicle are shown in Figure 4.47. It can be observed from the transverse velocity plot that the change in velocity is gradual and peaks at 18 km/h.

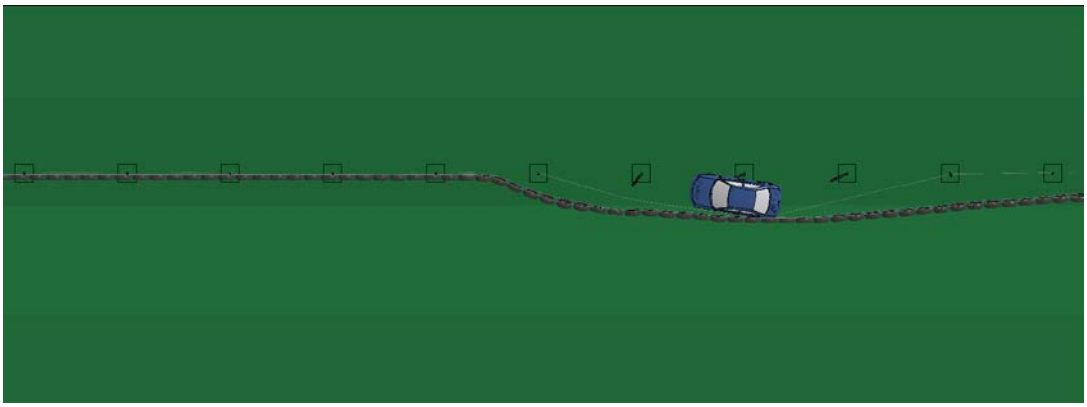

Top view

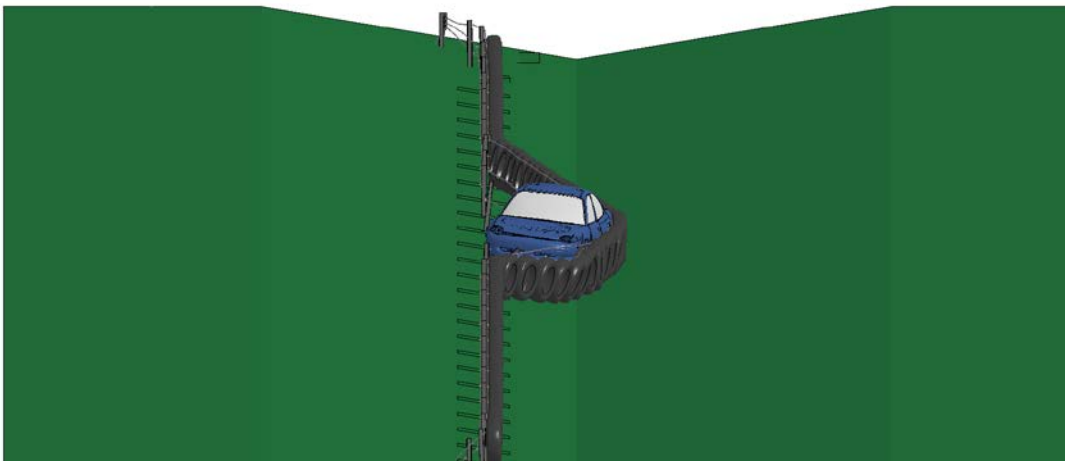

Front view

Figure 4.46: Maximum deflection of EDC_J1 for front side mid-span impact on sloped (placement 1) median.

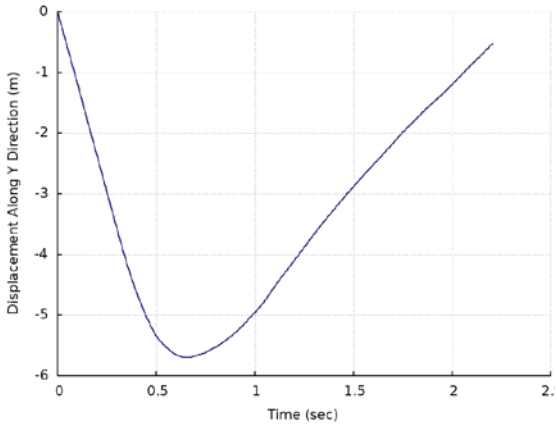

Transverse displacement

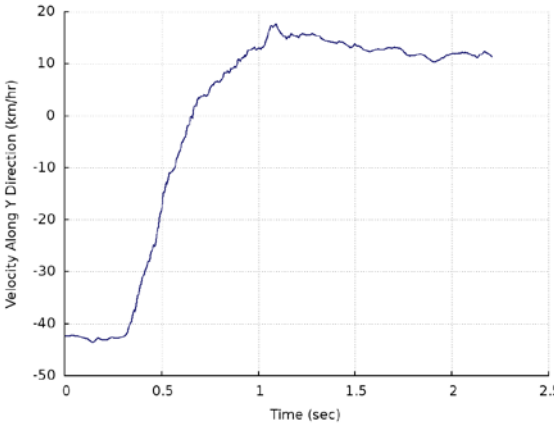

Transverse velocity

Figure 4.47: Transverse displacement and velocity of Neon impacting the front side mid-span of EDC_J1 on sloped (placement 1) median.

4.2.3 Sloped median (placement 2)

4.2.3.1 Front side post impact

Figure 4.48 shows the vehicle trajectory of Dodge Neon impacting the EDC_J1 tire-cable median barrier. The EDC_J1 barrier is shown in its deformed state with the Neon tire tracks marked in white. It can be observed that the vehicle penetrates the barrier and hence an exit box has not been shown for this case.

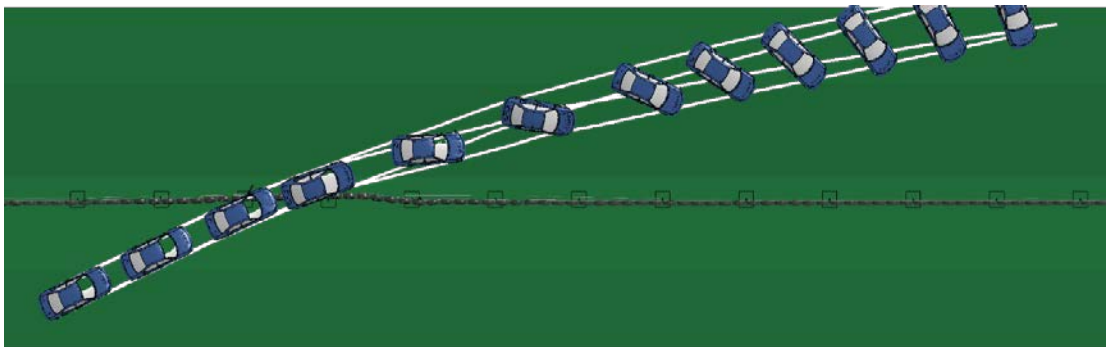

Figure 4.48: Vehicle trajectory for front side post impact of Neon with EDC_J1 on sloped (placement 2) median.

Figure 4.49 shows the yaw, pitch and roll angles of the vehicle. Both the pitch and roll angle values remain within a range of 20° and thus the barrier passed MASH evaluation criterion F. The changes in yaw angle suggest that vehicle spins out as it travels towards the opposing travel lane and increases the possibility of secondary collision.

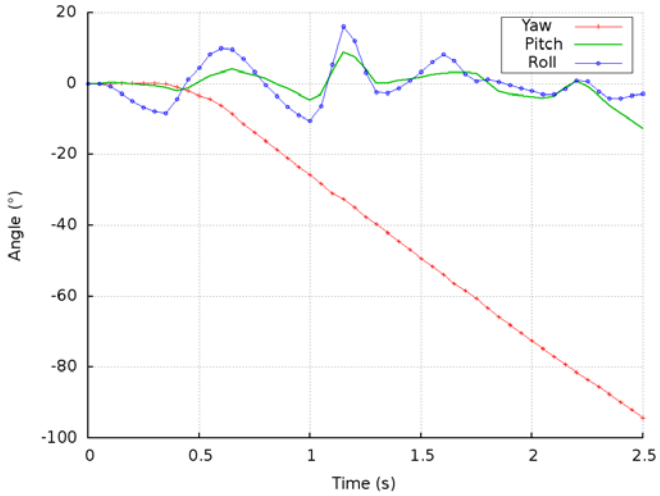

Figure 4.49: Yaw, pitch and roll angles for front side post of Neon with EDC_J1 on sloped (placement 2) median.

Figure 4.50 shows the state of maximum deflection of the barrier. The maximum deflection of the barrier was 1.28 meter before the vehicle overrode it and occurred at 0.46 seconds into the simulation. In this case, the post bends immediately upon impact by the vehicle and takes down the attached cables and barrier tires with it. This creates a ramp like area at the impact location and the vehicle is easily able to override the barrier and move to the opposing travel lane without much resistance. Figure 4.51 shows the vehicle barrier interaction for this case.

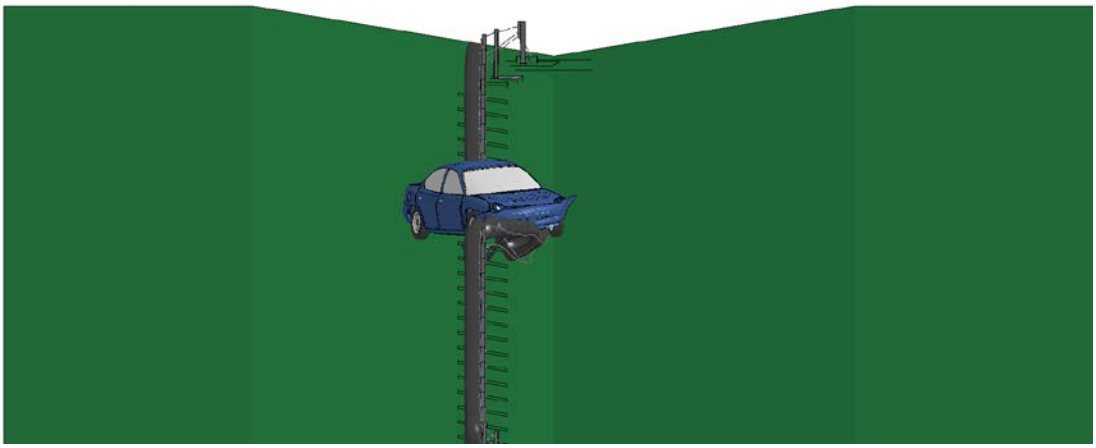

Figure 4.50: Maximum deflection of EDC_J1 for front side post impact on sloped (placement 2) median.

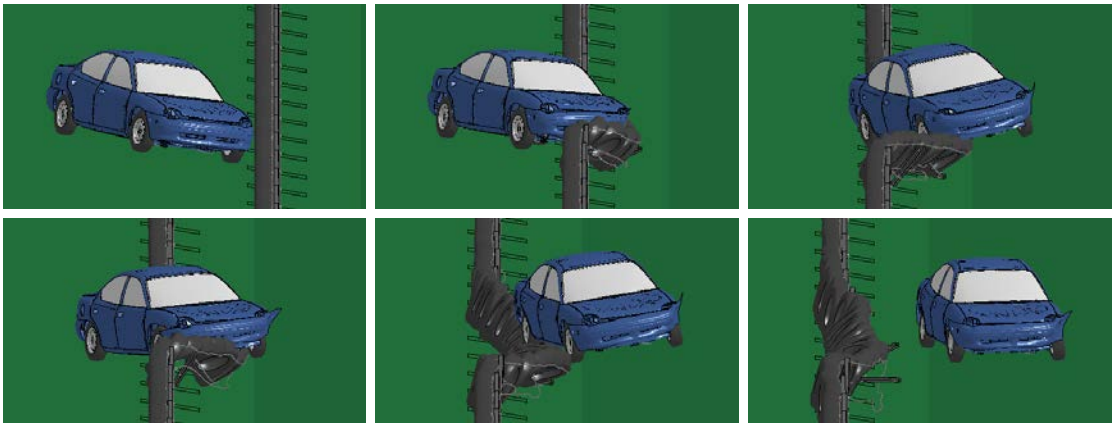

Figure 4.51: Neon interaction with EDC_J1 on sloped (placement 2) median for front side post impact.

The vehicle displacement in Y direction (transverse displacement) and the velocity in Y direction (transverse velocity), calculated at the CG (center of gravity) of the vehicle are shown in Figure 4.52. It can be observed that the displacement graph shows a continuous increase in the transverse displacement value indicating non-redirection of the vehicle. The transverse velocity also appears to have reduced but does not go below 13 km/h indicating a high possibility of secondary collision with the oncoming vehicles in the opposing lane.

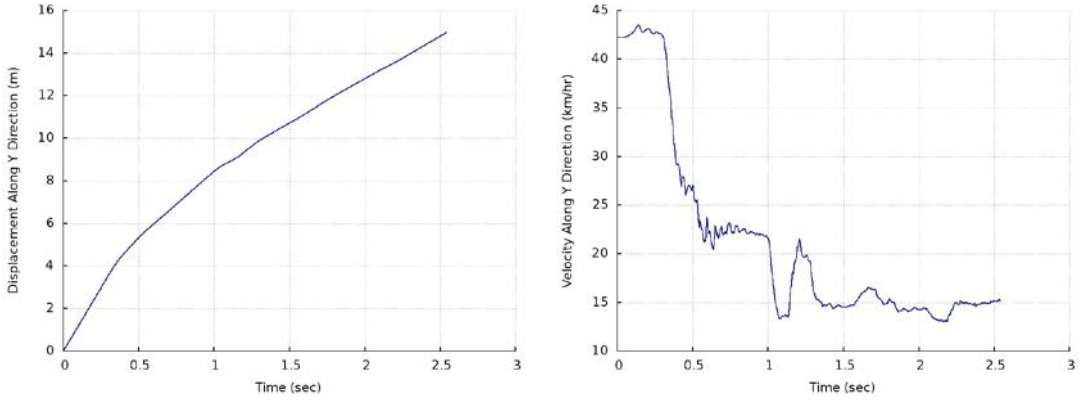

Transverse displacement Transverse velocity

Figure 4.52: Transverse displacement and velocity of Neon impacting the front side post of EDC_J1 on sloped (placement 2) median.

4.2.3.2 Front side mid-span impact

Figure 4.53 shows the vehicle trajectory of Dodge Neon impacting the EDC_J1 tire-cable median barrier. The EDC_J1 barrier is shown in its deformed state with the Neon tire tracks marked in white and the exit box shown in yellow. It can be observed that all four tire tracks of the vehicle fit in the exit box and thus this barrier design passes MASH exit box criterion N.

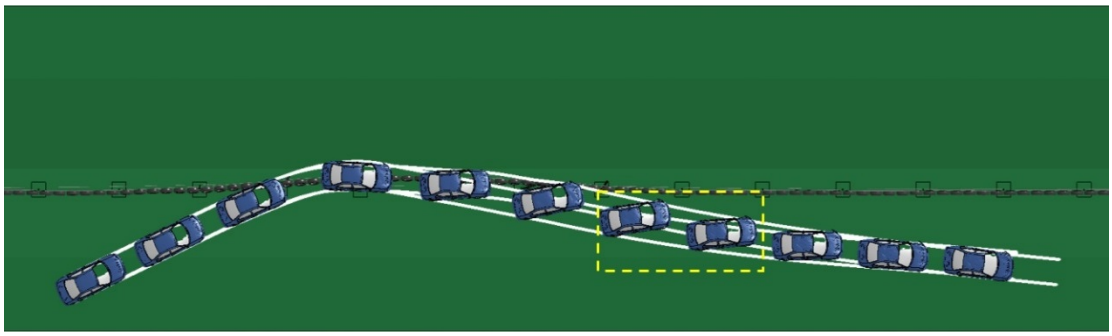

Figure 4.53: Vehicle trajectory and exit box for front side mid-span impact of Neon with EDC_J1 on sloped (placement 2) median.

Figure 4.54 shows the yaw, pitch and roll angles of the vehicle. Both the pitch and roll angle values remain well within a range of 15° and thus the barrier passes MASH evaluation criterion F. The changes in yaw angle suggest that vehicle does not spin out while being redirected and thus provides better control to the driver post redirection.

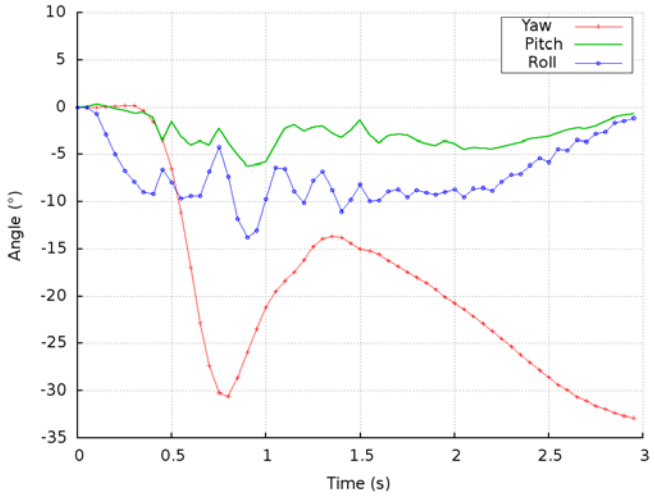

Figure 4.54: Yaw, pitch and roll angles for front side mid-span of Neon with EDC_J1 on sloped (placement 2) median.

Figure 4.55 shows the state of maximum deflection of the barrier. The maximum displacement of the barrier was 2.01 meter and occurred at 0.75 seconds into the simulation. The vehicle displacement in Y direction (transverse displacement) and the velocity in Y direction (transverse velocity), calculated at the CG (center of gravity) of the vehicle are shown in Figure 4.56. It can be observed from the transverse velocity plot that the change in velocity is gradual but it does not stabilize and may reduce further.

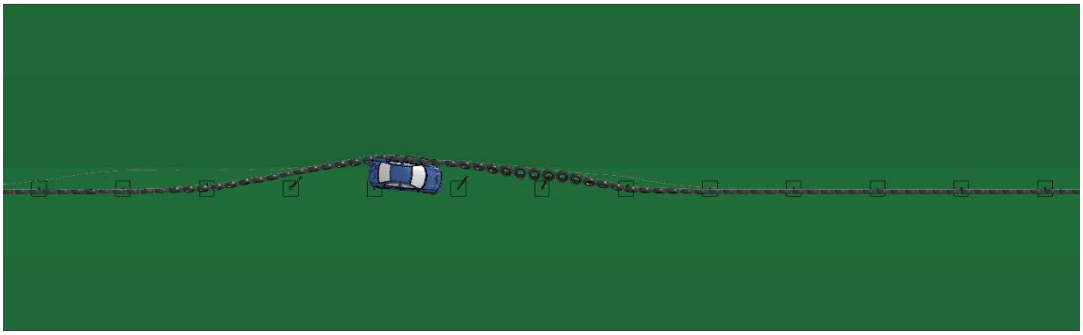

Top view

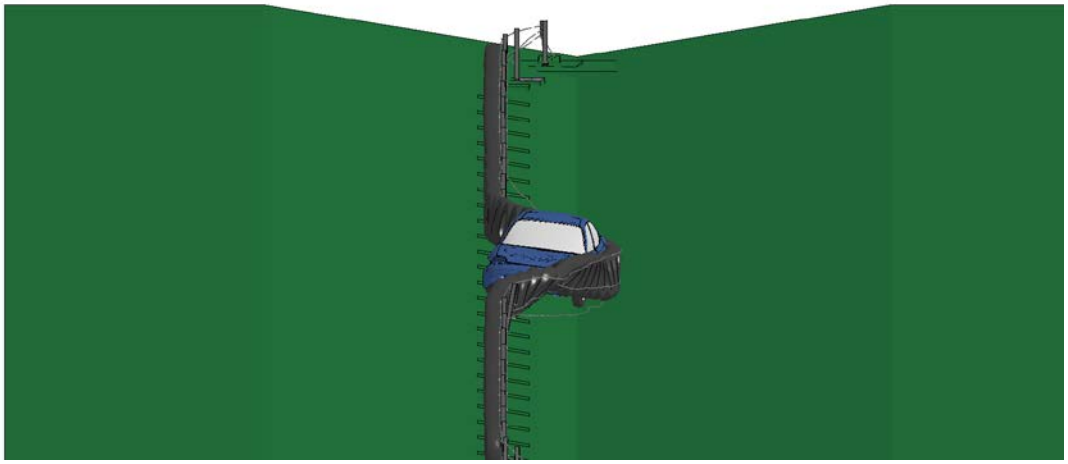

Front view

Figure 4.55: Maximum deflection of EDC_J1 for front side mid-span impact on sloped (placement 2) median.

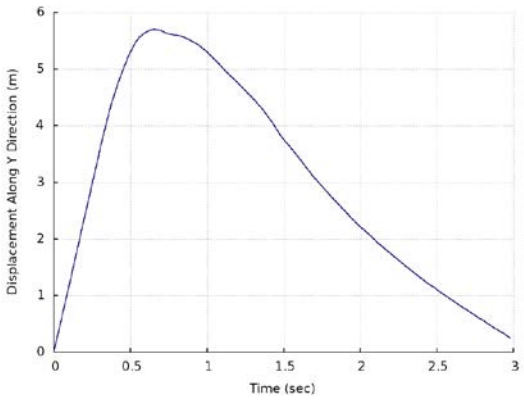

Transverse displacement

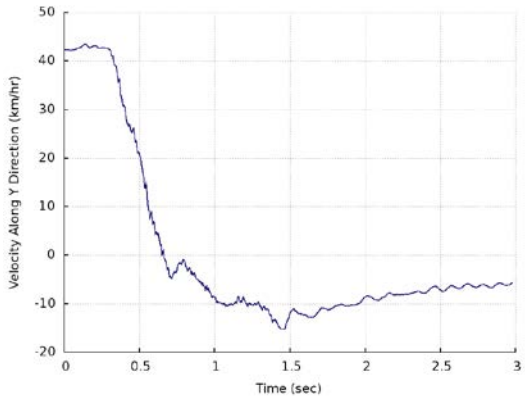

Transverse velocity

Figure 4.56: Transverse displacement and velocity of Neon impacting the front side mid-span of EDC_J1 on sloped (placement 2) median.

4.2.3.3 Back side post impact

Figure 4.57 shows the vehicle trajectory of Dodge Neon impacting the EDC_J1 tire-cable median barrier. The EDC_J1 barrier is shown in its deformed state with the

Neon tire tracks marked in white. At the end of the simulation, the vehicle is redirected and remains in contact with the barrier and hence no exit box is shown.

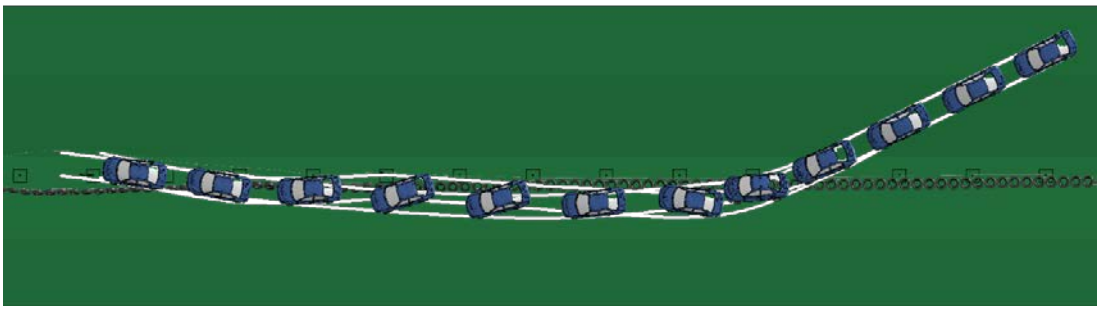

Figure 4.57: Vehicle trajectory for back side post impact of Neon with EDC_J1 on sloped (placement 2) median.

Figure 4.58 shows the yaw, pitch and roll angles of the vehicle. Both the pitch and roll angle values remain within the limit of 75° and thus the simulation passes MASH evaluation criterion F. The changes in yaw angle suggest that vehicle does not follow a smooth redirecting pattern.

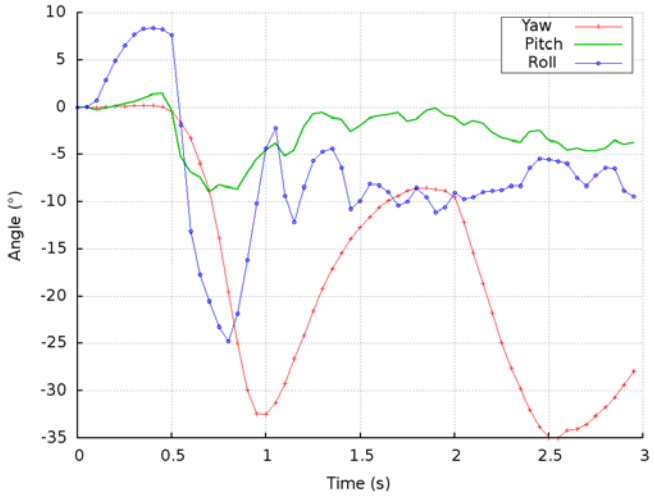

Figure 4.58: Yaw, pitch and roll angles for back side post impact of Neon with EDC_J1 on sloped (placement 2) median.

Figure 4.59 shows the state of maximum deflection of the barrier. The maximum deflection of the barrier was 2.78 meter and occurred at 1.47 seconds into the simulation. The vehicle displacement in Y direction (transverse displacement) and the velocity in Y direction (transverse velocity), calculated at the CG (center of gravity) of the vehicle are shown in Figure 4.60. It can be observed from the transverse velocity plot that the change in velocity is gradual and starts becoming zero towards the end of the simulation.

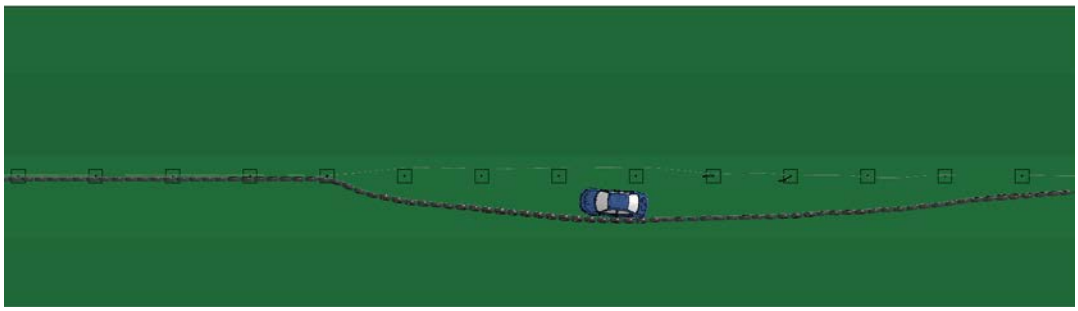

Top view

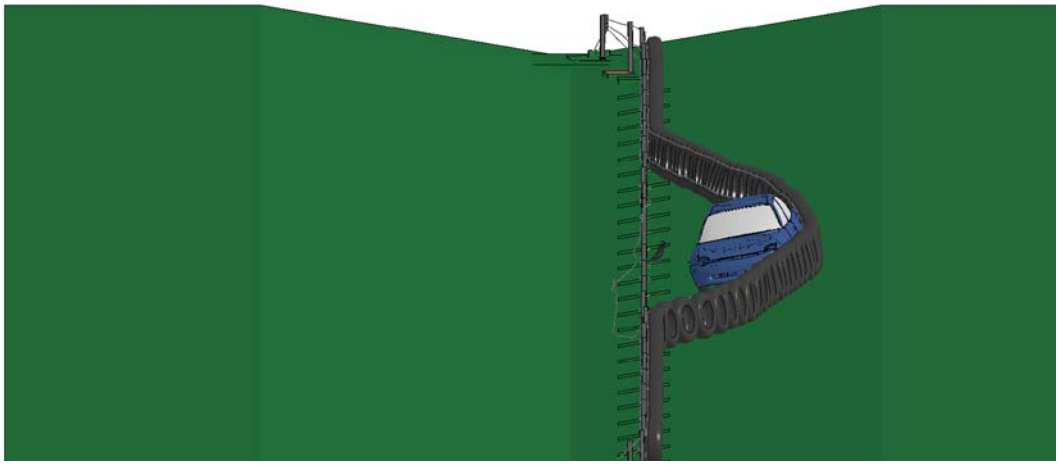

Front view

Figure 4.59: Maximum deflection of EDC_J1 for back side post impact on sloped (placement 2) median.

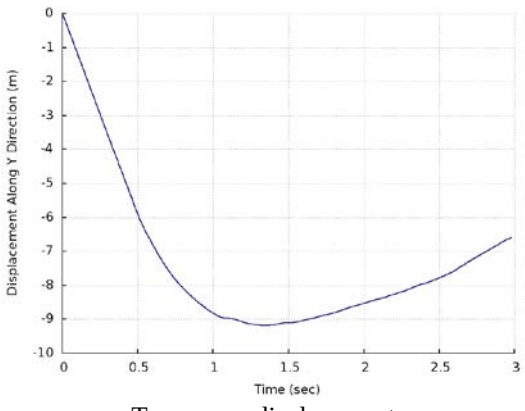

Transverse displacement

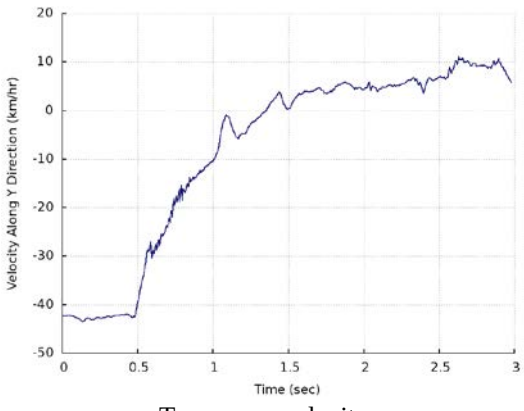

Transverse velocity

Figure 4.60: Transverse displacement and velocity of Neon impacting the back side post of EDC_J1 on sloped (placement 2) median.

4.2.3.4 Back side mid-span impact

Figure 4.61 shows the vehicle trajectory of Dodge Neon impacting the EDC_J1 tire-cable median barrier. The EDC_J1 barrier is shown in its deformed state with the Neon tire tracks marked in white. At the end of the simulation, the vehicle is redirected and remains in contact with the barrier and hence no exit box is shown.

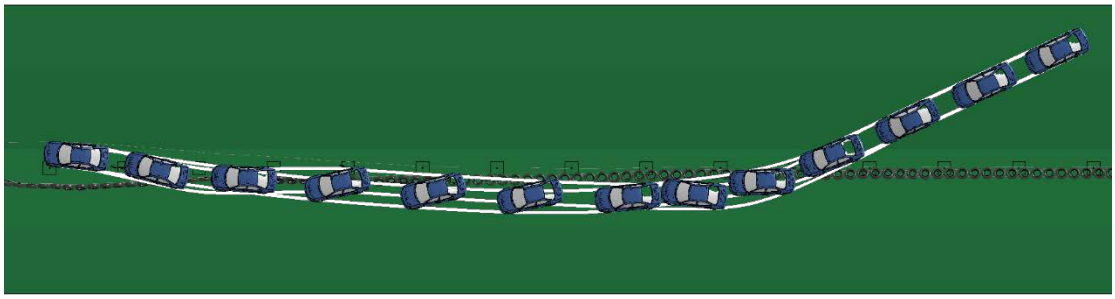

Figure 4.61: Vehicle trajectory and exit box for back side mid-span impact of Neon with EDC_J1 on sloped (placement 2) median.

Figure 4.62 shows the yaw, pitch and roll angles of the vehicle. Both the pitch and roll angle values remain well within a range of 15° and thus the barrier passed MASH evaluation criterion F. The changes in yaw angle suggest that vehicle does not follow a smooth redirecting pattern but no spin out was observed.

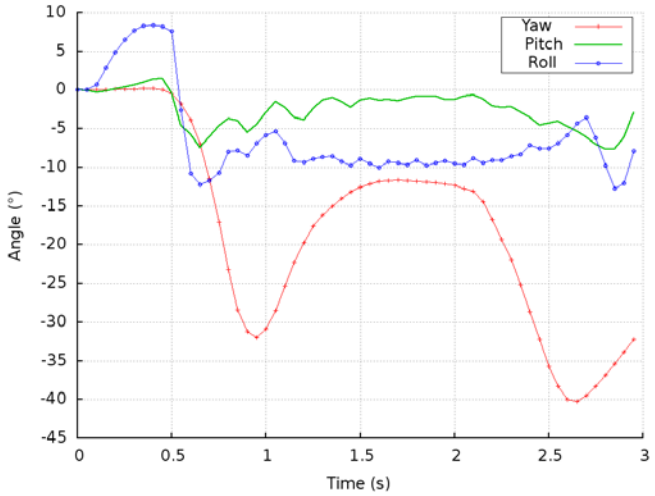

Figure 4.62: Yaw, pitch and roll angles for back side mid-span impact of Neon with EDC_J1 on sloped (placement 2) median.

Figure 4.63 shows the state of maximum deflection of the barrier. The maximum deflection of the barrier was 3.03 meter and occurred at 1.36 seconds into the simulation. The vehicle displacement in Y direction (transverse displacement) and the velocity in Y direction (transverse velocity), calculated at the CG (center of gravity) of the vehicle are shown in Figure 4.64. It can be observed from the transverse velocity plot that the change in velocity is gradual and starts becoming zero towards the end of the simulation.

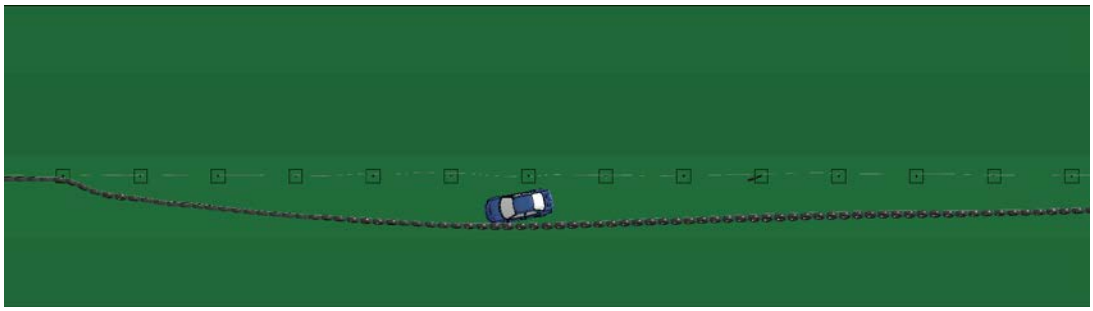

Top view

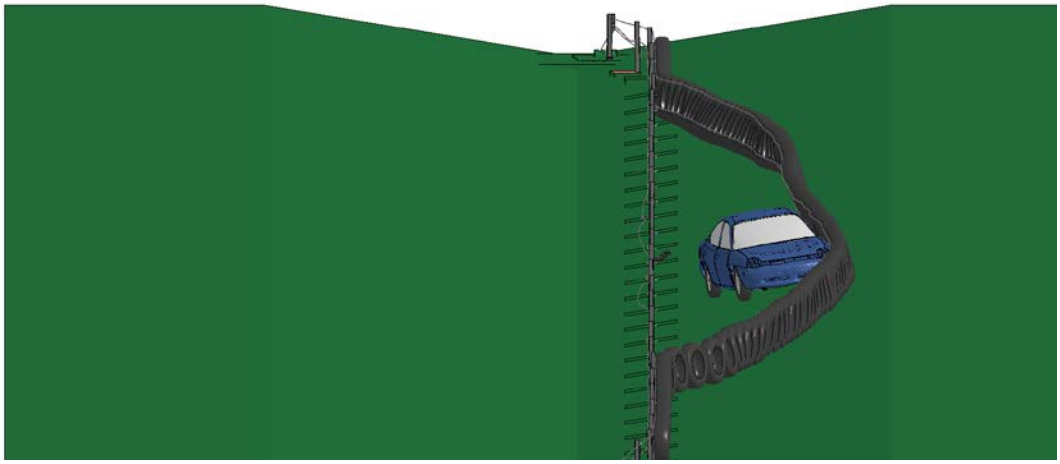

Front view

Figure 4.63: Maximum deflection of EDC_J1 for back side mid-span impact on sloped (placement 2) median.

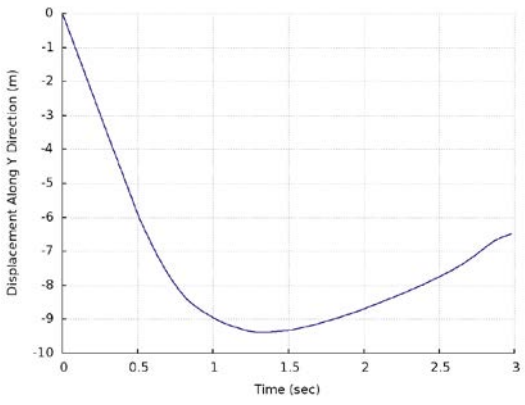

Transverse displacement

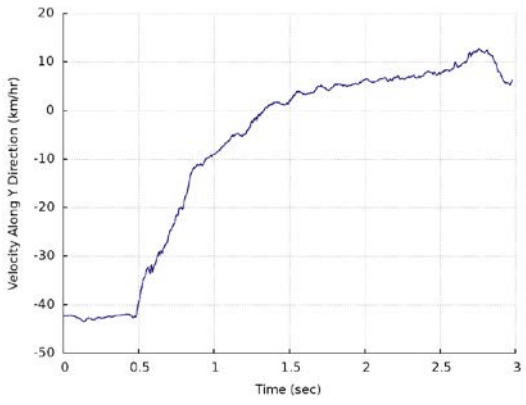

Transverse velocity

Figure 4.64: Transverse displacement and velocity of Neon impacting the back side mid-span of EDC_J1 on sloped (placement 2) median.

4.3 Case 3 simulations results

Case 3 simulations were planned to be conducted according to Table 3.3. However, a numerically stable model was not achieved for certain cases. A few simulations were completed without any major issues and others are still being debugged. Table 4.4 displays completed simulations for Case 3 along with the results for barrier designs.

Table 4.4: Results for Case 3.

Barrier	Median	Impact side	Impact point	Results
TCMB_U1	Flat	Front	Post	Override
EDC_U1	Flat	Front	Post	Override
EDC_J1	Sloped (placement 1)	Front	Post	Override
	Sloped (placement 1)	Back	Post	Redirected

4.3.1 Front side post impact on flat median for TCMB_U1

Figure 4.65 shows the vehicle trajectory of Ford F250 impacting the EDC_J1 tire-cable median barrier. The EDC_J1 barrier is shown in its deformed state with the F250 tire tracks marked in white. It can be seen that the truck does not redirect and lose contact with the barrier in this case and hence an exit box is not shown.

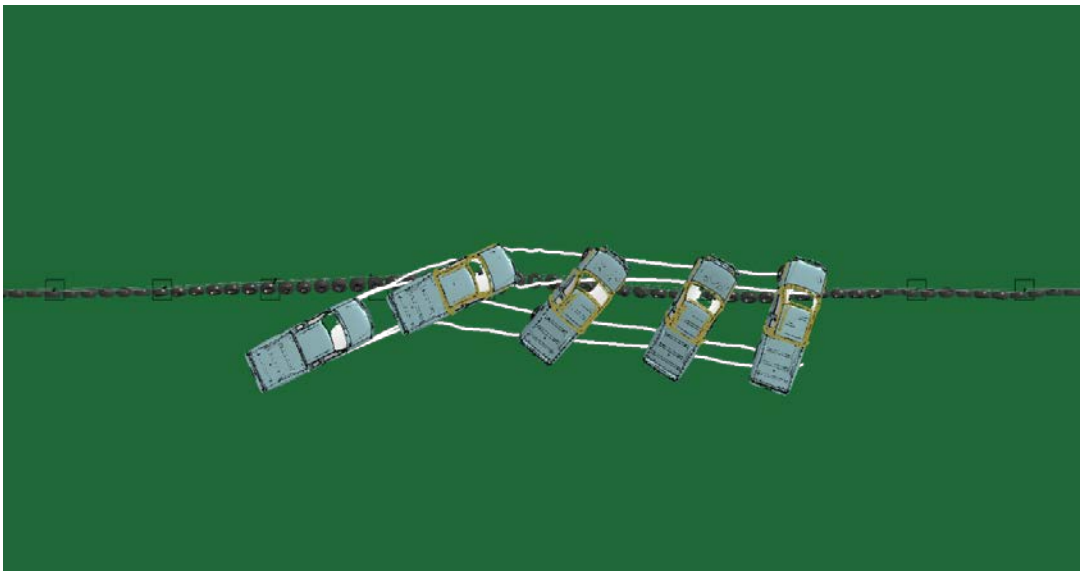

Figure 4.65: Vehicle trajectory for front side post impact of F250 with TCMB_U1 on flat median.

Figure 4.66 shows the yaw, pitch and roll angles of the vehicle. Both the pitch and roll angle values remain within the limit of 75° and thus the simulation passes MASH evaluation criterion F. The changes in yaw angle suggest that vehicle does not follow a smooth redirecting pattern.

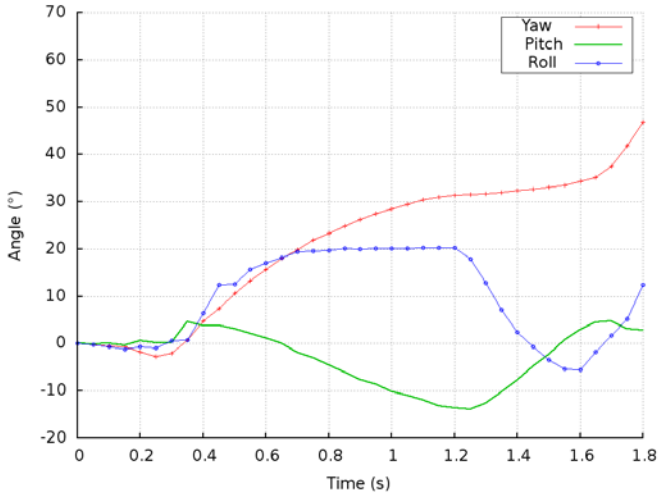

Figure 4.66: Yaw, pitch and roll angles for front side post of F250 with TCMB_U1 on flat median.

Figure 4.67 shows the state of maximum deflection of the barrier. This occurs at 0.31 secs into the simulation. For TCMB_U1 design an extra rigidity has been observed in the barrier due to the usage of U shaped hook bolts instead of J shaped hook bolts. The extra rigidity combined with movement of the lower part of the barrier tires makes this barrier inherently unstable. Due to this, the vehicle is unable to displace the barrier tires and cables in the transverse direction for a longer period of time resulting into excessive reaction force on the vehicle itself. In this case, the barrier tires turn the truck's front left tire exposing the anti-sway bar. The oscillating barrier tires pull on the anti-sway bar all the while keeping the truck tire turned. Since the cables and barrier tires cannot move laterally to absorb the impact, the truck is forced to move in the upward direction and is launched in the air and finally lands on the barrier. This is not a smooth redirection and can possibly be very dangerous to the passengers sitting inside the vehicle. Figure 4.68 shows the vehicle barrier interaction for this case.

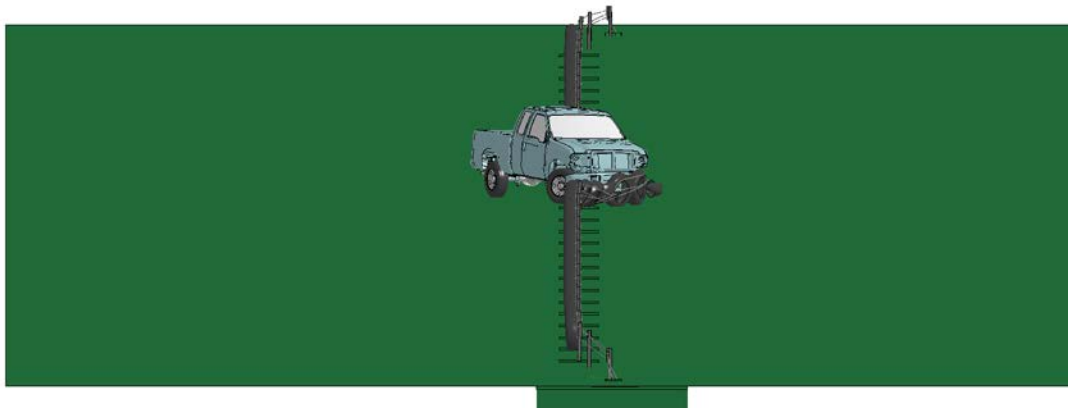

Figure 4.67: Maximum deflection of TCMB_U1 for front side post impact by F250 on flat median.

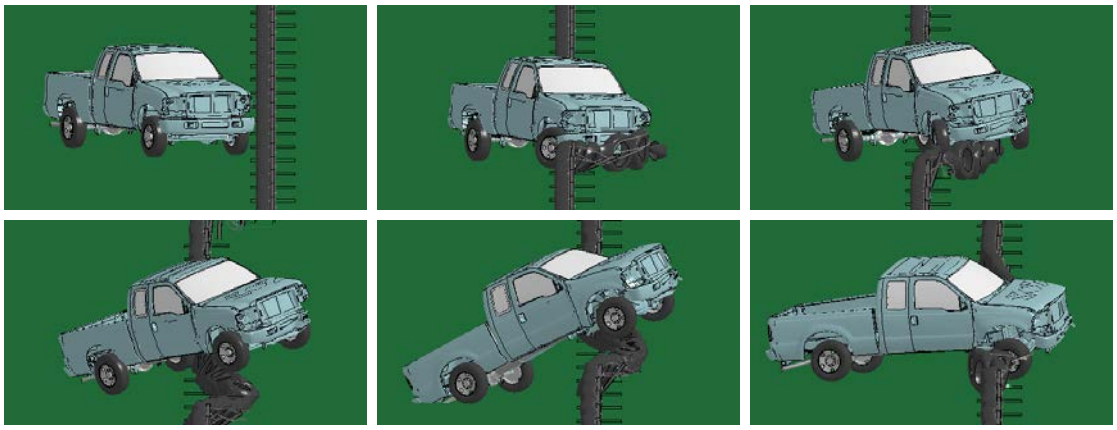

Figure 4.68: Ford interaction with TCMB_U1

The vehicle displacement in Y direction (transverse displacement) and the velocity in Y direction (transverse velocity), calculated at the CG (center of gravity) of the vehicle are shown in Figure 4.69. It can be seen from the displacement plot that the truck has been redirected however, a close look at the velocity profile suggests a sudden change in the direction and magnitude of the velocity in the transverse direction indicating that redirection was not smooth and possibly not safe.

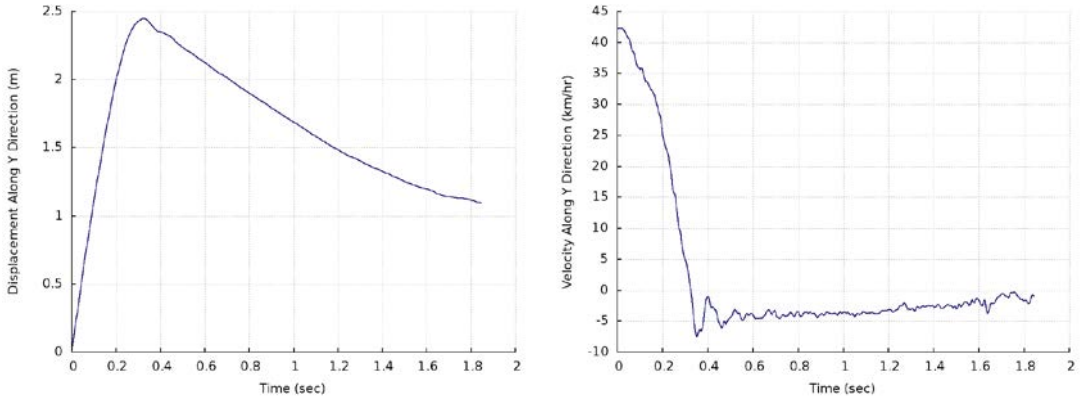

Transverse displacement Transverse velocity

Figure 4.69: Transverse displacement and velocity of F250 impacting the front side post of TCMB_U1 on flat median.

4.3.2 Front side post impact on flat median for EDC_U1

Figure 4.70 shows the vehicle trajectory of Ford F250 impacting the EDC_J1 tire-cable median barrier. The EDC_J1 barrier is shown in its deformed state with the F250 tire tracks marked in white. It can be observed that the vehicle penetrates the barrier and hence an exit box has not been shown for this case.

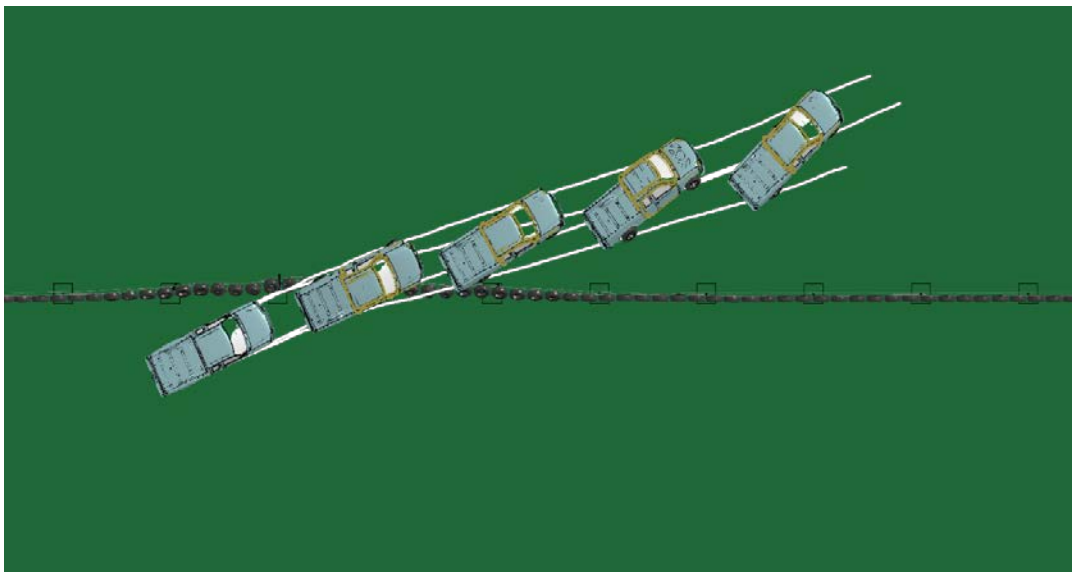

Figure 4.70: Vehicle trajectory for front side post impact of F250 with EDC_U1 on flat median.

Figure 4.71 shows the yaw, pitch and roll angles of the vehicle. Both the pitch and roll angle values remain within the limit of 75° and thus the barrier passes MASH evaluation criterion F. The yaw angle does not diverge too much and is indicative of the fact that vehicle may not spin out after overriding the barrier.

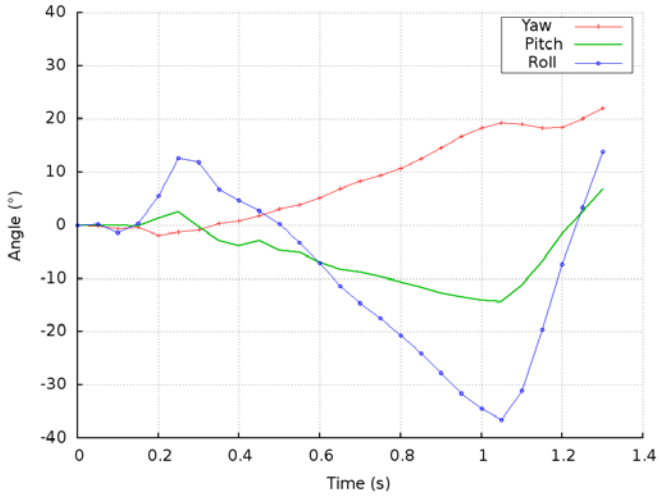

Figure 4.71: Yaw, pitch and roll angles for front side post of F250 with EDC_U1 on flat median.

Figure 4.72 shows the state of maximum deflection of the barrier. This occurs at 0.18 secs into the simulation. For EDC_U1 design an extra rigidity was observed in the barrier due to the usage of U shaped hook bolts. Due to this, the vehicle is unable to displace the barrier tires and cables in the transverse direction for a longer period of time resulting into excessive reaction force on the vehicle. Also as vehicle advances into the barrier, the extra rigidity forces cables and posts to bend which in turn bends the barrier tires creating a ramp. The vehicle is launched in the vertical direction due to the formation of this ramp and overrides the barrier proceeding towards the opposite travel lane. Figure 4.73 shows the vehicle barrier interaction for this case.

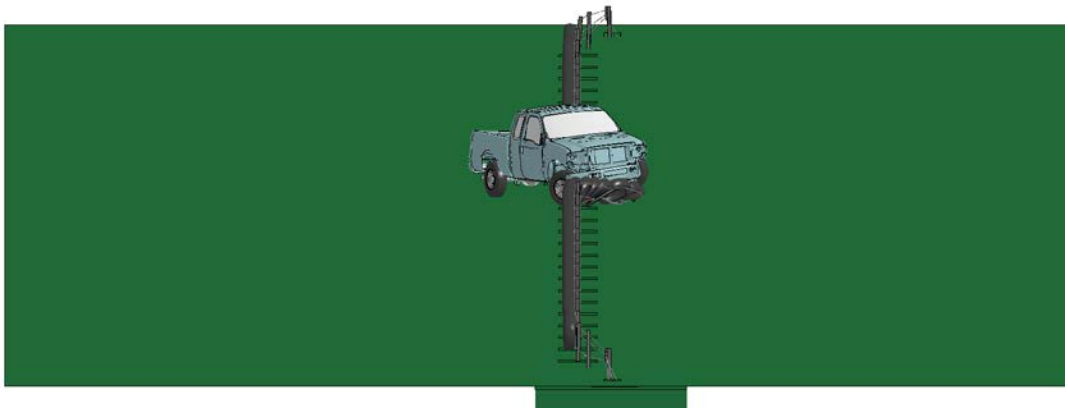

Figure 4.72: Maximum deflection of EDC_U1 for front side post impact by F250 on flat median.

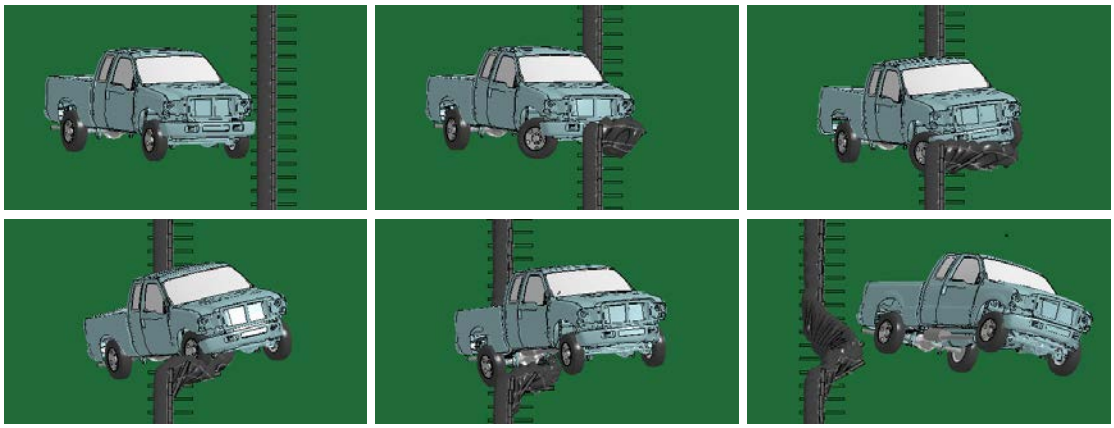

Figure 4.73: Ford interaction with EDC_U1

The vehicle displacement in Y direction (transverse displacement) and the velocity in Y direction (transverse velocity), calculated at the CG (center of gravity) of the vehicle are shown in Figure 4.74. It can be observed that the displacement graph shows a continuous increase in the transverse displacement value indicating non-redirection of the vehicle. The transverse velocity also appears to have reduced but does not go below 20 km/h indicating a high possibility of secondary collision with the oncoming vehicles in the opposing lane.

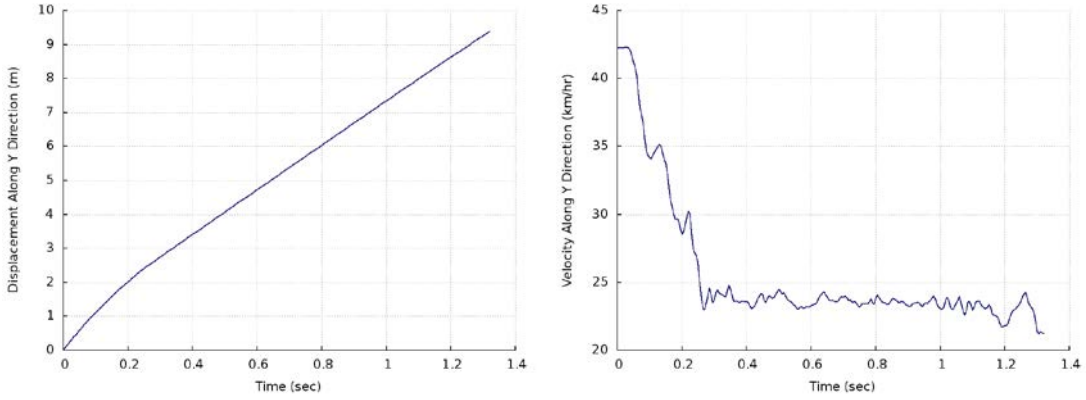

Transverse displacement Transverse velocity

Figure 4.74: Transverse displacement and velocity of F250 impacting the front side post of EDC_U1 on flat median.

4.3.3 Back side post impact on sloped (placement 1) median for EDC_J1

Figure 4.75 shows the vehicle trajectory of Ford F250 impacting the EDC_J1 tire-cable median barrier. The EDC_J1 barrier is shown in its deformed state with the F250 tire tracks marked in white. It can be observed that the vehicle penetrates the barrier and hence an exit box has not been shown for this case.

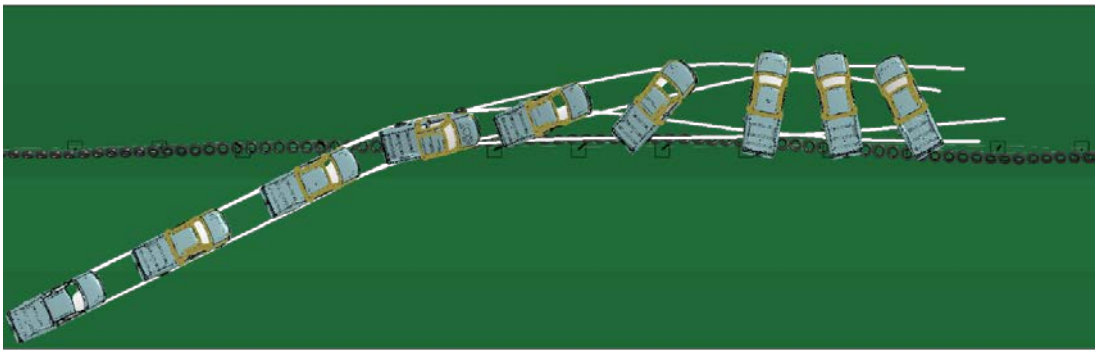

Figure 4.75: Vehicle trajectory and exit box for back side post impact of F250 with EDC_J1 on sloped (placement 1) median.

Figure 4.76 shows the yaw, pitch and roll angles of the vehicle. Both the pitch and roll angle values remain within a range of 20° and thus the simulation passes MASH evaluation criterion F. The changes in yaw angle suggest that vehicle appears to redirect after impact however, later on the continuous increase in the positive direction indicates that the vehicle spins inwards as it penetrates the barrier.

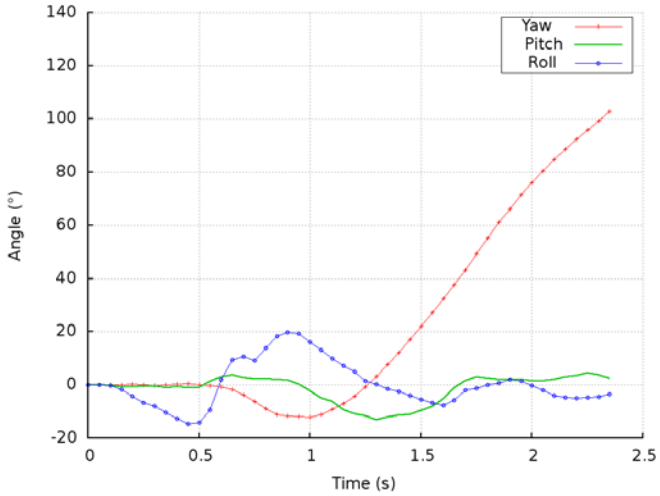

Figure 4.76: Yaw, pitch and roll angles for back side post of F250 with EDC_J1 on sloped (placement 1) median.

Figure 4.77 shows the state of maximum deflection of the barrier. This occurs at 1.26 seconds into the simulation. In this case, the post bends immediately upon impact by the vehicle and takes down the attached cables and barrier tires with it. This creates a ramp like area at the impact location and the vehicle is easily able to override the barrier and move to the opposite travel lane without much resistance. The front tires of the truck override the barrier and land on the shoulder of the opposite lane. At this moment, the rear tires are still in contact with the barrier tires. This causes the truck to spin in a counter clockwise direction causing the rear tires to lose contact with the barrier and override it. Figure 4.78 shows the vehicle barrier interaction for this case.

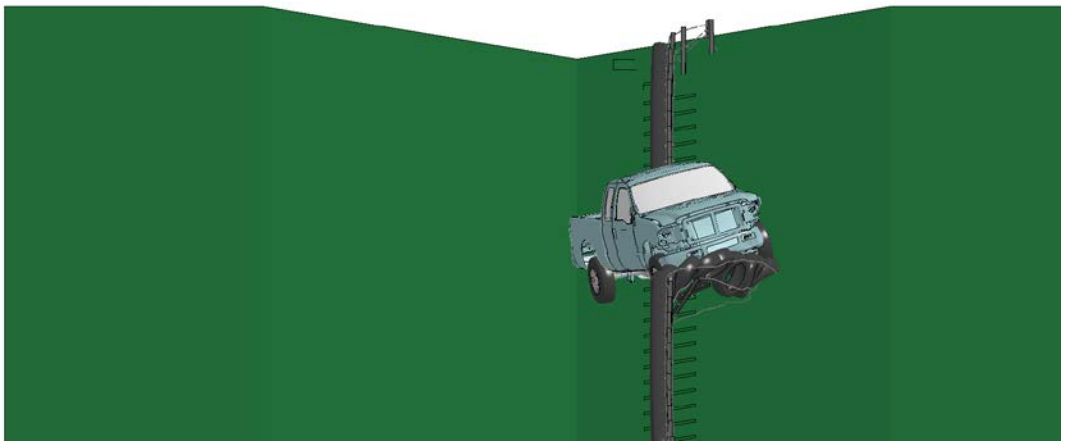

Figure 4.77: Maximum deflection of EDC_J1 for back side post impact by F250 on sloped (placement 1) median.

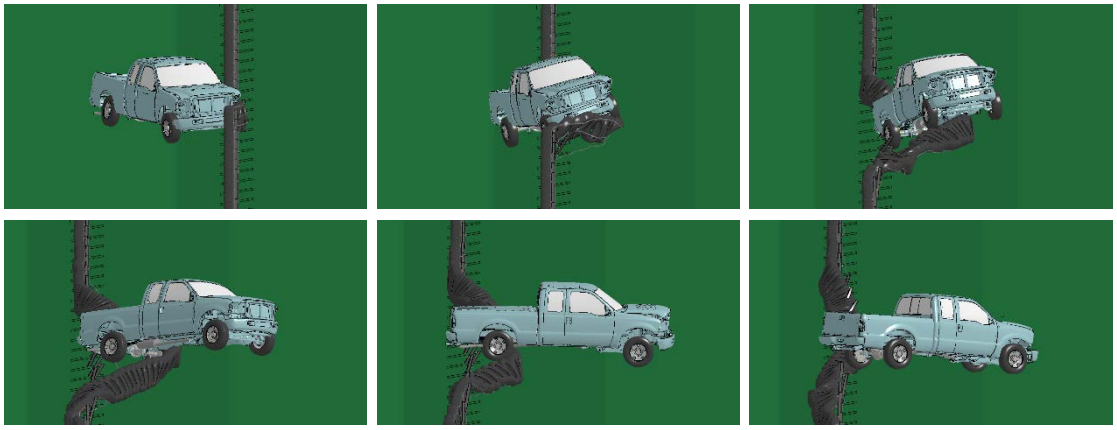

Figure 4.78: Ford interaction with EDC_J1 on sloped (placement 1) median for back side post impact

The vehicle displacement in Y direction (transverse displacement) and the velocity in Y direction (transverse velocity), calculated at the CG (center of gravity) of the vehicle are shown in Figure 4.79. It can be observed that the displacement graph shows a continuous increase in the transverse displacement value indicating non-redirection of the vehicle. The transverse velocity also appears to have reduced and goes below 0 km/h indicating a low probability of the truck crashing into oncoming vehicles in the opposite lane.

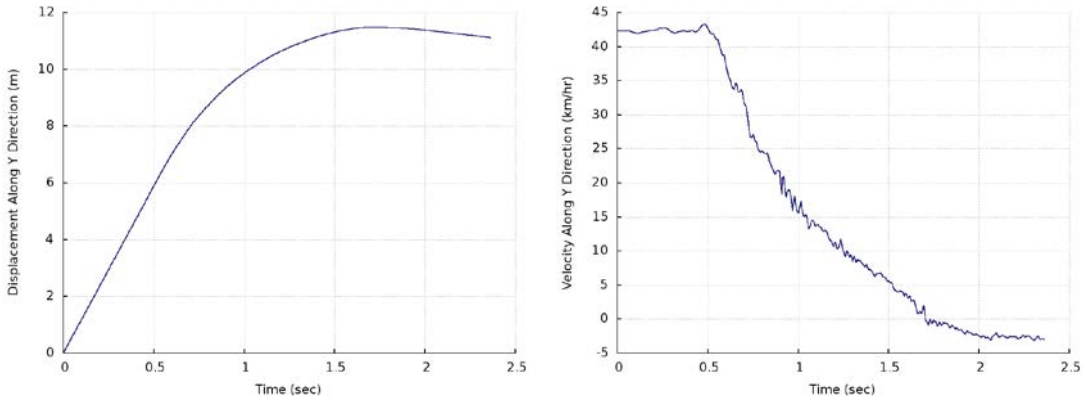

Transverse displacement Transverse velocity

Figure 4.79: Transverse displacement and velocity of F250 impacting the back side post of EDC_J1 on sloped (placement 1) median.

4.3.4 Front side post impact on sloped (placement 1) median for EDC_J1

Figure 4.80 shows the vehicle trajectory of Dodge Neon impacting the EDC_J1 tire-cable median barrier. The EDC_J1 barrier is shown in its deformed state with the F250 tire tracks marked in white and the exit box shown in yellow. At the end of simulation, the vehicle has lost contact with the barrier and it can be extrapolated that EDC_J1 passes MASH exit box criterion N based on Figure 4.80 and Figure 4.81 which shows constant yaw angle values after 2.5 seconds.

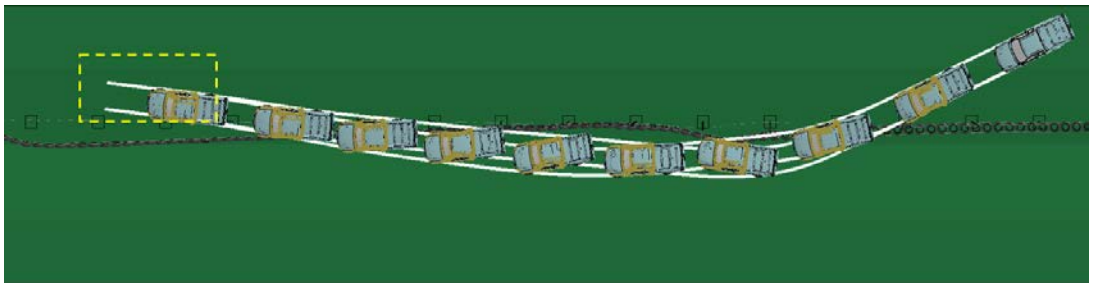

Figure 4.80: Vehicle trajectory and exit box for front side post impact of F250 with EDC_J1 on sloped (placement 1) median.

Figure 4.81 shows the yaw, pitch and roll angles of the vehicle. Both the pitch and roll angle values remain well within a range of 20° and thus the simulation passes MASH evaluation criterion F.

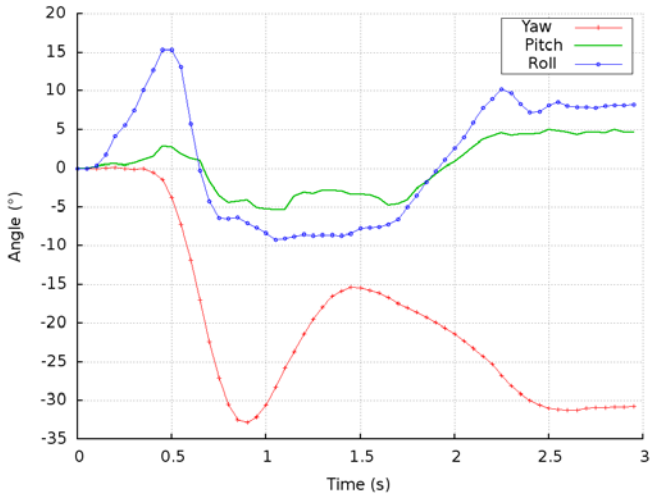

Figure 4.81: Yaw, pitch and roll angles for front side post of F250 with EDC_J1 on sloped (placement 1) median.

Figure 4.82 shows the state of maximum deflection of the barrier. This occurs at 0.95 seconds into the simulation. The vehicle displacement in Y direction (transverse displacement) and the velocity in Y direction (transverse velocity), calculated at the CG (center of gravity) of the vehicle are shown in Figure 4.83. It can be observed from the transverse velocity plot that the change in velocity is gradual and vehicle velocity starts reducing after 2.5 seconds.

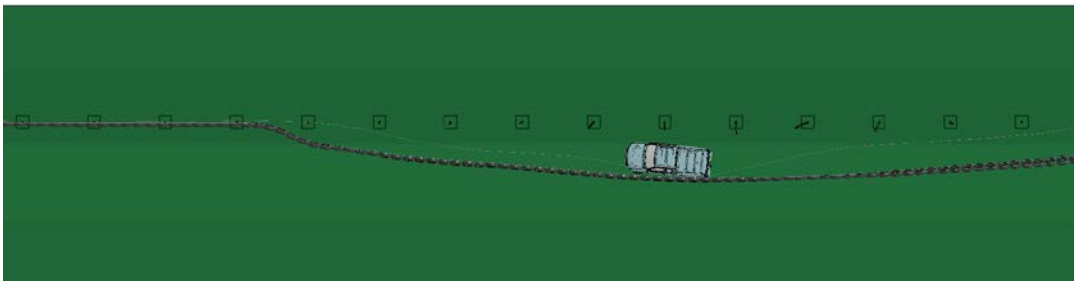

Top view

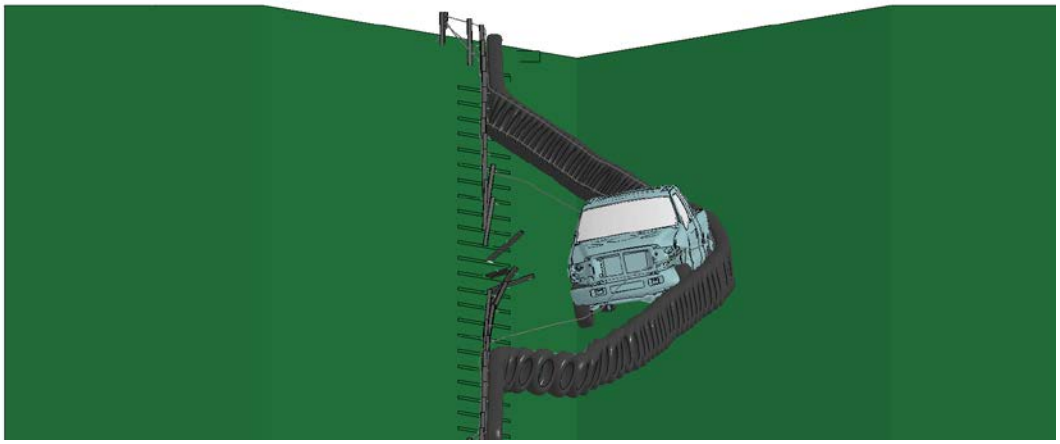

Front view

Figure 4.82: Maximum deflection of EDC_J1 for front side post impact by F250 on sloped (placement 1) median.

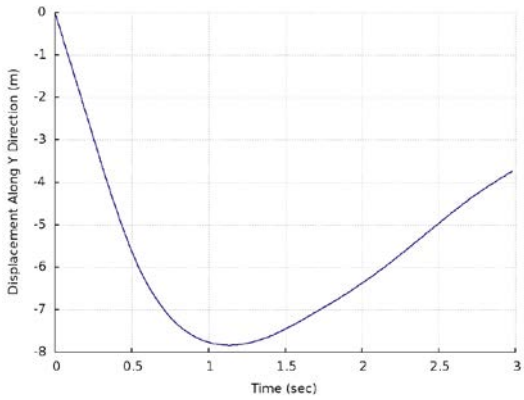

Transverse displacement

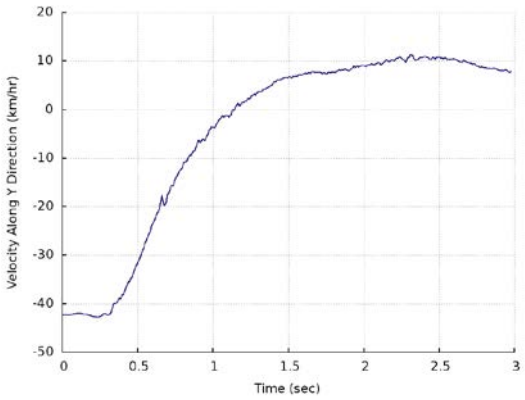

Transverse velocity

Figure 4.83: Transverse displacement and velocity of F250 impacting the front side post of EDC_J1 on sloped (placement 1) median.

CHAPTER 5 : COMPARISON OF TIRE-CABLE MEDIAN BARRIER WITH CURRENT DESIGN CABLE MEDIAN BARRIER

In this chapter, simulation results presented in chapter 4 have been compared with the results of full scale crash simulations conducted for the NCDOT project 2017-13. The NCDOT project focused on evaluation of two retrofit cable median barrier designs along with the evaluation of current NCDOT design for cable barriers on flat and sloped medians. Results from the impact simulations on flat and sloped medians for the current cable barrier were compared to results from impact simulations on flat and sloped (placement 2) medians for the EDC_J1 tire-cable median barrier.

The comparison criteria included maximum barrier deflection, post impact trajectory, barrier damage evaluation, post impact vehicle velocity and remarks on vehicle barrier interaction. The barrier damage criterion included posts that were bent or severely distorted and would need to be replaced completely. It also included damage to the hook bolts that failed by yielding on undamaged posts and would need replacement. Post impact behavior of the vehicle was compared with the help of post impact trajectory of the vehicle, its yaw, pitch and roll angles and the velocity profile of the vehicle. Maximum barrier deflection was the maximum movement of the barrier in the transverse direction (Y direction) and is indicative of the stiffness of the barrier. Vehicle barrier interaction was studied to account for cables that overrode, underrode and engaged the vehicle. Due to limited results available for the Ford F250 truck, comparisons were made only for Dodge Neon. Table 5.1 provides an overview of the results for current design and EDC_J1 tire-cable design.

Table 5.1: Comparison of results for current design and EDC_J1 barrier.

Median	Impact side and point	Current design results	EDC_J1 results
Flat median	Front side post	Redirected	Redirected
	Front side mid-span	Redirected	Redirected
	Back side post	Redirected	Redirected
	Back side mid-span	Penetrated	Redirected
Sloped median	Front side post	Overturned	Override
	Front side mid-span	Redirected	Redirected
	Back side post	Penetrated	Redirected
	Back side mid-span	Penetrated	Redirected

5.1 Front side post impact on flat median

Figure 5.1 shows the post impact trajectory of Dodge Neon for current NCDOT cable median barrier design and EDC_J1 tire-cable median barrier design. In both cases, the vehicle is redirected by the barrier. It can be clearly seen that the current design does not pass MASH exit box criterion but EDC_J1 design does. Figure 5.2 shows a comparison of the yaw, pitch and roll angles for the two barrier designs. For both cases, the roll and pitch angles remain within the limit of 75° and thus pass MASH evaluation criterion F. Comparison of the yaw angle suggests that in case of current design the vehicle will continue to spin out as it is being redirected and for the EDC_J1 design it will continue to advance in an almost straight line providing for better control from the driver post redirection. Figure 5.3 shows the comparison of velocity profile of the vehicle between current design and EDC_J1 design. It can be seen that at a time of approximately 2.2 seconds into the simulation, the velocity of vehicle is around 66 km/h for current design and around 60 km/h for the EDC_J1 barrier. The velocity for EDC_J1

remains constant thereafter and a decrease in speed of about 40 km/h is observed for EDC_J1 barrier as compared to a decrease of 34 km/h for the current design.

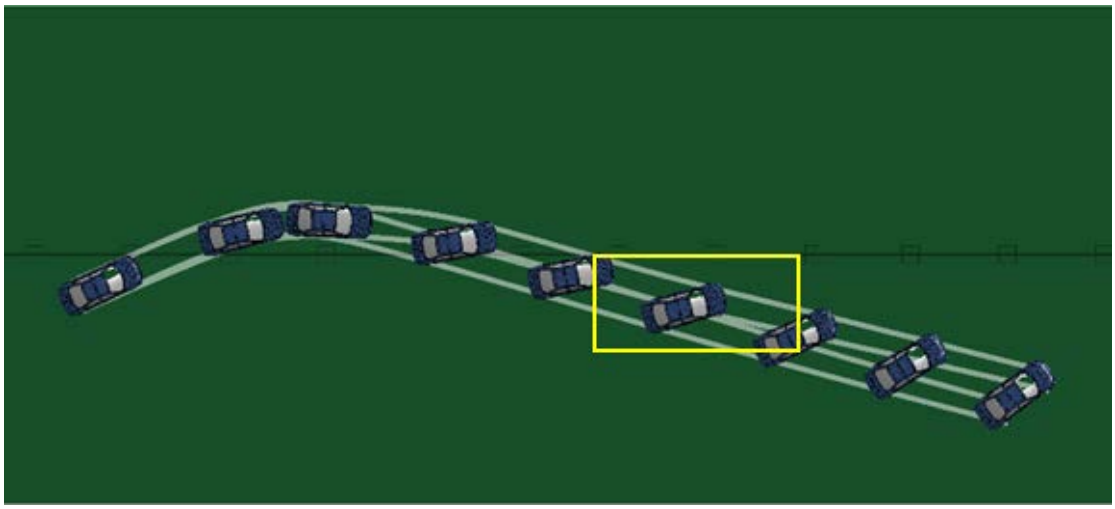

Vehicle trajectory for current design

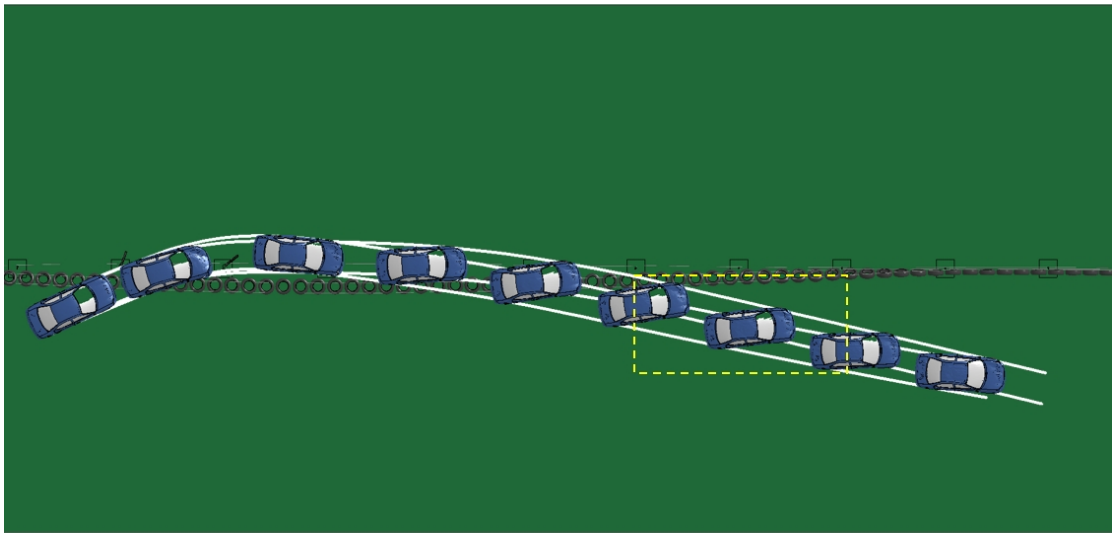

Vehicle trajectory for EDC_J1 design

Figure 5.1: Comparison of vehicle trajectories between current design and EDC_J1 design for front side post impact on flat median.

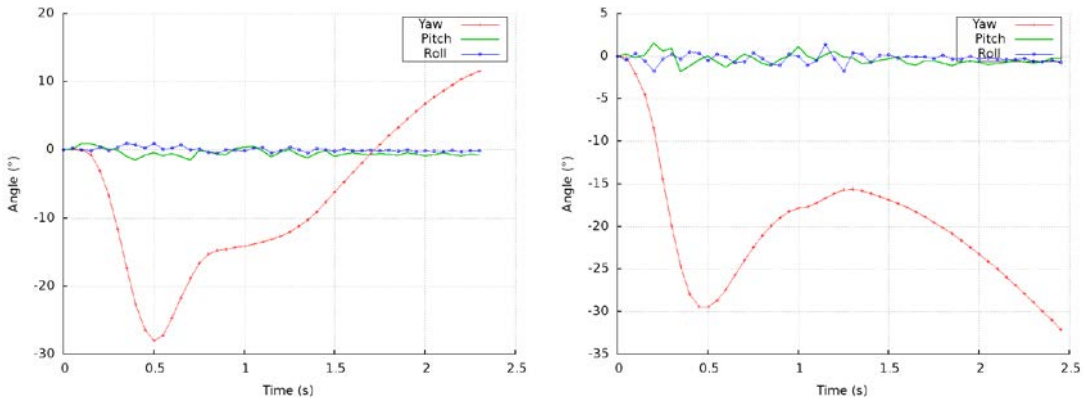

Yaw, pitch and roll angles for current design

Yaw, pitch and roll angles for EDC_J1 design

Figure 5.2: Comparison of yaw, pitch and roll angles between current design and EDC_J1 design for front side post impact on flat median.

Maximum deflection of current design cable barrier is 2.61 meters and occurs at 0.48 seconds into the simulation. Maximum deflection of EDC_J1 tire cable barrier is 1.86 meters and occurs at 0.475 seconds into the simulation. Thus, it is seen that the retrofit design is stiffer and able to redirect the vehicle in less space as compared to the current design cable barrier. Barrier damage evaluation results showed that number of posts damaged for the current design were 5 and the number of hook bolts damaged were 19. Comparatively, the number of posts damaged for EDC_J1 barrier were 5 and number of hook bolts damaged were 15. It can be observed that EDC_J1 barrier has less damage compared to current design for this case. Vehicle barrier engagement study found that for current design barrier, the top cable overrode the vehicle while middle and bottom cable engaged the vehicle. The bottom cable maintained contact with the vehicle and supported its redirection while the middle cable lost contact at about 1 second into the simulation and did not further aid in redirection. In case of EDC_J1 design, the barrier tires attached to the top and bottom cable are constantly in contact with the vehicle and aid in its redirection while the middle cable does not come in contact with the vehicle and provides minimum assistance in redirecting the vehicle.

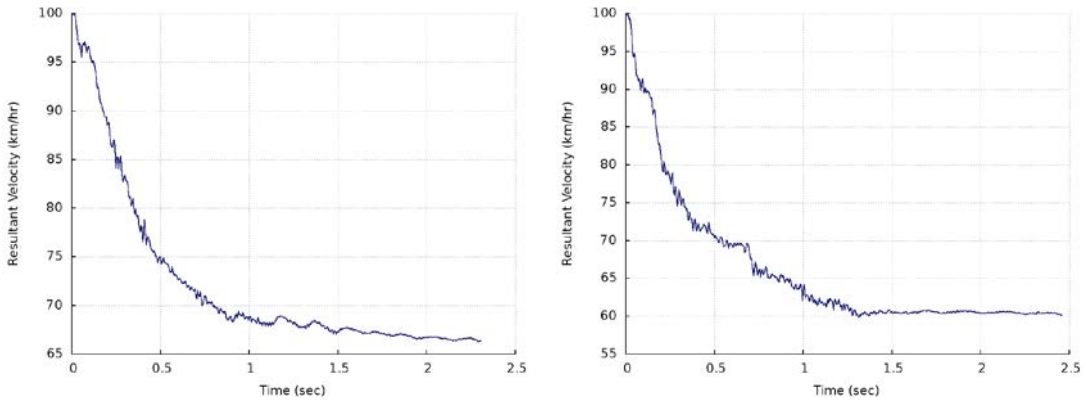

Resultant vehicle velocity for current design Resultant vehicle velocity for EDC_J1 design

Figure 5.3: Comparison of resultant vehicle velocities between current design and EDC_J1 design for front side post impact on flat median.

5.2 Front side mid-span impact on flat median

Figure 5.4 shows the post impact trajectory of Dodge Neon for current NCDOT cable median barrier design and EDC_J1 tire-cable median barrier design. In both cases, the vehicle is redirected by the barrier. It can be seen that for this case, the current design passes MASH exit box criterion but EDC_J1 design does not. Figure 5.5 shows a comparison of the yaw, pitch and roll angles for the two barrier designs. For both cases, the roll and pitch angles remain within the limit of 75° and thus pass MASH evaluation criterion F. Comparison of the yaw angle suggests that in case of current design, the vehicle has negative yaw angle and will continue to travel in a straight line post impact. However in case of EDC_J1 barrier design, the vehicle has a continuously increasing positive yaw angle which suggests vehicle spin out and loss of control for the driver post redirection. Figure 5.6 shows the comparison of velocity profile of the vehicle between current design and EDC_J1 design. It can be seen that at a time of 2.4 seconds into the simulation, the velocity of vehicle is around 67 km/h for current design and around 61 km/h for the EDC_J1 barrier. The vehicle velocity for EDC_J1 remains

almost constant thereafter and a decrease in speed of about 39 km/h is observed for EDC_J1 barrier as compared to a decrease of 33 km/h for the current design.

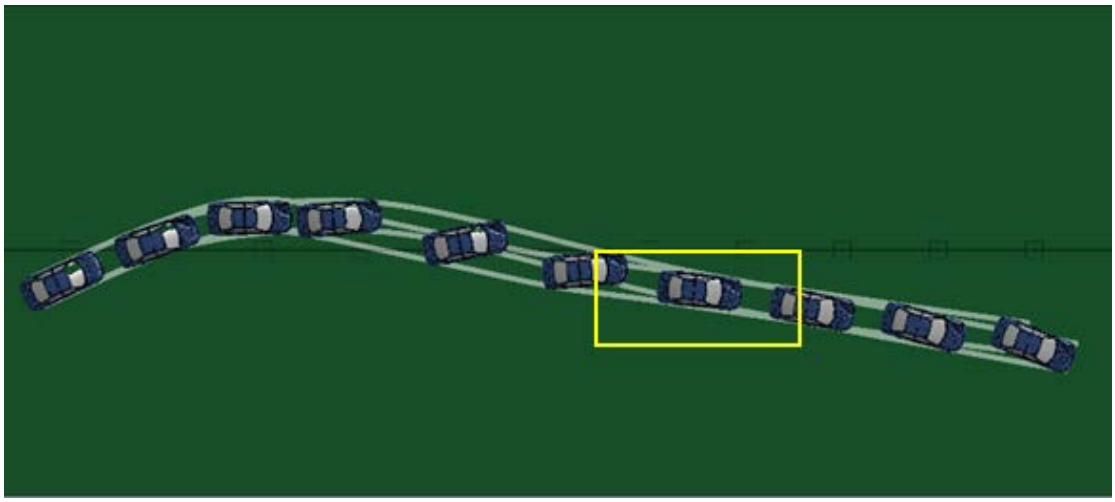

Vehicle trajectory for current design.

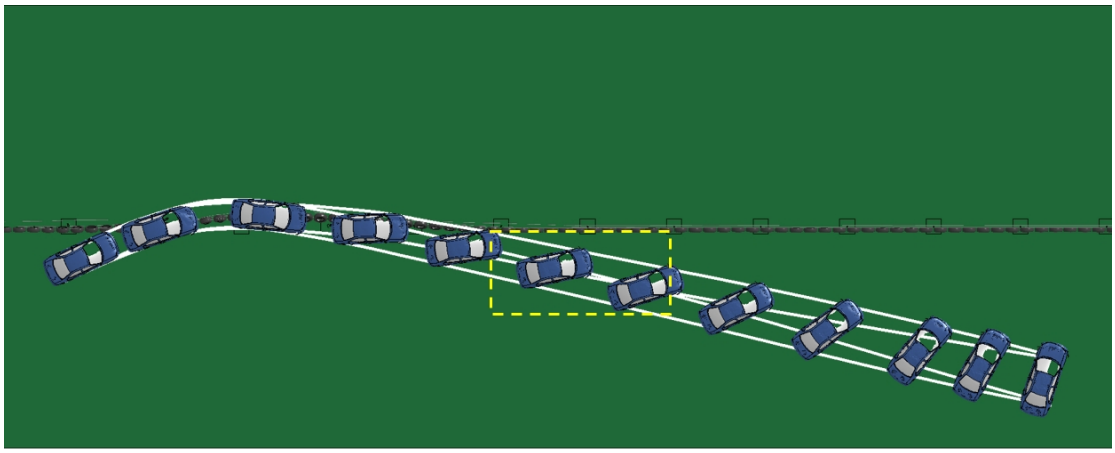

Vehicle trajectory for EDC_J1 design

Figure 5.4: Comparison of vehicle trajectories between current design and EDC_J1 design for front side mid-span impact on flat median.

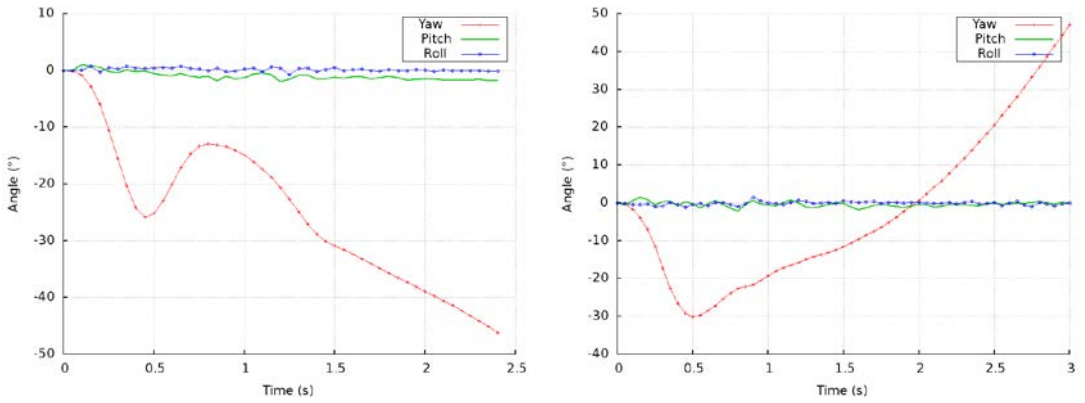

Yaw, pitch and roll angles for current design

Yaw, pitch and roll angles for EDC_J1 design

Figure 5.5: Comparison of yaw, pitch and roll angles between current design and EDC_J1 design for front side mid-span impact on flat median.

Maximum deflection of current design cable barrier is 2.67 meters and occurs at 0.48 seconds into the simulation. Maximum deflection of EDC_J1 tire cable barrier is 1.88 meters and occurs at 0.48 seconds into the simulation. Thus, it is seen that the retrofit design is stiffer and able to redirect the vehicle in less space as compared to the current design cable barrier. Barrier damage evaluation results showed that number of posts damaged for the current design were 6 and the number of hook bolts damaged were 18. Comparatively, the number of posts damaged for EDC_J1 barrier were 5 and number of hook bolts damaged were 10. It can be observed that EDC_J1 barrier has less damage compared to current design for this case. Vehicle barrier engagement study found that for current design barrier, the top cable overrode the vehicle while middle and bottom cable engaged the vehicle. The bottom cable maintained contact with the vehicle and supported its redirection while the middle cable lost contact at about 1 second into the simulation and did not further aid in redirection. In case of EDC_J1 design, the barrier tires attached to the top and bottom cable are constantly in contact with the vehicle and aid in its redirection while the middle cable does not come in

contact with the vehicle and provides minimum assistance in redirecting the vehicle. This result is similar to front side post impact described before.

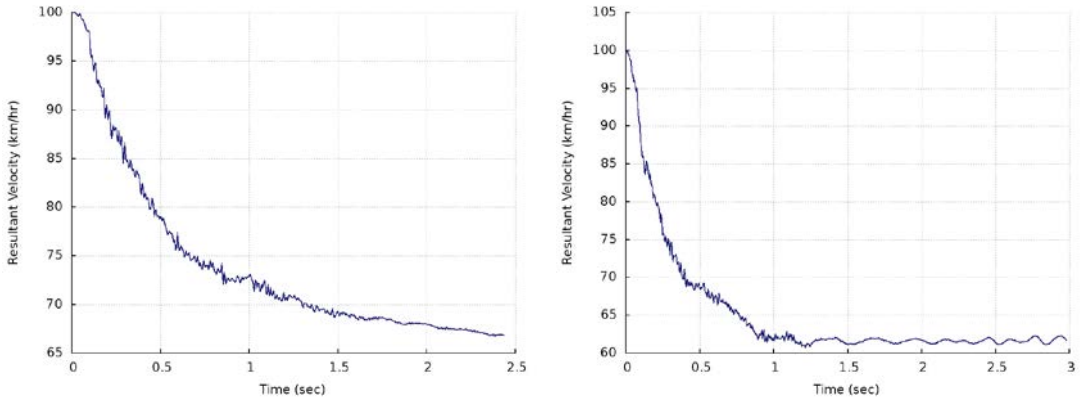

Resultant vehicle velocity for current design Resultant vehicle velocity for EDC_J1 design

Figure 5.6: Comparison of resultant vehicle velocities between current design and EDC_J1 design for front side mid-span impact on flat median.

5.3 Back side post impact on flat median

Figure 5.7 shows the post impact trajectory of Dodge Neon for current NCDOT cable median barrier design and EDC_J1 tire-cable median barrier design. In both cases, the vehicle is redirected by the barrier. It is observed that in this case, both the barrier designs fail to pass the MASH exit box criterion. Figure 5.8 shows a comparison of the yaw, pitch and roll angles for the two barrier designs. For both cases, the roll and pitch angles remain within the limit of 75° and thus pass MASH evaluation criterion F. Comparison of the yaw angle suggests that in case of current design, the vehicle has negative yaw angle and will continue to travel in a straight line post impact. However in case of EDC_J1 barrier design, the vehicle has a continuously increasing positive yaw angle which suggests vehicle spin out and loss of control for the driver post redirection. Figure 5.9 shows the comparison of velocity profile of the vehicle between current design and EDC_J1 design. It can be seen that at a time of 1.9 seconds into the

simulation, the velocity of vehicle is around 69 km/h for current design and around 61 km/h for the EDC_J1 barrier. The velocity for EDC_J1 remains constant thereafter and a decrease in speed of about 39 km/h is observed for EDC_J1 barrier as compared to a decrease of 31 km/h for the current design.

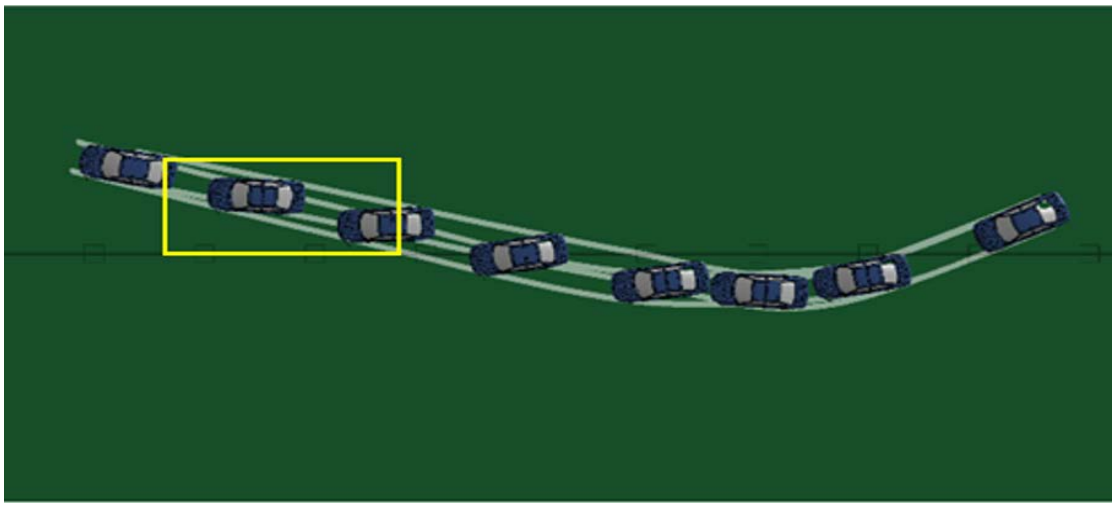

Vehicle trajectory for current design.

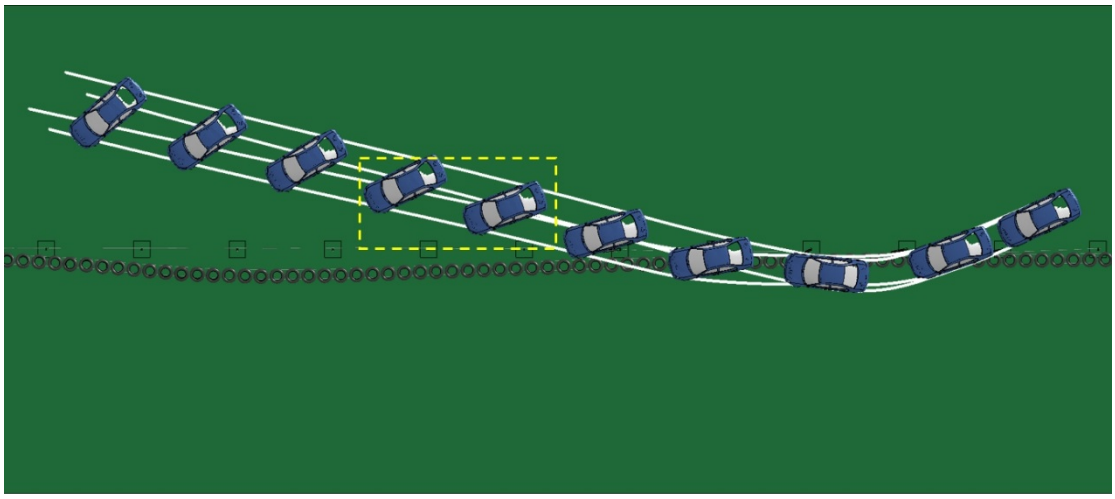

Vehicle trajectory for EDC_J1 design.

Figure 5.7: Comparison of vehicle trajectories between current design and EDC_J1 design for back side post impact on flat median

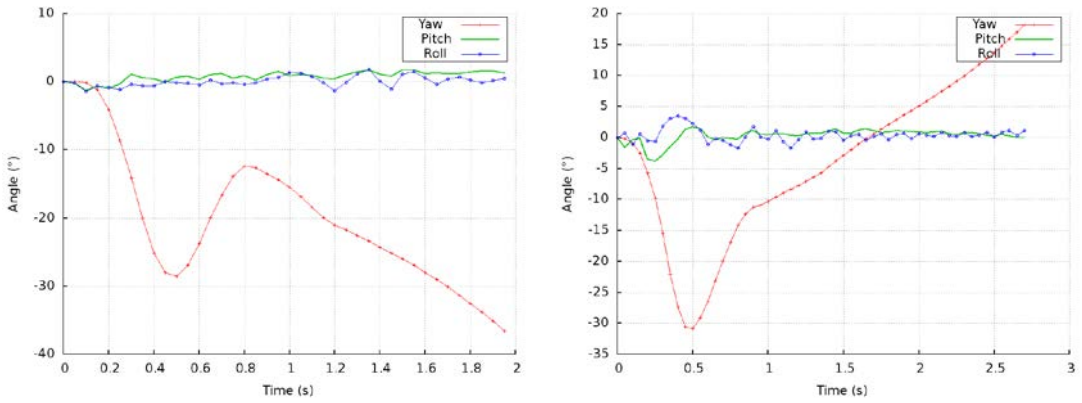

Yaw, pitch and roll angles for current design

Yaw, pitch and roll angles for EDC_J1 design

Figure 5.8: Comparison of yaw, pitch and roll angles between current design and EDC_J1 design for back side post impact on flat median.

Maximum deflection of current design cable barrier is 2.79 meters and occurs at 0.5 seconds into the simulation. Maximum deflection of EDC_J1 tire cable barrier is 2.23 meters and occurs at 0.46 seconds into the simulation. Thus, it is seen that the retrofit design is stiffer and able to redirect the vehicle in less space as compared to the current design cable barrier. Barrier damage evaluation results showed that number of posts damaged for the current design were 7 and the number of hook bolts damaged were 24. Comparatively, the number of posts damaged for EDC_J1 barrier were 5 and number of hook bolts damaged were 47. It can be observed that EDC_J1 barrier has more damage compared to current design it terms of the destroyed hook bolts for this case. However, replacement of hook bolts is cheaper compared to replacement of posts and hence repair costs will be less for EDC_J1 barrier. Vehicle barrier engagement study found that for current design barrier, all three cables engaged the vehicle. The middle cable maintained contact with the vehicle for the entire duration and supported its redirection while the top and bottom cable lost contact at about 1.2 seconds into the simulation and did not further aid in redirection. In case of EDC_J1 design, all three cables along with the barrier tires engage the vehicle. However, the barrier tires lose

contact with the vehicle as it is redirected and moving parallel to the lateral axis. The middle cable remains in contact with the vehicle throughout and aids in redirection.

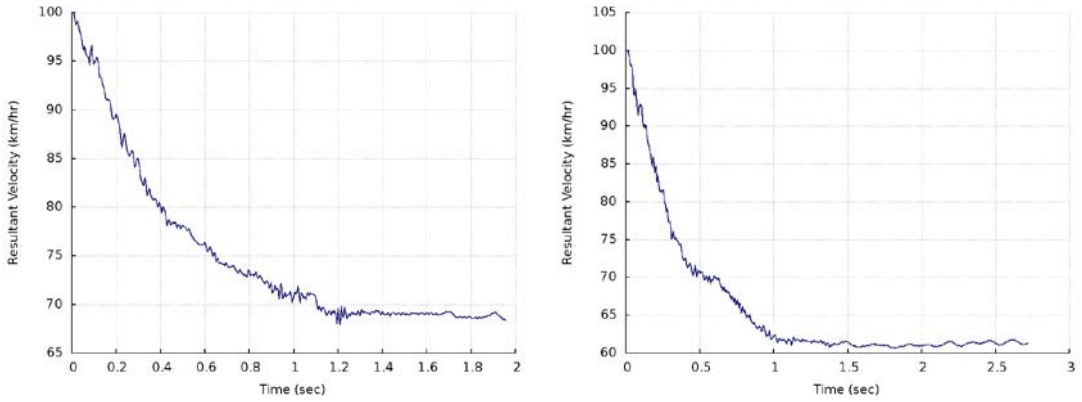

Resultant vehicle velocity for current design Resultant vehicle velocity for EDC_J1 design

Figure 5.9: Comparison of resultant vehicle velocities between current design and EDC_J1 design for back side post impact on flat median.

5.4 Back side mid-span impact on flat median

Figure 5.10 shows the post impact trajectory of Dodge Neon for current NCDOT cable median barrier design and EDC_J1 tire-cable median barrier design. The current design failed to redirect the vehicle and hence exit box criterion is not applicable. The EDC_J1 design managed to redirect the vehicle but failed the MASH exit box criterion. Figure 5.11 shows a comparison of the yaw, pitch and roll angles for the two barrier designs. For both cases, the roll and pitch angles remain within 10° indicating that vehicle remained upright. The EDC_J1 design passed the MASH evaluation criterion F. Comparison of the yaw angle suggests that in case of current design, the vehicle will continue to spin out as it approaches the oncoming traffic lane after penetration and for the EDC_J1 design it will continue to spin out after redirection increasing the possibility of a secondary collision due to loss of control by the driver. Figure 5.12 shows the comparison of velocity profile of the vehicle between current

design and EDC_J1 design. It can be seen that for current design, the velocity of vehicle after penetration is 76 km/h at the end of simulation and points towards higher severity of collision with oncoming vehicles. The post impact velocity of vehicle for EDC_J1 barrier is 65 km/h and occurs at 1.9 seconds into the simulation. Although this velocity is still high, the tire cable barrier was successful in redirecting the vehicle while the current design could not.

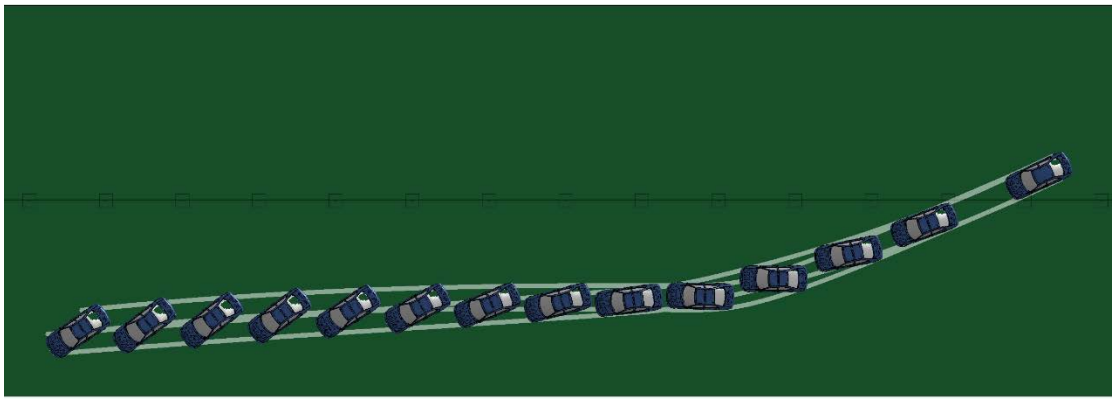

Vehicle trajectory for current design

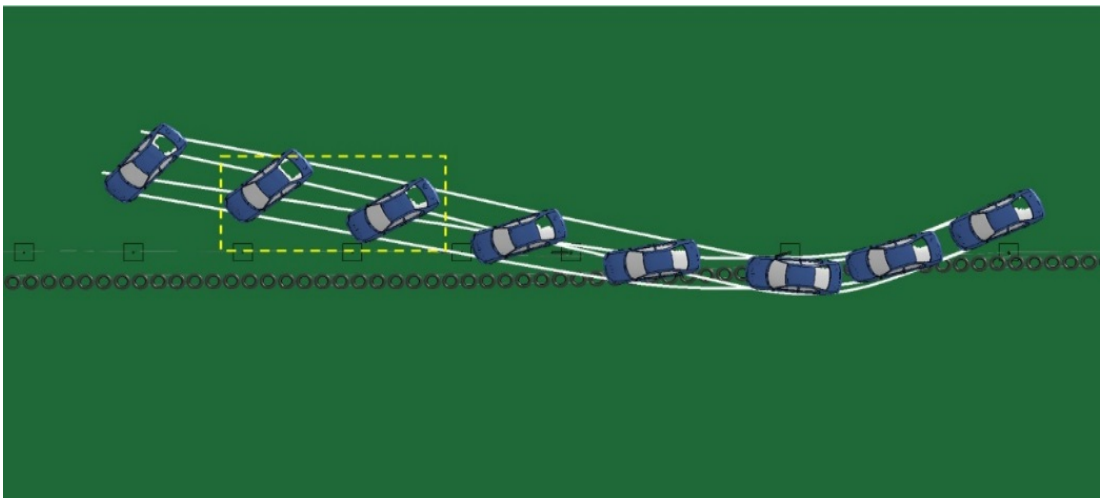

Vehicle trajectory for EDC_J1 design

Figure 5.10: Comparison of vehicle trajectories between current design and EDC_J1 design for back side mid-span impact on flat median.

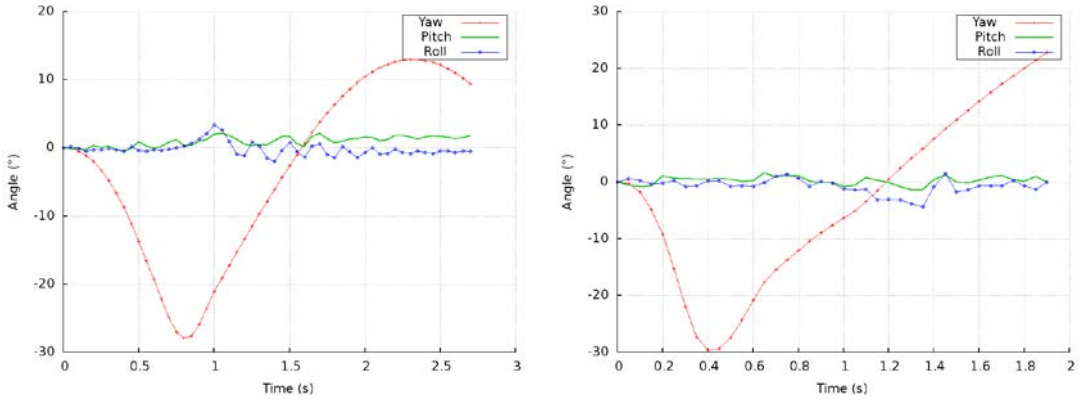

Yaw, pitch and roll angles for current design

Yaw, pitch and roll angles for EDC_J1 design

Figure 5.11: Comparison of yaw, pitch and roll angles between current design and EDC_J1 design for back side mid-span impact on flat median.

Maximum deflection of current design cable barrier is 7.09 meters and occurs at 1 seconds into the simulation. Maximum deflection of EDC_J1 tire cable barrier is 2.11 meters and occurs at 0.42 seconds into the simulation. Thus, it is seen that the retrofit design is stiffer and able to redirect the vehicle in less space as compared to the current design cable barrier which allowed for the penetration of vehicle onto the opposing travel lane. Barrier damage evaluation results showed that number of posts damaged for the current design was 1 and the number of hook bolts damaged were 34. Comparatively, the number of posts damaged for EDC_J1 barrier were 6 and number of hook bolts damaged were 41. Even though EDC_J1 barrier has slightly more damage compared to current design for this case, it successfully redirected the vehicle. Vehicle barrier engagement study found that for current design barrier, the top and middle cables overrode the vehicle upon impact while the bottom cable engaged the vehicle and remained in contact until it underrode and lost contact with the vehicle. In case of EDC_J1 design, all three cables along with the barrier tires engage the vehicle. However, the barrier tires lose contact with the vehicle as it is redirected and moving

parallel to the lateral axis. The middle cable remains in contact with the vehicle throughout and aids in redirection.

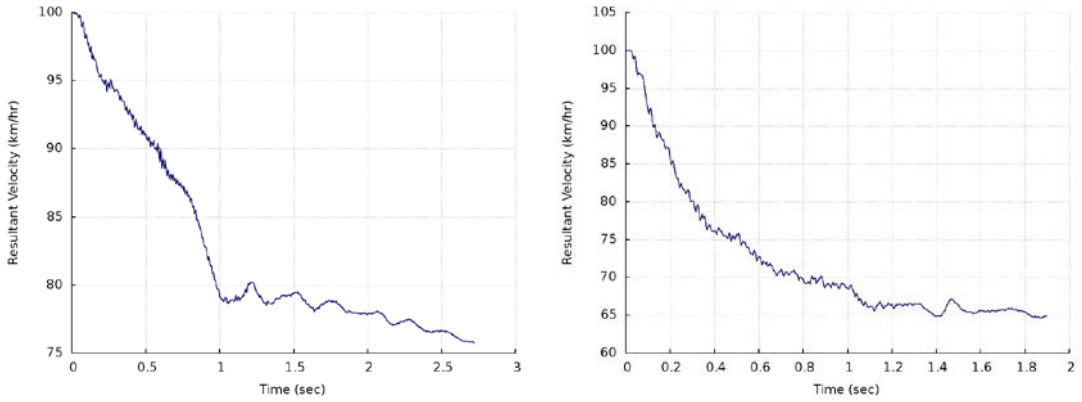

Resultant vehicle velocity for current design Resultant vehicle velocity for EDC_J1 design

Figure 5.12: Comparison of resultant vehicle velocities between current design and EDC_J1 design for back side mid-span impact on flat median.

5.5 Front side post impact on sloped median

Figure 5.13 shows the post impact trajectory of Dodge Neon for current NCDOT cable median barrier design and EDC_J1 tire-cable median barrier design. It can be seen that both the barriers failed to redirect the vehicle safely. In case of the current design, the vehicle was overturned and remained in contact with the barrier at the end of simulation while for the EDC_J1 design the vehicle jumped over the barrier and crossed into opposing traffic lane. Hence, no exit box is shown for both the cases. Figure 5.14 shows a comparison of the yaw, pitch and roll angles for the vehicle with two barrier designs. The roll angle value is more than permissible limit of 75° for the current design and hence it fails the MASH criterion F. Roll and pitch angle values for the EDC_J1 barrier are within 20° and thus pass the MASH criterion F. The yaw angle for EDC_J1 barrier suggests that the vehicle will continue to spin out as it enters the opposing travel lane increasing the probability and severity of a secondary collision

with oncoming traffic. Figure 5.15 shows the comparison of velocity profile of the vehicle between current design and EDC_J1 design. It can be seen that for current design, the vehicle has overturned at the end of simulation and has a speed of 55 km/h. This is a highly dangerous scenario because it increases the risk of occupant injury manifold. The EDC_J1 barrier does not perform better in terms of post impact velocity either. At the end of simulation, the vehicle has crossed into the opposing travel lane and continues with a velocity of 76 km/h increasing the probability and severity of secondary crash with oncoming vehicles.

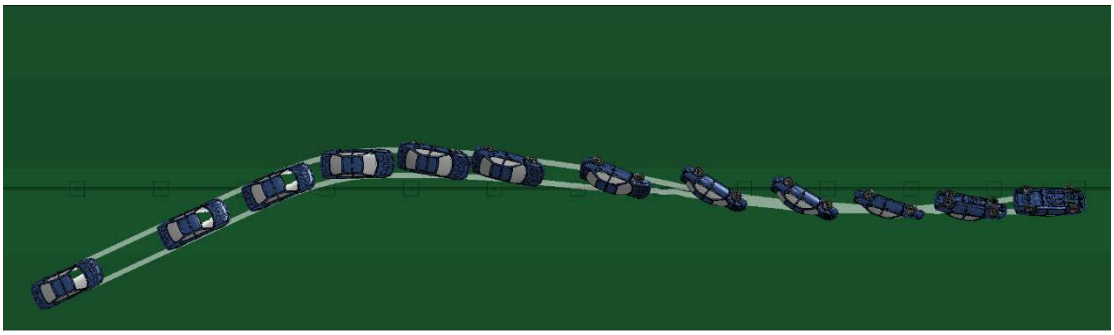

Vehicle trajectory for current design

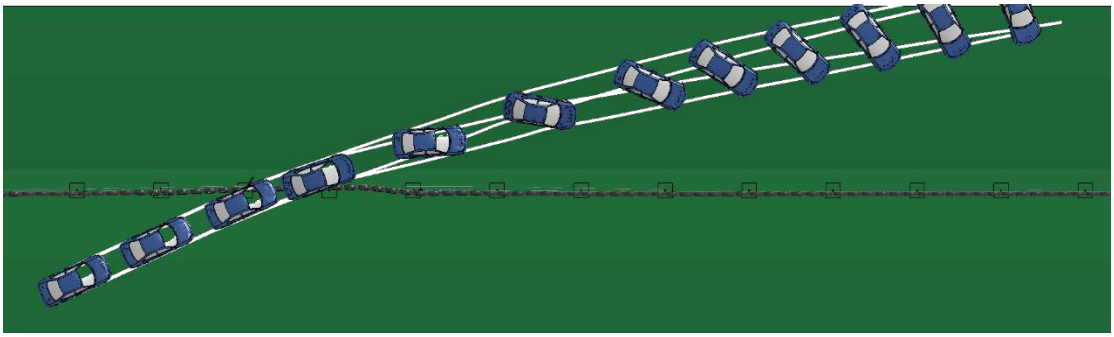

Vehicle trajectory for EDC_J1 design

Figure 5.13: Comparison of vehicle trajectories between current design and EDC_J1 design for front side post impact on sloped median.

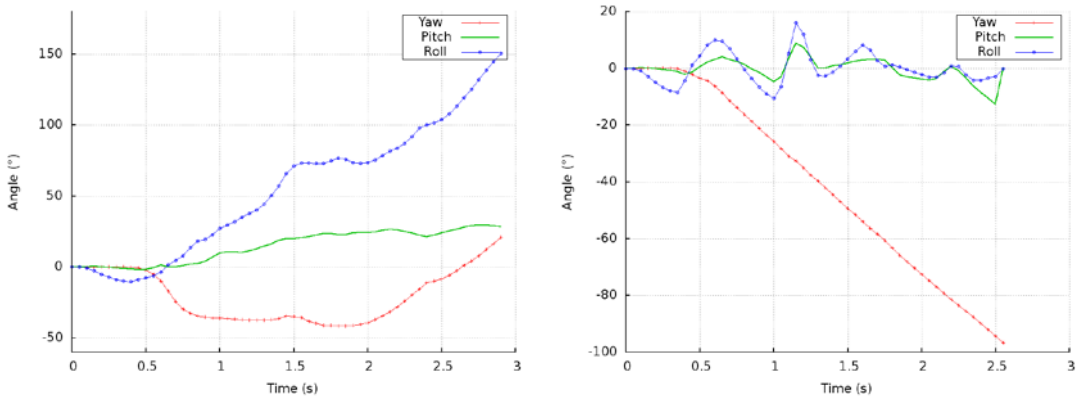

Yaw, pitch and roll angles for current design

Yaw, pitch and roll angles for EDC_J1 design

Figure 5.14: Comparison of yaw, pitch and roll angles between current design and EDC_J1 design for front side post impact on sloped median.

Maximum deflection of current design cable barrier is 2.62 meters and occurs at 0.785 seconds into the simulation. Maximum deflection of EDC_J1 tire cable barrier is 1.28 meters and occurs at 0.465 seconds into the simulation. Barrier damage evaluation results showed that number of posts damaged for the current design were 12 and the number of hook bolts damaged were 11. Comparatively, the number of posts damaged for EDC_J1 barrier were 5 and number of hook bolts damaged were 4. Even though EDC_J1 barrier seems to have less damage post impact compared to the current design, it was not able to contain the vehicle within the median or redirect it. Most of the damage for the current design is due to the vehicle rollover and skidding. Vehicle barrier engagement study found that for current design barrier, middle cable underrides the vehicle upon impact. The top and bottom cable engage the vehicle and put it on a redirection course, however they get stuck on the inner side of the hood and pull it causing the vehicle to flip. In case of EDC_J1 design, the post bends along with the cable and tires upon impact. This does not allow for proper engagement between the barrier and vehicle. The vehicle uses the bend portion of the barrier as a ramp and clears the barrier with relative ease and at high speed.

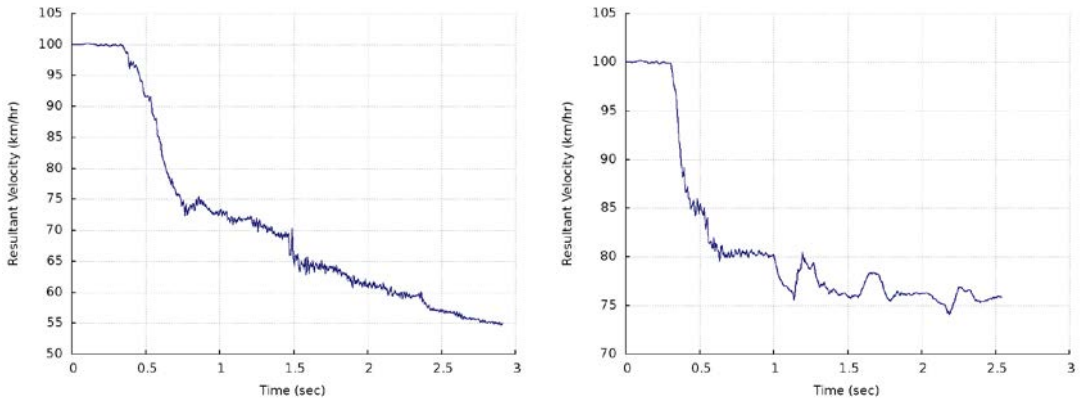

Resultant vehicle velocity for current design Resultant vehicle velocity for EDC_J1 design

Figure 5.15: Comparison of resultant vehicle velocities between current design and EDC_J1 design for front side post impact on sloped median.

5.6 Front side mid-span impact on sloped median

Figure 5.16 shows the post impact trajectory of Dodge Neon for current NCDOT cable median barrier design and EDC_J1 tire-cable median barrier design. In both cases, the vehicle is redirected by the barrier. It can be clearly seen that both designs pass MASH exit box criterion N. Figure 5.17 shows a comparison of the yaw, pitch and roll angles for the two barrier designs. For both cases, the roll and pitch angles remain within the limit of 75° and thus pass MASH evaluation criterion F. Comparison of the yaw angle suggests that in case of current design the vehicle will continue to spin out as it is being redirected and for the EDC_J1 design it will continue to advance in an almost straight line providing for better control from the driver post redirection. Figure 5.18 shows the comparison of velocity profile of the vehicle between current design and EDC_J1 design. It can be seen that at a time of 2.6 seconds into the simulation, the velocity of vehicle is around 64 km/h for current design and around 62 km/h for the EDC_J1 barrier. The velocity for EDC_J1 remains constant thereafter and a decrease in speed of about 38 km/h is observed for EDC_J1 barrier as compared to a decrease of 36 km/h for the current design.

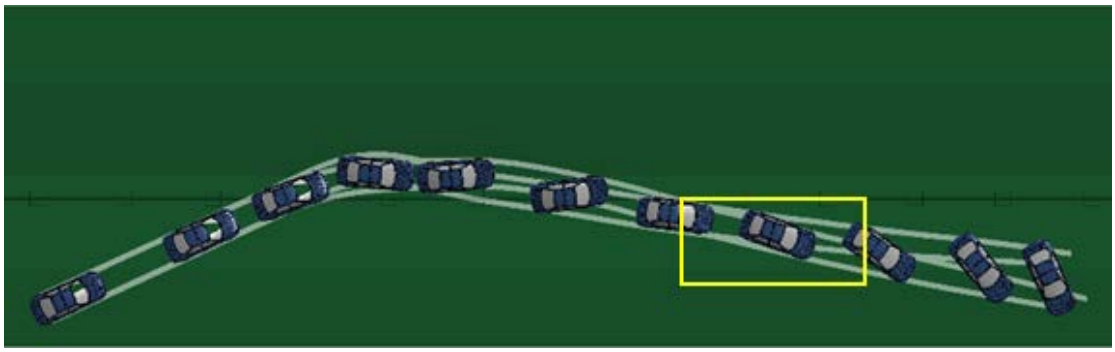

Vehicle trajectory for current design

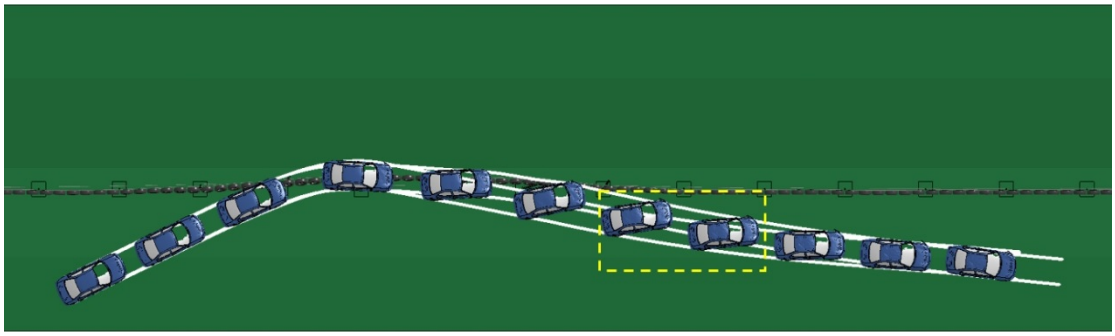

Vehicle trajectory for EDC_J1 design

Figure 5.16: Comparison of vehicle trajectories between current design and EDC_J1 design for front side mid-span impact on sloped median.

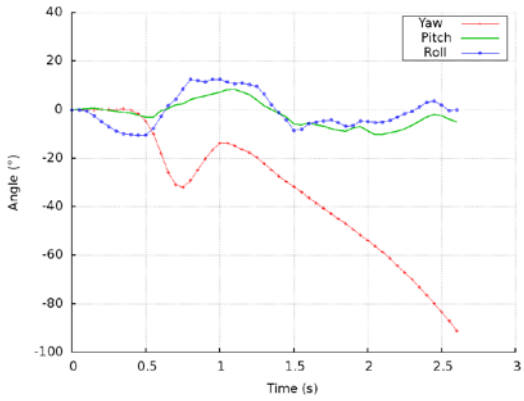

Yaw, pitch and roll angles for current design

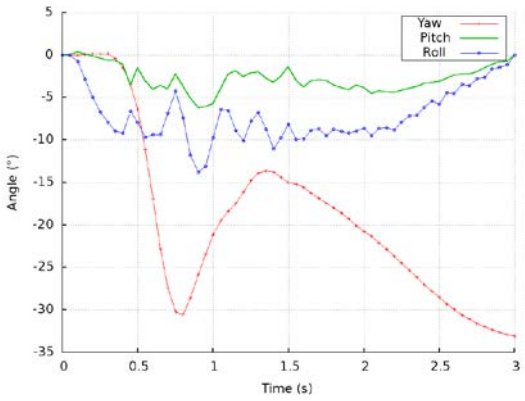

Yaw, pitch and roll angles for EDC_J1 design

Figure 5.17: Comparison of yaw, pitch and roll angles between current design and EDC_J1 design for front side mid-span impact on sloped median.

Maximum deflection of current design cable barrier is 2.45 meters and occurs at 0.74 seconds into the simulation. Maximum deflection of EDC_J1 tire cable barrier is 2.01 meters and occurs at 0.755 seconds into the simulation. Thus, it is seen that the

retrofit design is stiffer and able to redirect the vehicle in less space as compared to the current design cable barrier. Barrier damage evaluation results showed that number of posts damaged for the current design were 6 and the number of hook bolts damaged were 9. Comparatively, the number of posts damaged for EDC_J1 barrier were 6 and number of hook bolts damaged were 7. It can be observed that EDC_J1 barrier has less damage compared to current design for this case. Vehicle barrier engagement study found that for current design barrier, all three cables engaged the vehicle and aided in redirection. In case of EDC_J1 design, the barrier tires attached to the top and bottom cable are constantly in contact with the vehicle and aid in its redirection while the middle cable does not come in contact with the vehicle and provides minimum assistance in redirecting the vehicle.

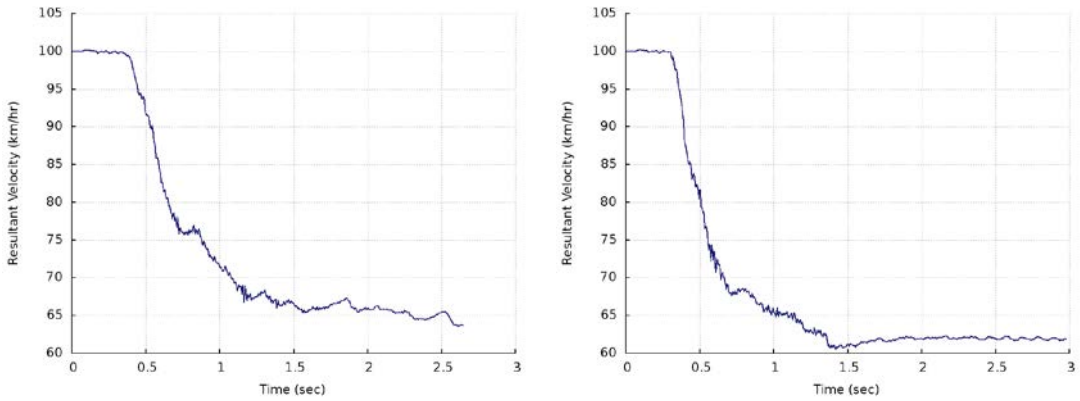

Resultant vehicle velocity for current design Resultant vehicle velocity for EDC_J1 design

Figure 5.18: Comparison of resultant vehicle velocities between current design and EDC_J1 design for front side mid-span impact on sloped median.

5.7 Back side post impact on sloped median

Figure 5.19 shows the post impact trajectory of Dodge Neon for current NCDOT cable median barrier design and EDC_J1 tire-cable median barrier design. The current design failed to redirect the vehicle and hence exit box criterion is not

applicable. The EDC_J1 design managed to redirect the vehicle and remained in contact with the barrier at the end of simulation and hence exit box cannot be shown. For EDC_J1 design, the vehicle is trapped between barrier tires and the middle cable. Figure 5.20 shows a comparison of the yaw, pitch and roll angles for the two barrier designs. For both cases, the roll and pitch angles remain within the limit of 75° and thus pass MASH evaluation criterion F. Comparison of the yaw angle suggests that in case of current design, the vehicle will continue to spin slightly as it approaches the oncoming traffic lane and for the EDC_J1 design it will continue to advance in an almost straight line providing for better control from the driver post redirection. Figure 5.21 shows the comparison of velocity profile of the vehicle between current design and EDC_J1 design. It can be seen that for current design, the velocity of vehicle after penetration is 79 km/h at the end of simulation and points towards higher severity of collision with oncoming vehicles. The post impact velocity of vehicle for EDC_J1 barrier is 61 km/h and occurs at 3 seconds into the simulation.

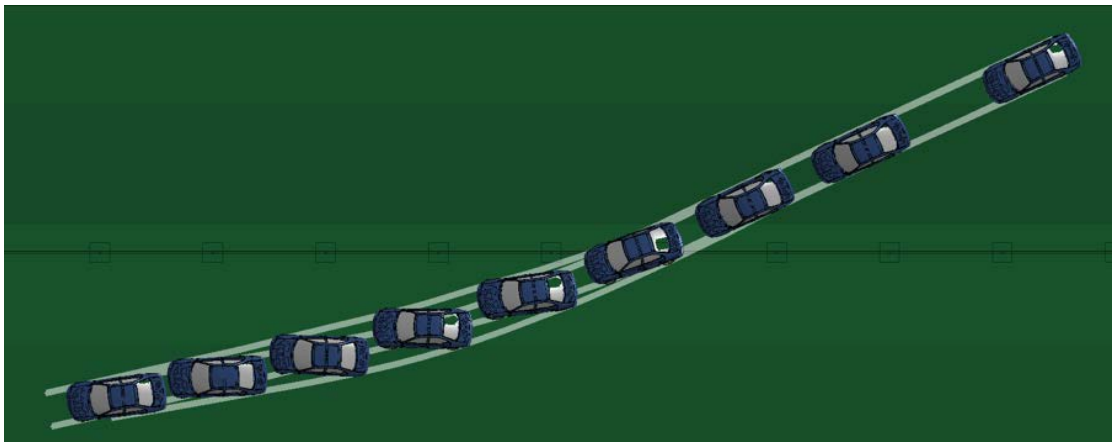

Vehicle trajectory for current design

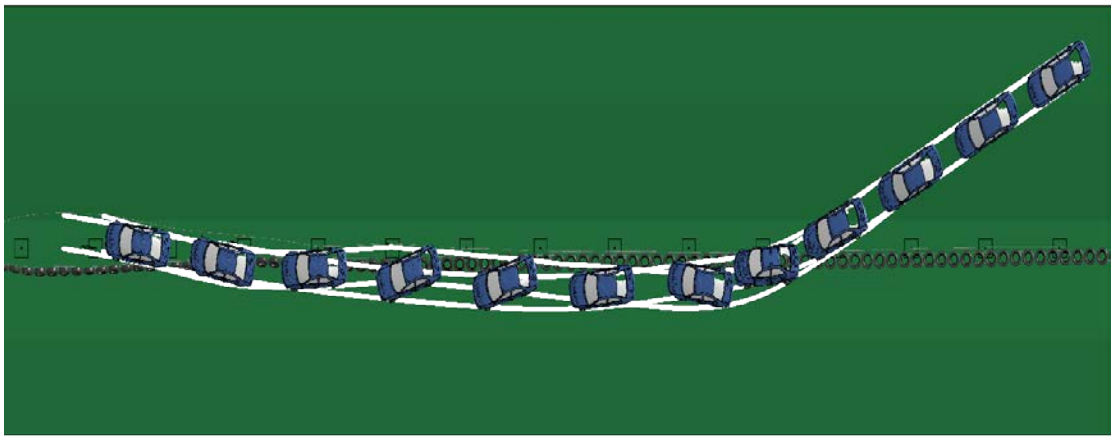

Vehicle trajectory for EDC_J1 design

Figure 5.19: Comparison of vehicle trajectories between current design and EDC_J1 design for back side post impact on sloped median.

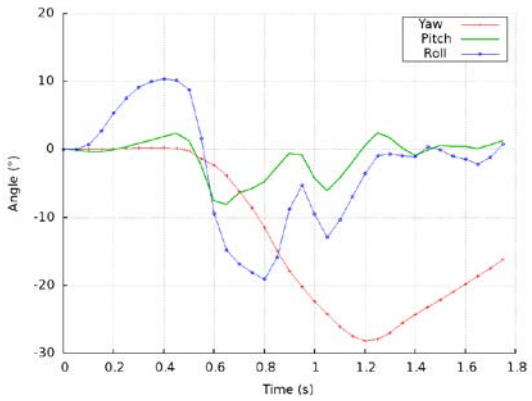

Yaw, pitch and roll angles for current design

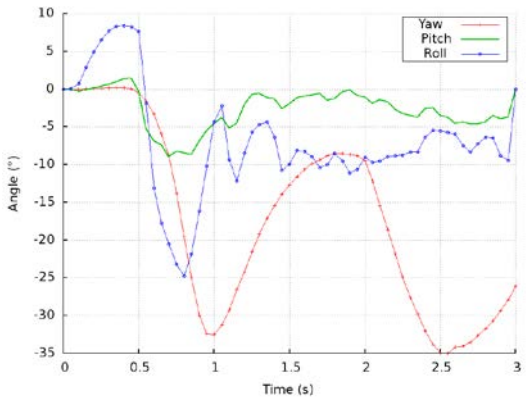

Yaw, pitch and roll angles for EDC_J1 design

Figure 5.20: Comparison of yaw, pitch and roll angles between current design and EDC_J1 design for back side post impact on sloped median.

Maximum deflection of current design cable barrier is 5.27 meters and occurs at 1.3 seconds into the simulation. Maximum deflection of EDC_J1 tire cable barrier is 2.78 meters and occurs at 1.47 seconds into the simulation. Thus, it is seen that the retrofit design is stiffer and able to redirect the vehicle in less space while the current design fails to redirect the vehicle. Barrier damage evaluation results showed that number of posts damaged for the current design was 1 and the number of hook bolts damaged were 40. Comparatively, the number of posts damaged for EDC_J1 barrier were 6 and number of hook bolts damaged were 48. Even though EDC_J1 barrier has slightly more damage compared to current design for this case, it successfully redirected the vehicle. Vehicle barrier engagement study found that for current design barrier, the top and middle cables overrode the vehicle upon impact while the bottom cable engaged the vehicle and remained in contact until 1.3 seconds into the simulation after which it underrode and lost contact with the vehicle. In case of EDC_J1 design, the barrier tires attached to the top and bottom cable are constantly in contact with the vehicle and aid in its redirection while the middle cable was overridden upon impact. The middle cable prevents reentering of the vehicle in the travel lane by trapping it between barrier tires and itself.

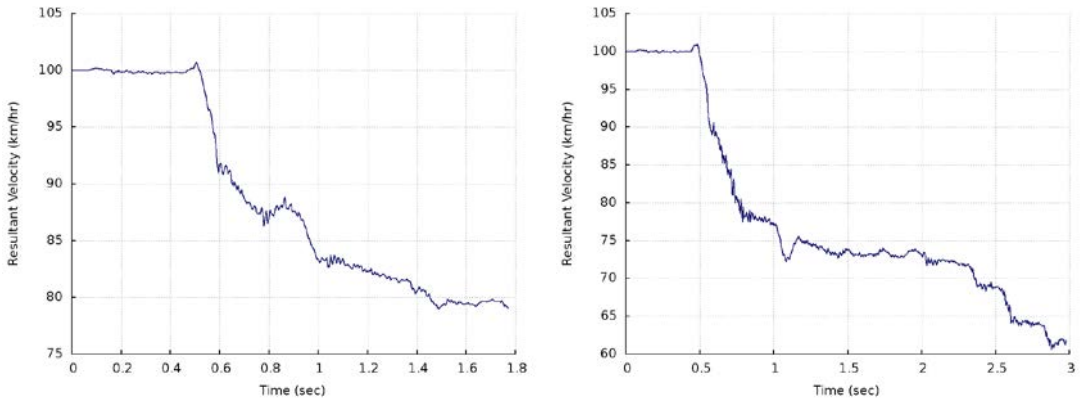

Resultant vehicle velocity for current design Resultant vehicle velocity for EDC_J1 design

Figure 5.21: Comparison of resultant vehicle velocities between current design and EDC_J1 design for back side post impact on sloped median.

5.8 Back side mid-span impact on sloped median

Figure 5.22 shows the post impact trajectory of Dodge Neon for current NCDOT cable median barrier design and EDC_J1 tire-cable median barrier design. The current design failed to redirect the vehicle and hence exit box criterion is not applicable. The EDC_J1 design managed to redirect the vehicle and remained in contact with the barrier at the end of simulation and hence exit box cannot be shown. For EDC_J1 design, the vehicle is trapped between barrier tires and the middle cable. Figure 5.23 shows a comparison of the yaw, pitch and roll angles for the two barrier designs. For both cases, the roll and pitch angles remain within the limit of 75° and thus pass MASH evaluation criterion F. Comparison of the yaw angle suggests that in case of current design, the vehicle will continue to spin out as it approaches the oncoming traffic lane and for the EDC_J1 design it will continue to advance in an almost straight line providing for better control from the driver post redirection. Figure 5.24 shows the comparison of velocity profile of the vehicle between current design and EDC_J1 design. It can be seen that for current design, the velocity of vehicle after penetration is 87 km/h at the end of simulation and points towards higher severity of collision with

oncoming vehicles. The post impact velocity of vehicle for EDC_J1 barrier is 61 km/h and occurs at 3 seconds into the simulation.

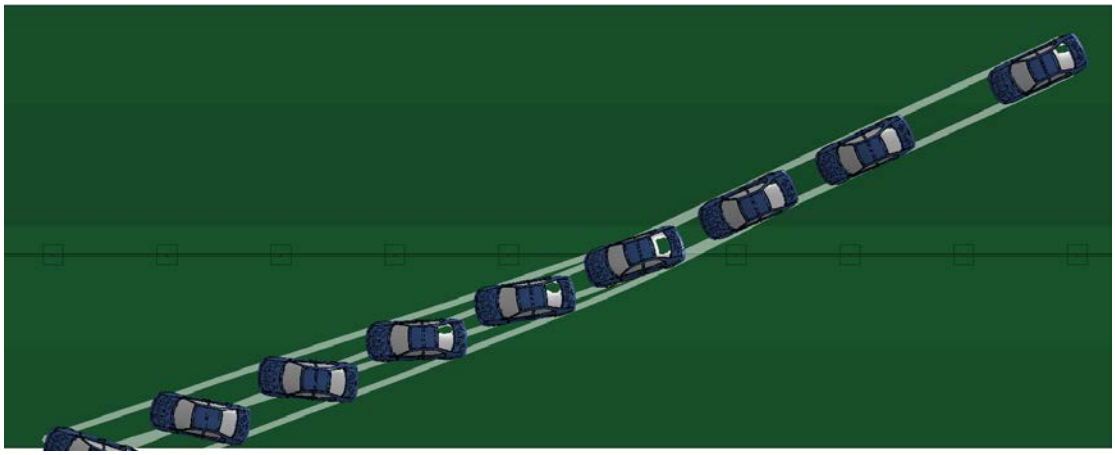

Vehicle trajectory for current design

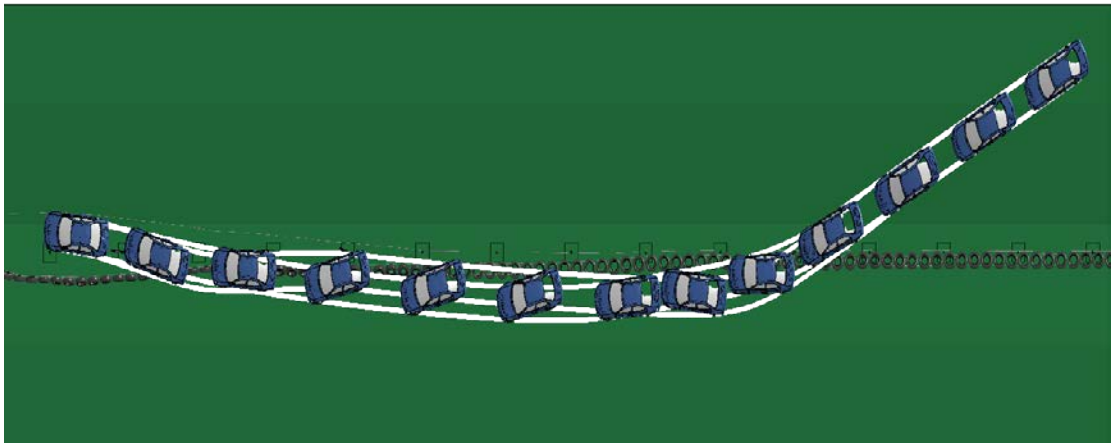

Vehicle trajectory for EDC_J1 design

Figure 5.22: Comparison of vehicle trajectories between current design and EDC_J1 design for back side mid-span impact on sloped median.

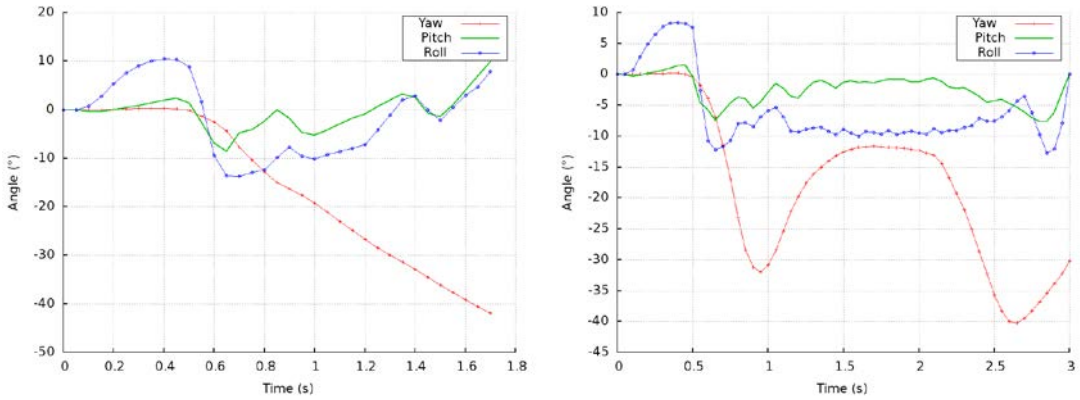

Yaw, pitch and roll angles for current design Yaw, pitch and roll angles for EDC_J1 design

Figure 5.23: Comparison of yaw, pitch and roll angles between current design and EDC_J1 design for back side mid-span impact on sloped median.

Maximum deflection of current design cable barrier is 1.129 meters and occurs at 0.8 seconds into the simulation. Maximum deflection of EDC_J1 tire cable barrier is 3.03 meters and occurs at 1.36 seconds into the simulation. Thus, it is seen that the retrofit design is stiffer and able to redirect the vehicle in less space while the current design fails to redirect the vehicle. Barrier damage evaluation results showed that number of posts damaged for the current design was 1 and the number of hook bolts damaged were 22. Comparatively, the number of posts damaged for EDC_J1 barrier were 5 and number of hook bolts damaged were 54. Even though EDC_J1 barrier has slightly more damage compared to current design for this case, it successfully redirected the vehicle. Vehicle barrier engagement study found that for current design barrier, all three cables overrode the vehicle upon impact. In case of EDC_J1 design, the barrier tires attached to the top and bottom cable are constantly in contact with the vehicle and aid in its redirection while the middle cable was overridden upon impact. The middle

cable prevents reentering of the vehicle in the travel lane by trapping it between barrier tires and itself.

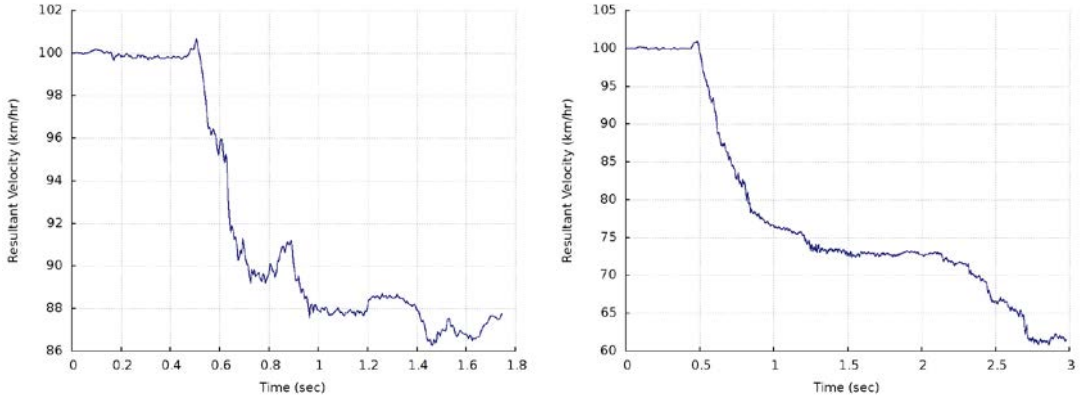

Resultant vehicle velocity for current design Resultant vehicle velocity for EDC_J1 design

Figure 5.24: Comparison of resultant vehicle velocities between current design and EDC_J1 design for back side mid-span impact on sloped median.

CHAPTER 6 : CONCLUSIONS AND FUTURE WORK

In this thesis work, a retrofit design for cable median barrier has been studied. The idea behind this design was to combine reclaimed tires with cable barriers and create a viable barrier design. This would help put the reclaimed tires to good use and also enhance the performance of cable barriers in an economic way. Finite element (FE) simulations were conducted to evaluate the performance of retrofit barrier under MASH TL-3 conditions.

A systematic procedure was followed while deciding the tire-cable median barrier design. In Case 1, the least retrofitting approach was used to decide the first design TCMB_J1. On its failure, TCMB_U1 design was analyzed. It was observed that the free movement of the lower part of the barrier tires proved ineffective in stopping and redirecting the vehicles. Hence, decision was made to change the heights of the middle and bottom cable so as to support the barrier tire uniformly on its sidewall. In this way, EDC_J1 and EDC_U1 designs were conceived. Simulation results proved that EDC_U1 was too stiff and could not redirect vehicle safely but EDC_J1 was successful in containing and redirecting the smaller sedan.

Case 2 entailed further investigation of EDC_J1 barrier design. This design was evaluated on flat and sloped medians. Simulation results showed that EDC_J1 barrier was able to redirect the vehicle for all the cases barring two. The performance of EDC_J1 barrier was especially good on the flat median as it managed to redirect the vehicle for both post and mid-span impact from front and back side. The two simulations in which EDC_J1 barrier failed to redirect the vehicle were back side post

impact on sloped median for placement 1 and front side post impact on sloped median for placement 2.

Case 3 involved simulations with all four tire-cable median barrier designs and a Ford F250 truck. Due to numerical issues, all the simulations initially planned for this case could not be completed in time for the presentation of this work. However, four simulations were successfully completed and their results have been shared in this thesis. Simulation results for TCMB_U1 and EDC_U1 barriers showed that these designs were unable to successfully redirect the truck in a safe manner. These results were found to be consistent with the ones obtained for Neon. Investigation of EDC_J1 barrier on sloped median for placement 1 showed that the barrier successfully redirected the truck for front side post impact but could not retain the vehicle for back side post impact.

Comparison of barrier performance between current design cable median barrier and EDC_J1 barrier showed that the latter was objectively better at redirecting small sedan Neon on flat and sloped medians. A major issue with the current design cable median barrier was that cables would easily override the vehicle which would allow it to penetrate the barrier. However in case of EDC_J1 barrier, no override was observed for the compared cases. Current design cable median barrier was able to redirect the vehicle in four cases out of a total of eight and the EDC_J1 barrier was able to redirect the vehicle in seven out of a total eight cases.

This research provided valuable insights regarding placement of tires on a cable median barrier and its effect on the system. Finite element analysis proved to be a useful tool in design evaluation of retrofit median barriers. It can be concluded that EDC_J1 barrier is a good alternative for current design cable median barriers for redirecting

small sedans on a flat median. Although improvements were observed on the sloped median with EDC_J1 barrier, further investigations are recommended.

This research work could not conclusively put forth the effects of impact of trucks with the EDC_J1 barrier. As part of future work for this research, numerical issues in the Ford F250 FE model combined with tire-cable median barrier FE model will be understood and resolved. Full scale simulations will be run with the truck to better understand tire-cable median barrier performance. Further investigation into the hook bolt strength will be carried out to improve on the impact scenarios involving substantial post and hook bolt damage. Another area of future work will involve incorporating failure of the hook bolt to post attachment for the TCMB_U1 and EDC_U1 designs. Realistic design and modeling of barrier tire to cable attachment with failure criteria will also be included in future work. All these areas of future work will help understand the tire-cable median barriers better and a superior retrofit design may be possible.

REFERENCES

Bernaquez, N., & Sabourin, I. (1996). IMPACT ABSORBING BARRIERS FOR HIGHWAYS.

Burns, K., & Bell, K. (2016). Performance Evaluation of a Cable Median Barrier System on an Oregon Highway with a Narrow Median. Transportation Research Record 2588, (2588), 137–144.

Cooner, S. A., Rathod, Y. K., Alberson, D. C., Bligh, R. P., & Stephen, E. (2009). Performance Evaluation of Cable Median Barrier Systems in Texas (Vol. 7).

Diem, R. (2003). METHOD AND DEVICE FOR BRAKING VEHICLES.

Fang, H., Li, N., Disogra, M., Gutowski, M., & Weggel, D. C. (2012). Recommendations for Placement of Cable Median Barriers on 6:1 and 4:1 Sloped Medians with Horizontal Curvatures.

Fang, H., Weggel, D. C., Bi, J., & Martin, M. E. (2009). Finite Element Evaluation of Two Retrofit Options to Enhance the Performance of Cable Median Barriers.

Graham, M. D., Burnett, W. C., Gibson, J. L., Freer, R. H., & Engineer, A. (1967). New Highway Barriers: The Practical Application of Theoretical Design. Highway Research Record 174.

Hallquist, J. O. (2006). “LS-DYNA Theory Manual.” Livermore Software Technology Corporation. Livermore, CA.

Hiser, N. R., & Reid, J. D. (2005). Modeling slip base mechanisms. International Journal of Crashworthiness, 8265. *<http://doi.org/10.1533/ijcr.2005.0361>*

Hughes, T. J. R., Taylor, R. L., Sackman, J. L., Curnier, A., & Kanoknukulchai, W. (1976). A finite element method for a class of contact-impact problems. *Computer Methods in Applied Mechanics and Engineering*, *8*(3). http://doi.org/https://doi.org/10.1016/0045-7825 (76)90018-9

Hunter, W. W., Stewart, J. R., Eccles, K. A., Huang, H. F., Council, F. M., & Harkey, D. L. (1997). Three-Strand Cable Median Barrier in North Carolina In-Service Evaluation. Transportation Research Record 1743, (1), 97–103.

Ibrahimbegovic, A. (2006). *Nonlinear Solid Mechanics*. Springer Netherlands. *<http://doi.org/10.1007/978-90-481-2331-5>*

Kramer, R. (2001). VEHICLE CRASH WALL.

Laker, I. B., & Naylor, A. W. (1973). Development and Proving Tests of a Four-Rope Safety Fence. Transportation Research Record 1419.

LSTC (2007). “LS-DYNA keyword user’s manual - version 971.” Livermore Software Technology Corporation (LSTC), Livermore, CA.

Marzougui, D., Mohan, P., Dao, C., Kan, S., & Opiela, K. (2007). Performance Evaluation of Low-Tension Three-Strand Cable Median Barriers. Transportation Research Record 2025, 34–44.

MASH (2009). “Manual for assessing safety hardware (MASH).” American Association of State Highway and Transportation Officials (AASHTO), Washington D.C.

Mohan, P., Marzougui, D., Meczkowski, L., Bedewi, N., Mohan, P., Marzougui, D., Bedewi, N. (2010). Finite element modeling and validation of a 3- strand cable guardrail system. International Journal of Crashworthiness, 8265(August). *<http://doi.org/10.1533/ijcr.2005.0345>*

Moon, D. (1993). IMPACT ABSORBING BARRIER AND THE METHOD OF CONSTRUCTING SAME.

NCAC (web1). “NCAC finite element models.” *<http://www.ncac.gwu.edu/vml/models.html>*

CCSA (web2). “CCSA finite element models.” *<https://www.ccsa.gmu.edu/models/>*

Phillips, R., Tyrell, A., Bryden, J., & Fortuniewicz, J. (1990). CABLE GUIDERAIL BREAKAWAY TERMINAL ENDS.

Robert, W., Cody, S., & John, D. (2012). Improved Models of Cable-to-Post Attachments for High-Tension Cable Barriers (2012) (Vol. 851).

Sposito, B., & Johnston, S. (1998). THREE-CABLE MEDIAN BARRIER FINAL REPORT.

Stolle, C. S. (2014). Factors Contributing to Cable Median Barrier Penetrations. In Transportation Research Board 93rd Annual Meeting.

Stolle, C. S., & Reid, J. D. (2011). Development of a wire rope model for cable guardrail simulation. International Journal of Crashworthiness, 16(3), 331–341. *<http://doi.org/Doi 10.1080/13588265.2011.586609>*

Stolle, C. S., & Sicking, D. L. (2013). Impact Conditions Associated with Cable Median Barrier Failures. In Transportation Research Board 92nd Annual Meeting.

Suri Bala (web3). “Tied interface.” *<https://www.d3view.com/blog>*

Talbott, A. (2005). TIRE FENCE.

Vincent, C. (1974). GO-CART GUARD RAIL.

Walker, B. (1972). ENERGY ABSORBER.

Wang, Q., Fang, H., Li, N., Weggel, D. C., & Wen, G. (2013). An efficient FE model of slender members for crash analysis of cable barriers. Engineering Structures, 52, 240–256. < *http://doi.org/10.1016/j.engstruct.2013.02.027* >

Way, M., & Pas, J. (1974). HIGHWAY SAFETY TIRE DEVICE.

Yang, W., Bendana, L. J., & Bruno, N. J. (1979). Performance of Cable Guiderail in New York. Transportation Research Record 1419.

Yoho, L. (1976). VEHICULAR ENERGY ABSORBER.

Yunick, H. (1997). RACE TRACK WITH NOVEL CRASH BARRIER AND METHOD.